Effects of strength hardening, stiffness degradation, strength deteriorarion and pinching on the seismic response of SDoF systems

Bougioukos Apostolos | March, 2017

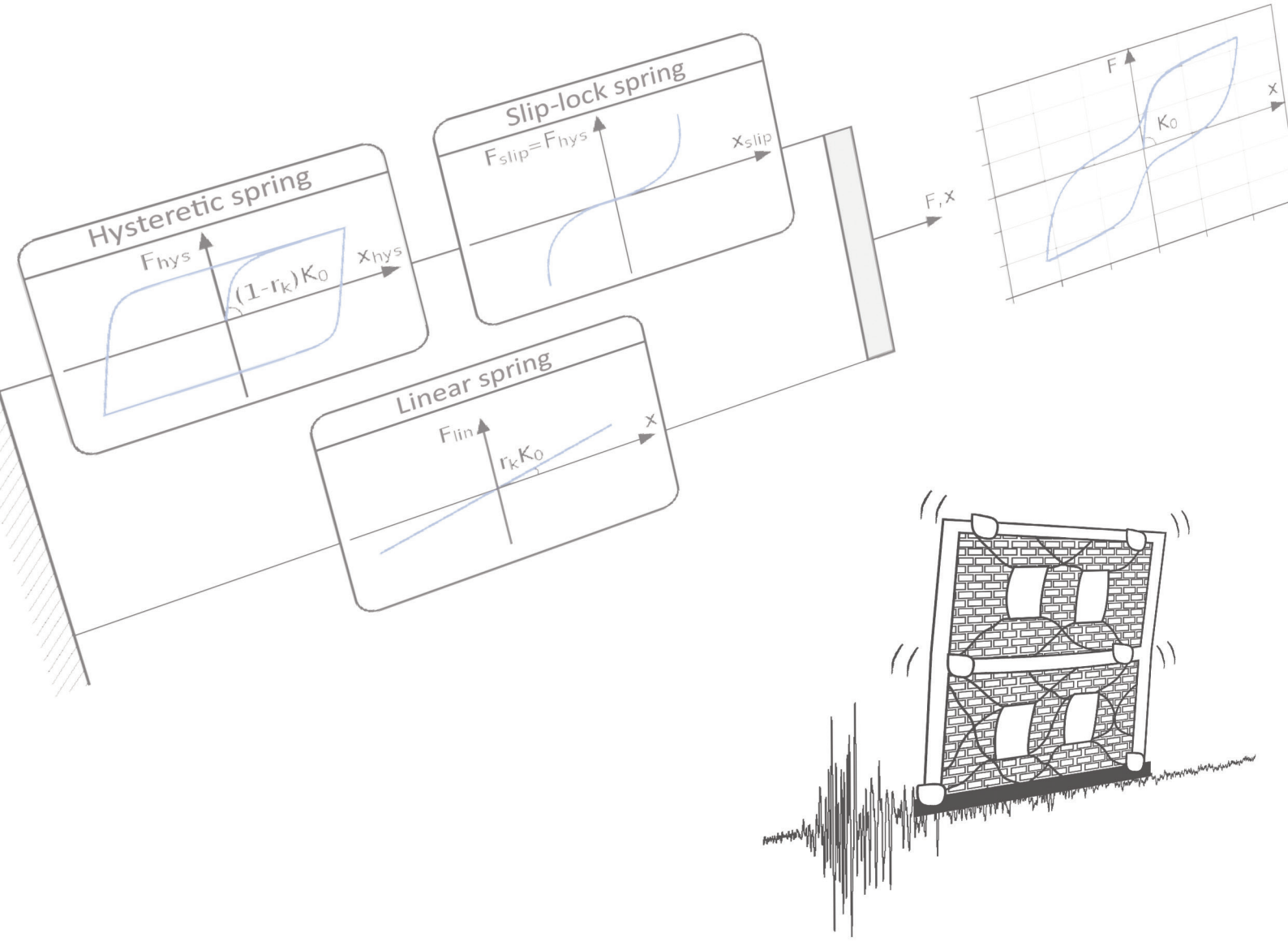

Witteveen Bos

TU Delft

Effects of strength hardening, stiffness degradation, strength deterioration and pinching on the seismic response of SDoF systems

Apostolos Bougioukos

March 2017,

Delft University of technology

Coordinators:

Andrei Metrikine
Professor
Section of Structural Mechanics
Faculty of Civil Engineering and Geosciences
Delft University of Technology
E-mail: A.Metrikine@tudelft.nl

Apostolos Tsouvalas
Assistant professor
Section of Offshore Engineering
Faculty of Civil Engineering and Geosciences
Delft University of Technology
E-mail: A.Tsouvalas@tudelft.nl

Karel van Dalen
Researcher/Lecturer Structural Mechanics
Section of Structural Mechanics
Faculty of Civil Engineering and Geosciences
Delft University of Technology
E-mail: K.N.vanDalen@tudelft.nl

Floris Besseling
Structural / Geotechnical Project Engineer
Witteveen+Bos
E-mail: floris.besseling@witteveenbos.com

Acknowledgments

First of all, I would like to express my gratitude to my daily supervisors Dr. Apostolos Tsouvals and Ir. Floris Besseling, whose comments and guidance greatly improved this study. They allowed me to elaborate my own ideas and let this study to be my own work, but at the same time they steered me in the right direction whenever they thought it was needed.

I would also like to acknowledge Prof. Andrei Metrikine for his valuable comments on critical moments of this graduation work. Prof. Andrei Metrikine encouraged me to be more critical and less judgmental on other researchers' findings, while at the same time he taught me to search for the physics behind every result.

Additionally, I would like to thank all my friends in Delft for being next to me the last two and a half years. Special thanks to Marianthi Sousamli who in addition proofread this study, but also to my friends: Giorgos Katsaounis, Panos Mitsis and Lampros Roussos with whom we spent many hours in the library of TU Delft.

Furthermore, I must express my gratitude to my family for their financial and psychological support all these years of my studies. Especially I would like to thank my sister Maria Bougioukou for her assistance on the design of the cover page of this study.

Last but not least I would like to thank my girlfriend, Kim Schipper for her understanding, her patience and her encouragement during the challenging moments that I faced the last period of my graduation work. She was always there when I needed support and her aid was critical for the completion of this graduation work.

Contents

Abstract

One of the most commonly used seismic analysis methods, over the last few decades is the equivalent lateral force method. This procedure, which was initially intended for elastic design of structures, has been extended to inelastic design, with the incorporation of the behaviour factor q or with the integration of response spectrum procedures with non-linear static pushover analysis. The behaviour factor, which is meant to reduce the elastic forces, depends on the ductility capacity of each structure. However, the connection between the ductility ratio and the behaviour factor has been approximated by employing an elastic-perfectly plastic hysteretic system, which is a very simplistic form of inelastic behaviour. Meanwhile, the last decades, a number of non-linear effects, that develop during the cyclic loading of an earthquake on different types of structures have been identified. The influence of those effects on the response of single degree of freedom (SDoF) systems subjected to seismic load has been recognized by various authors.

The purpose of this work is to enhance the understanding of the impact of various typically observed effects on the seismic response of structures. Models that incorporate the effects of strength hardening, stiffness degradation, strength deterioration and pinching are examined and their response is compared to the response of the elastic-perfectly plastic system. The non-linear models are subjected to an ensemble of 167 earthquake ground motions, which is divided into eight different groups according to the magnitude of the earthquake, the significant duration, the soil conditions while one more group consists of signals similar to the ground motions of the area of Groningen. The response measures that are examined have been selected through an extensive investigation of various damage indices and measures proposed in the literature. Through this investigation, it is concluded that the measures of the maximum displacement response, the residual displacement, the total hysteretic energy, the total dissipated by viscous damping energy and the total input energy are sufficient to describe the response of a structure subjected to seismic load.

The results of this investigation showed that these non-linear effects influence more the response of the systems with short eigen-period. The effect that seems to affect the most the response is the pinching effect. Additionally, it is shown that there is high dependency between the frequency content and the deviations of the response calculated by the models that incorporate this non-linear effects and the response calculated by elastoplastic model.

1 Introduction

Nowadays, the seismic design of a structure can be performed through several different methods. Among them, the most commonly used in the design codes, are the equivalent lateral force analysis, the modal response spectrum analysis and the time history analysis (Eurocode 8; NEHRP 2009). Despite the fact that the last metho is more sophisticated, the most popular ones are the equivalent lateral force analysis and the modal response spectrum analysis. There are mainly two reasons for this. Firstly, these methods are meant for regular structures, that can be well represented by single degree of freedom systems; and indeed, the majority of structures around the world can be classified as regular. Secondly, they are very simple methods based on response spectra, which are used for decades.

The response spectrum method is based on the fact that the dynamic load of an earthquake is treated as static lateral load distributed along the height of the structure according to the fundamental mode of vibration of the structure. Initially, this method was developed for elastic design of structures. However, with the introduction of the inelastic design spectra it has been extended to structures which are expected to respond inelastically to the design earthquake (Kappos 1998). The inelastic design spectra are constructed based on the reduction of the ordinates of the elastic design spectra by a behaviour factor (q). The behaviour factor is linked to the concept of ductility capacity[1] of a structural system, through relationships that are defined by assuming that the inelastic behaviour of structures can be represented by elastic-perfectly plastic hysteretic models (Bozorgnia & Campbell 2004; Bojórquez & Ruiz 2004; Akkar 2014).

However, several authors (Park et al. 1988; Reinhorn et al. 1988; Kunnath et al. 1990; Sivaselvan & Reinhorn 1999; Sivaselvan & Reinhorn 2000; Ibarra et al. 2005; Sivaselvan 2013; Kottari et al. 2014) through laboratory tests have proved that the behaviour of structural systems subjected to cyclic lateral load deviates from the behaviour of elastic-perfectly plastic model. This observation triggered the motivation of this study to examine quantitatively the degree that the response of a structure subjected to ground motion would change if instead of the simplistic elastoplastic model, a more advanced model that accounts for several non-linear effects would have been used.

It is a fact that a lot of earlier studies (Rahnama & Krawinkler 1993; Sashi K Kunnath et al. 1997; Oh et al. 2000; Oh et al. 2000; Sivaselvan & Reinhorn 2000; Naeim et al. 2000; Ruiz-García & Miranda 2003; Medina & Krawinkler 2004; Rodgers, Janise E.; Mahin 2004; FEMA P440A 2009) have already investigated these non-linear effects. Nevertheless, all of them examined either the influence of only one of those effects, or the influence of all of these effects considering only the maximum inelastic displacement as a response measure. This is done by determining the magnitude of the maximum inelastic displacement for models that account for the non-linear effects and compare it with the magnitude of the maximum inelastic displacement of the elastic-perfectly plastic model.

However, this study attempts to take the whole investigation one step further in five different ways. Firstly, by employing a very advanced general hysteretic model developed by Ray and Reinhorn (2014). This model, which combines characteristics of earlier models (Park et al. 1987; Sashi K Kunnath et al. 1997; Sivaselvan & Reinhorn 2000), has been proved to capture accurately the non-linear effects of ductile and brittle materials as well. Secondly, by evaluating the level of the impact of the non-linear effects according to five different response parameters; the maximum inelastic displacement, the residual displacement, the total dissipated hysteretic energy, the total viscous dissipated energy and the total input energy. These choices are the result of an extensive literature review of damage indices at an initial stage of this study.

Thirdly, by dividing the whole ensemble of 167 ground motions into eight different groups according to the earthquake magnitude, the significant duration, the soil conditions and one group that consists of signals similar to the ground motions in Groningen. In this way, it can be observed, which type of ground motion characteristics influence more each of the non-linear behaviours. Fourthly, by presenting the different types of response in contour plots in respect of the yield force (F_y) and the initial elastic period. In addition to this diagram

[1] Ductility capacity is defined as the ratio between the ultimate displacement and the yield displacement of a structural system, as they determined through monotonic test.

a complementary diagram that presents the Fourier spectrum of the input motion is added, in order to examine also the influence of the signals in terms of their frequency content. Finally, in contrast with the previous researchers who assume that the yield force of all the models is equal to the yield force of the elastoplastic model, in this study it is assumed that the yield force of the elastoplastic model is equal to the maximum force of the system that incorporates the non-linear behaviours. This concept is closer to the procedure that is followed from the design codes to envelope the real force-displacement diagram. Therefore, the outcomes of this study can be used for the improvement of the design procedures.

1.1 Study objectives

The primary objective of this study is to give a better insight of the influence of several non-linear effects on the response of structural systems subjected to seismic loads. Secondary, objective is to evaluate these outcomes for the Groningen case where the structures usually have short eigen-period and the signals have significantly different frequency content compared to the tectonic earthquakes.

These objectives are accomplished by following two different types of investigation:

1. In the first one, a single model was examined
    1.1. The model is calibrated to fit the force-displacement curve of a pushover test of a masonry building that represents the structures in Groningen.
    1.2. The calibrated model is subjected to signals that represent the ground motions in Groningen and in order to calculate the maximum force and displacement response.
    1.3. The same structure under the same load is calculated by the response spectrum method and the results are compared
2. In the second one a sensitivity analysis was performed:
    2.1. Through an extensive literature review of the proposed damage indices, the response measures that can represent the behaviour of a structural system subjected to cyclic lateral load are identified.
    2.2. An additional literature review reveals the non-linear effects that appear during the cyclic loading of a structure.
    2.3. An advanced hysteretic model that captures these effects is chosen and according to that several systems are modeled.
    2.4. A careful selection of ground motions, to which the structural systems are subjected, took place.
    2.5. The influence of the non-linear effects is examined, by comparing various forms of response of the enhanced models to the more simplistic elastoplastic system.

1.2 Study scope

The scope of this study is to identify the sensitivity on the seismic response of various non-linear effects, of models that already have been proposed in the literature. In this manner, no attempt is made for the development of a new hysteric model or for the proposal of a new damage index. However, the author is confident that the observations of this research can set the basis of the construction of new rules, regarding the prediction of the response of inelastic systems.

Furthermore, this research focuses on single degree of freedom systems and therefore all the observations that are drawn correspond to structures for which the fundamental mode of vibration dominates the dynamic response of the system during earthquake excitation. There are two reasons for this choice. Firstly, a large number of simple structures in the real world can be reduced to single degree of freedom systems, with fair accuracy. Secondly, the investigation of multi degree of freedom systems, implies more than one natural periods, each one corresponding to a different vibration mode. On top of that the degree of participation of each of those modes should be taken into account as an additional parameter. Given the fact that the response of non-linear single degree of freedom systems subjected to seismic load is rather complex, both on the implementation and the interpretation, the involvement of a larger number of natural periods may lead to ambiguous and confusing results. In this respect, the results presented in this thesis must always be viewed in relation to simple structures or structures in which the dynamic response is dominated by a single mode of vibration throughout the excitation.

Additionally, the sensitivity analysis does not focus on one type of structures, but instead it attempts to encompass a broad spectrum of structural systems and materials. This means that the developed models are not calibrated to real laboratory tests; but rather than that they refer to idealized structural systems which appear two levels (a moderate and a high) of strength hardening, stiffness degradation, strength deterioration and pinching. These predefined levels have been incorporated to show the trend of the deviations compared to the elastic perfectly-plastic system. The later system is the basis of the current design codes.

1.3 Report structure

The report has been constructed in a way such that it presents the distinctive stages of the project. More specifically, the first chapter explains the conception of the study, the objectives that the author set and the scope of the study

The second chapter, focuses on the description of the main effects that have been observed on various structural systems subjected to cyclic lateral load through laboratory tests. More precisely, the evolution of the effects of strength hardening, stiffness degradation, strength deterioration and pinching is explained through a sequence of figures. In addition, earlier findings of the response of systems that incorporate these effects are included at the end of each paragraph.

In the third chapter, the development of the various models that are employed in this study is presented. Firstly, a brief overview of the hysteretic models is given that have been proposed in the literature, along with the general model that it is chosen in this particular study. This is followed by a description of the numerical method that has been applied and a more analytical presentation of the technics according to which the inelastic effects are incorporated in the models.

The fourth chapter introduces the ensemble of the ground motions that have been used as external loads to the single degree of freedom systems. Characteristics of the signals, including the magnitude, the peak ground acceleration, the significant duration, the fault distance, the mechanism of the event etc., can be seen however, in the Appendix C.

In the fifth chapter, a very detailed overview of the damage indices is provided as developed by various authors for structures subjected to seismic load. The damage indices have been classified into different categories, according to the response parameter examined. The primary reason for this overview is to identify which response parameters are sufficient to characterize the behaviour of a structure.

In the sixth chapter, the results of the analyses are presented and discussed. The significance of the non-linear effects of strength hardening, stiffness degradation, strength deterioration and pinching are evaluated for the response parameters chosen in the previous chapter. The results are presented in the form of contour plots which illustrate the response of the elastoplastic systems normalized by the response of the advanced systems, with respect to the yield force and the reference elastic period chosen.

Finally, in the seventh chapter, several conclusions are drawn and recommendations for future studies are given.

2 Seismic response of inelastic systems

2.1 Hysteresis

Hysteresis is a non-linear behaviour that is encountered in several physical phenomena (e.g. plasticity, electricity, inelasticity, friction, magnetism) and as a term appears in various disciplines (e.g. science, engineering, chemistry, economics, biology and experimental psychology). According to Visintin (1994), hysteresis is characterized by memory and it is rate independent (rate independent memory effect).

However, in nature the response of structural systems is never independent of the rate of the applied load. Therefore, when the effect of the rate needs to be taken into account, viscosity is introduced. As a matter of fact, typically in seismic response of structures both viscosity and hysteresis contribute to the overall energy dissipated by the structure. Nevertheless, the viscous phenomena can be neglected and only hysteretic phenomena are encountered when the load is applied at a very low rate. In structural engineering, hysteresis is a phenomenological concept based on the fitting of experimental data and is usually depicted as a diagram of the response parameter ($f(x)$) versus the input parameter (x) (Figure 2.1 (c)) (Charalampakis 2009).

2.2 Elastic-perfectly plastic behaviour

In the literature, most of the studies that examine the behaviour of non-linear systems subjected to seismic load, assume that the cyclic response of the system can be described by an elastic-perfectly plastic model. This means that the yield force and the stiffness of the system are considered constant throughout the entire loading history, by being assigned to predefined values.

This behaviour can be captured by a simple non-degrading elastic-perfectly plastic hysteretic model (Figure 2.2). In such a model, the loading branch of the force-deformation diagram is linear elastic until the yield force is reached. After the yield force is reached, the stiffness of the system becomes zero until the force becomes smaller than the yield force. Regarding the unloading branch, its stiffness is equal to the (initial) stiffness of the loading branch. Despite its simplicity, such an assumption deviates from reality as it has been proven in experimental studies (Goel & El-tayem 1987; Venti & Engelhardt 1999; Elwood & Moehle 2003; Uriz & Mahin 2004; Liu & Astaneh-asl 2004).

Various studies (Park et al. 1988; Reinhorn et al. 1988; Kunnath et al. 1990; Sivaselvan & Reinhorn 1999; Sivaselvan & Reinhorn 2000; Ibarra et al. 2005; Sivaselvan 2013; Kottari et al. 2014) have already observed more complicated behaviour in different materials and structural systems. These studies argue that the behaviour of a structural system can be captured more accurately when a hysteretic model incorporates the effects of strength hardening, stiffness degradation, strength deterioration and pinching. In the following paragraphs, these effects are explained and results of earlier studies which examined their influence on the maximum displacement are discussed.

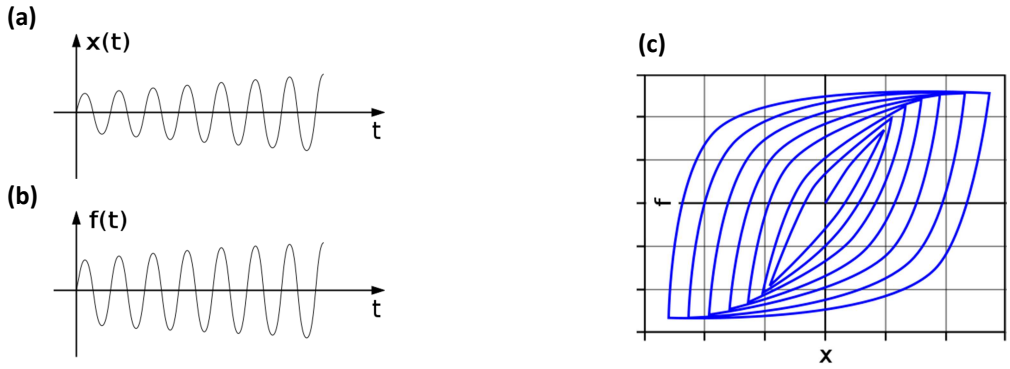

Figure 2.1. Hysteretic behaviour. (a) Input time history x(t), (b) response time history f(t), (c) hysteretic response diagram.

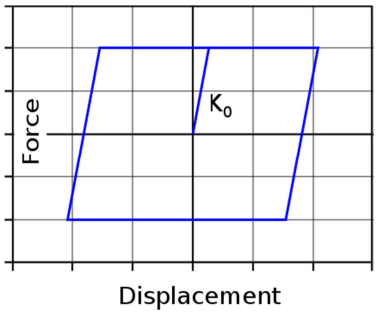

Figure 2.2. Elastic-perfectly plastic hysteretic loop.

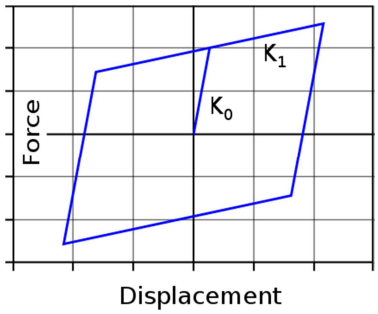

Figure 2.3. Hysteretic loop with strength hardening (bilinear).

2.3 Strength hardening

As explained above, the elastic-perfectly-plastic behaviour is a rough approximation of the real inelastic behaviour of structures subjected to lateral cyclic loading. It has been observed that the strength of many materials, structural elements and structural systems, does not remain constant after the yield force is exceeded; but instead it keeps increasing with a different rate, possessing some kind of strength hardening.

On material level, this phenomenon is called strain hardening. This is because in several non-brittle materials (e.g. metals and polymers) the strength is increasing, when after yielding they are subjected to large strain levels (Degarmo et al. 2003; Van Melick et al. 2003). On the structural element level, strength hardening occurs due to delayed mobilization of the entire cross-section after yielding (FEMA P440A 2009). On the structural system level, strength hardening is a result of the sequential yield of all the individual elements that compose the structural system (FEMA P440A 2009).

In the force displacement diagram, the strength hardening is represented by incorporating a positive post-yield stiffness (Figure 2.3). In the literature, very often, the post-yield stiffness is given as a ratio (stiffness ratio) of the initial elastic stiffness of the system. When the stiffness ratio is unity the post-yield stiffness is equal to the initial elastic stiffness and practically the system remains elastic. On the other hand, when the stiffness ratio is zero the post-yield stiffness is zero and the bilinear model yields to the elastic-perfectly plastic model (Figure 2.2).

Ruiz-García and Miranda (2003) investigated the influence of the strength hardening by comparing the maximum inelastic displacement of elastic-perfectly plastic systems to the one of bilinear systems with varying post-yield stiffness. They concluded that the maximum inelastic displacement is in general smaller for bilinear systems. This decrease becomes more apparent on systems with short structural period. The same authors (Jorge Ruiz-García & Miranda 2006) examined the effect of the strength hardening on the residual displacements. The conclusion of this study is that the residual displacement (as response parameter) is more sensitive to the strength hardening, compared to the maximum inelastic displacement.

2.4 Stiffness degradation

Stiffness degradation is a phenomenon usually observed in structural elements or systems which are subjected to cyclic lateral load. It has been shown to occur due to geometric non-linear effects and it becomes more severe with increasing deformations (Kunnath et al. 1990). The effect of this phenomenon becomes stronger when a structure is subjected to several large load reversals. The main cause of stiffness degradation in steel elements is fatigue (Whitworth 1998), while in reinforced concrete elements stiffness degrades due to cracking, loss of bond or interaction with high shear or axial stresses (FEMA P440A 2009).

Park et al. (1988) have suggested an empirical rule that predicts accurately the stiffness degradation of a system. According to this rule, the unloading branch of the force-displacement diagram targets a pivot point on the extrapolated branch of the initial elastic stiffness at a distance aF_y, on the force axis, of the opposite side. F_y represents the yield force of the system and a is a parameter that controls the level of stiffness degradation.

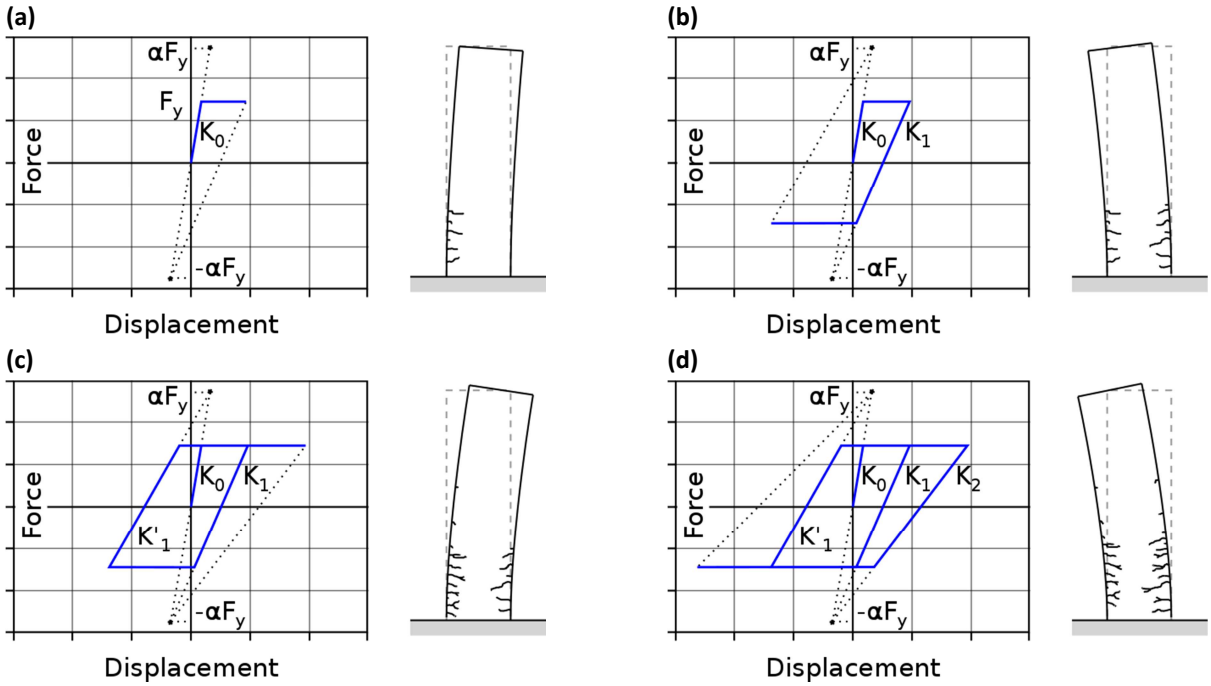

Figure 2.4. Evolution of stiffness degradation of a reinforced concrete column element subjected to cyclic lateral load.

When a is small the stiffness degradation effect is large and when a is very large (>200) there is almost no stiffness degradation.

The effect of stiffness degradation of a reinforced concrete column element is illustrated in the Figure 2.4. In this figure, it can be seen that larger displacement (further to the yield point), leads to higher stiffness degradation. Through geometry, Sivaselvan & Reinhorn (2000) defined the stiffness degradation factor R_k, according to which the magnitude of the decreased stiffness of the unloading branch can be determined. In the formula that these authors proposed (Eq. (2.1)) F_i and x_i are the force and the displacement respectively at the i^{th} step of the loading time history and K_0 is the initial elastic stiffness of the system. Most of the advanced hysteretic models implement this simple rule to capture the stiffness degradation effect of a structural system.

$$R_k = \frac{F_i + aF_y}{K_0 x_i + aF_y} \tag{2.1}$$

Various studies have been conducted (Rahnama & Krawinkler 1993; Oh et al. 2000; Naeim et al. 2000; Medina & Krawinkler 2004; Rodgers, Janise E.; Mahin 2004; FEMA P440A 2009) for the evaluation of the effects of stiffness degradation by comparing the maximum displacement of stiffness degrading systems to the maximum displacement of elastoplastic and bilinear systems. These studies have concluded that moderate and long period single degree of freedom degrading systems lead to maximum displacements similar to the elastoplastic and bilinear system. On the other hand, the maximum displacements of short period single degree of freedom degrading systems, are larger than the one experienced by elastoplastic and bilinear systems.

2.5 Strength deterioration

Strength deterioration refers to the reduction of the lateral strength of a structure that is subjected to cyclic lateral load. In some hysteretic models this reduction of strength is expressed as a function of the maximum displacement of each cycle (Rahnama & Krawinkler 1993), while in others as a function of the dissipated hysteretic energy (Park et al. 1988; Rahnama & Krawinkler 1993). As a result, models which are based on the former rule experience reduction of strength after the end of each cycle (cyclic strength deterioration), whereas models that are based on the latter rule experience strength reduction after each time step (in-cycle strength deterioration). However, most real-life structural systems experience the strength deterioration as a combination of the aforementioned mechanisms. This behaviour has been recognised by various authors

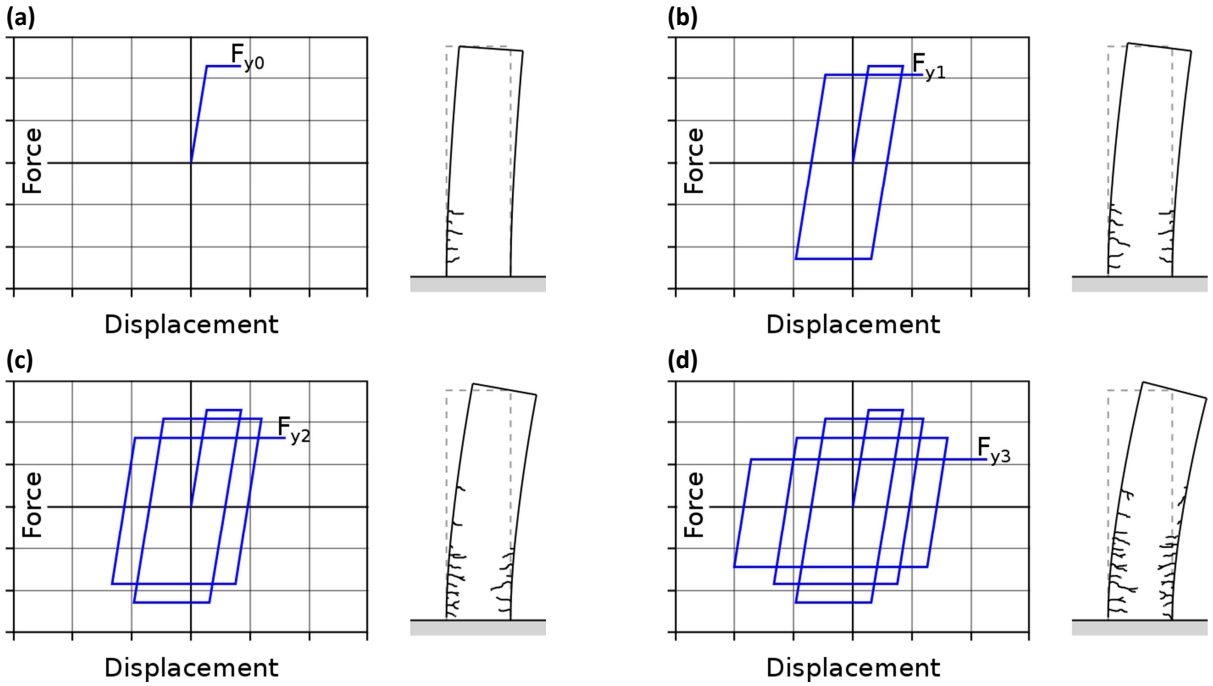

Figure 2.5. Evolution of cyclic strength deterioration of reinforced concrete column element subjected to cyclic lateral load. Level of yield strength: (a) at the initial stage, (b) after the first loading cycle, (c) after the second loading cycle and (d) after the third cyclic load.

(Park & Ang 1985; Reinhorn et al. 1988; Rahnama & Krawinkler 1993; Sivaselvan & Reinhorn 1999; Sivaselvan & Reinhorn 2000; Medina & Krawinkler 2004; Sivaselvan 2013; Kottari et al. 2014) who developed strength deterioration hysteretic models that incorporate both effects.

In the Figure 2.5, the initial yield strength of a reinforced concrete column element is illustrated (Figure 2.5 (a)), along with the level of strength deterioration experienced during the first (Figure 2.5 (b)), the second (Figure 2.5 (c)) and the third (Figure 2.5 (d)) loading cycle. In this sequence of subfigures, it becomes apparent the way with which the accumulation of hysteretic dissipated energy in combination with the increase of the maximum displacement leads to the decrease of the initial yield force in every loading cycle.

In this particular study the strength deterioration is integrated through the relationship introduced by Sivaselvan & Reinhorn (2000). This relationship (Eq. (2.2)) takes into account the effect of both the evolution of the maximum deformation and the accumulation of hysteretic energy on the strength deterioration. The maximum deformation is considered through the first term of Eq. (2.2), which accounts for the maximum deformation (x_{max}) appeared until the i^{th} time step and it is normalised by the ultimate displacement (x_{ult}).

The hysteretic energy is considered through the second term of Eq. (2.2), which accumulates the hysteretic energy (EH_i) that is dissipated by the model until the i^{th} time step (Eq. (2.3)) and it is normalised by the ultimate hysteretic energy that the model is expected to sustain (EH_{ult}) (i.e. The energy that is dissipated when the structural element is forced by a monotonic displacement until it reaches the ultimate displacement (x_{ult}) (Eq. (2.4)). The first term of Eq. (2.3) accumulates the total energy dissipated until the i^{th} time step, whereas the second term subtracts the elastic energy until the same time step. The deterioration parameters β_1 and β_2 of Eq. (2.2) control the degree that the maximum displacement and the accumulation of hysteretic energy affect the deterioration of strength respectively.

$$F_{yi} = F_{y0}\left(1-\left(\frac{|x_{\max}|}{x_{ult}}\right)^{1/\beta_1}\right)\left(1-\frac{\beta_2}{1-\beta_2}\frac{EH_i}{EH_{ult}}\right) \tag{2.2}$$

$$EH_i = \int_0^{x_i} F_i \cdot dx - \frac{F_i^2}{2R_k K_0} \tag{2.3}$$

$$EH_{ult} = \frac{F_{y0} x_y}{2} + F_{y0}\left(x_{ult} - x_y\right) \tag{2.4}$$

Several researchers (Oh et al. 2000; Naeim et al. 2000; Medina & Krawinkler 2004; Rodgers, Janise E.; Mahin 2004; FEMA P440A 2009) that investigated the influence of the strength deterioration on the maximum displacement, have proved that in moderate and long-period systems the maximum displacement is insensitive to strength deterioration. In contrast, in structural systems with short period, the presence of strength deterioration may lead to noticeable increase of the maximum displacement

2.6 Pinching

Another phenomenon that has been observed in structures subjected to cyclic lateral load is pinching. The term refers to the characteristic reduction of the actual area of the loops on the force-deformation diagram close to the point of origin after unloading. This shrinkage indicates large reduction in stiffness during the reloading, after unloading has occurred; which is followed by recovery of stiffness after a certain displacement. The introduction of such a behaviour leads to reduction of the amount of dissipated energy.

This phenomenon is observed mainly in brittle materials and it can be caused by different mechanisms. More specifically, in reinforced concrete elements, pinching is a result of opening of cracks when the element is forced to one direction. During the load reversal, sudden drop of stiffness will be observed until the cracks close and partial stiffness recovery occur. In timber elements, pinching is mainly a result of the opening and closing of gaps or pull-out of nails. Pinching is also observed in masonries primarily due to opening and closing of cracks (FEMA P440A 2009).

The behaviour of a reinforced concrete column element that experiences the pinching effect during cyclic lateral load is demonstrated in Figure 2.6. In the beginning, only a few closed cracks appear in the left side of the element (Figure 2.6 (a)). This is followed by load reversal, which leads to the development of open cracks in the right side of the element (Figure 2.6 (b)). This results in sudden drop of the stiffness, when the element is pushed towards the direction of the open cracks (Figure 2.6 (c)), until the cracks close and the stiffness partially returns to the initial level (Figure 2.6 (d)). If the element is forced to further deformation, cracks may open on the other side of the element as well (Figure 2.6 (e)). When the load changes direction, the stiffness reduces again (Figure 2.6 (f)) until the moment that the cracks shut (Figure 2.6 (g)). This behaviour is repeating, causing increase of the pinching effect in every subsequent loading cycle.

Similar to the effects of strength hardening, stiffness degradation and strength deterioration, several studies (Oh et al. 2000; Naeim et al. 2000; Medina & Krawinkler 2004; Rodgers, Janise E.; Mahin 2004; FEMA P440A 2009) have shown that in moderate and long-period structural systems, pinching does not affect significantly the maximum displacement. Meanwhile, the maximum displacement of systems with short structural period seems to be sensitive to the pinching effect, with increasing sensitivity as the structural period and the yield strength of the system decrease (FEMA P440A 2009).

As a concluding remark of this chapter it is underlined that the degree of stiffness degradation, strength deterioration and pinching behaviour depends not only on the characteristics of the system (such as the material characteristics, the structural system, the type of connections etc.), but also on the load history (such as the magnitude of the loading, the total duration, the number of loading cycles, the sequence of the loading cycles etc.) (Rahnama & Krawinkler 1993; Miranda 1993; FEMA P440A 2009). Some of those characteristics are taken into account in this study in the chapter 4.

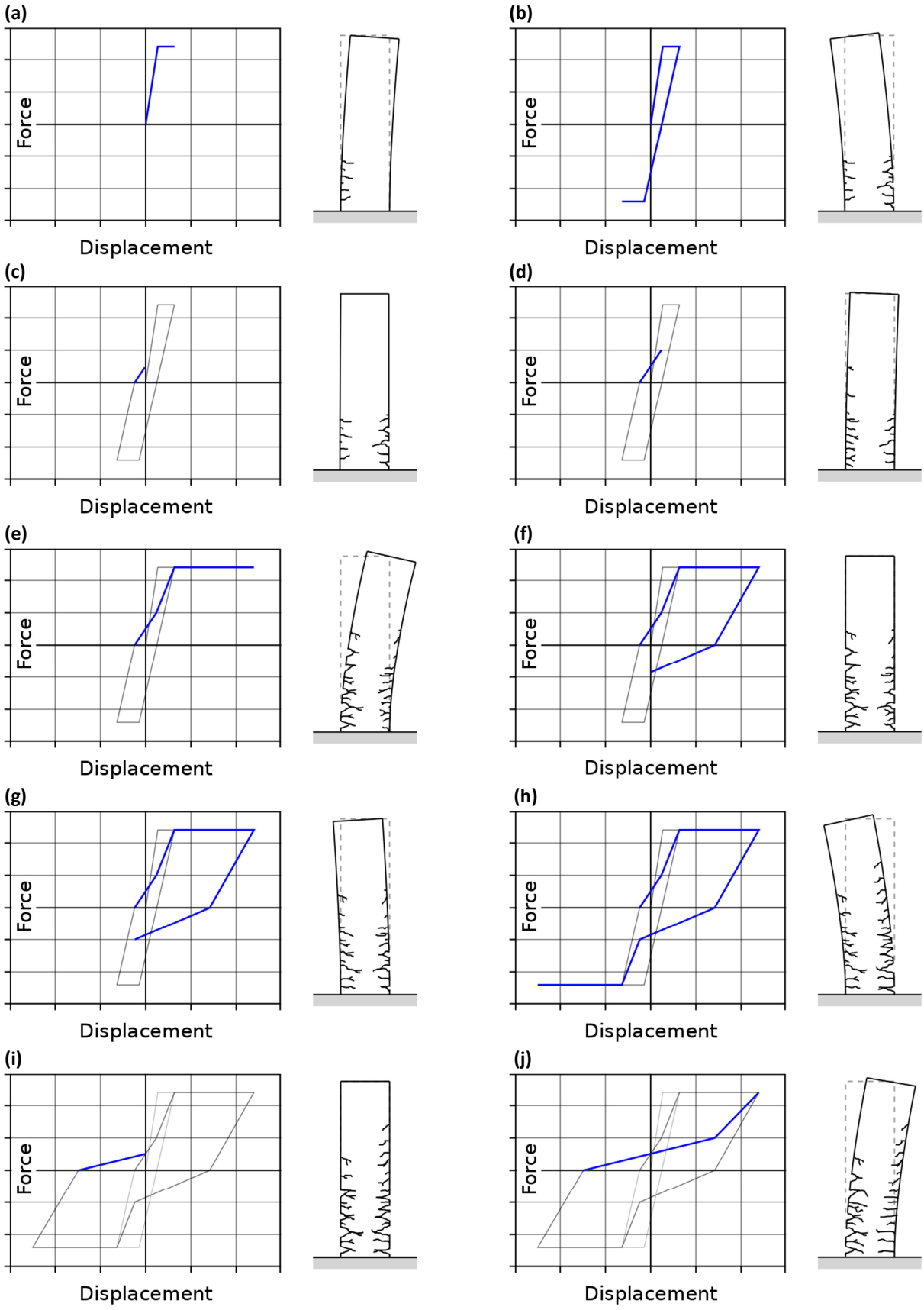

Figure 2.6: Evolution of pinching of a reinforced concrete column element subjected to cyclic lateral load.

3 Non-linear single degree of freedom systems

3.1 Equation of motion of single degree of freedom system

The governing equation of a single degree of freedom non-linear system subjected to an earthquake motion is given by the Eq. (3.1). In this equation $x(t)$, $\dot{x}(t)$, $\ddot{x}(t)$ represent the relative displacement, the relative velocity and the relative acceleration of the system respectively with respect to the ground, while $\ddot{x}_g(t)$ represents the ground acceleration. Furthermore, m and c denote the mass and the damping coefficient of the system, whereas $F(x,\dot{x})$ represents the non-linear restoring force of the system (Oh et al. 2000; Chopra 2012).

$$m\ddot{x}(t)+c\dot{x}(t)+F(x,\dot{x})=-m\ddot{x}_g(t) \tag{3.1}$$

This behaviour is illustrated by the model of the Figure 3.9. The restoring force is a function of time and its formulation depends on the inelastic characteristics of the system. In the simplest forms of: (i) elastoplastic hysteretic system and (ii) bilinear with strength hardening hysteretic system, the response can be represented by the models in the Figure 3.1 (a) and Figure 3.2 respectively. If additionally to this behaviour, stiffness degradation, stiffness deterioration and pinching are considered, phenomenological models are developed as will be explained in the following paragraphs.

Alternatively, the governing equation may be given in a normalized form (Eq. (3.2)), when the terms of both sides of the Eq. (3.1) are divided by the product of the mass times the yield displacement ($mx_y \neq 0$).

$$\ddot{\mu}(t)+2\xi\omega_0\dot{\mu}(t)+\omega_0^2\tilde{F}(x,\dot{x})=-\frac{\ddot{x}_g(t)}{x_y} \tag{3.2}$$

Where,

$\omega_0=\frac{k_0}{m}$: is the elastic circular frequency,

$\mu(t)=\frac{x(t)}{x_y}$: is the displacement ductility ratio and therefore: $\dot{\mu}(t)=\frac{\dot{x}(t)}{x_y}$ and $\ddot{\mu}(t)=\frac{\ddot{x}(t)}{x_y}$,

$\xi=\frac{c}{2m\omega_0}$: is the damping ratio and

$\tilde{F}(x,\dot{x})=\frac{F(x,\dot{x})}{m\omega_0^2 x_y}=\frac{F(x,\dot{x})}{k_0 x_y}=\frac{F(x,\dot{x})}{F_{y0}}$: is the restoring force normalized by the initial yield force of the system.

3.2 Overview of existing hysteretic models

During the process of building a model capable to capture accurately the non-linear behaviour of a structural system, the most crucial aspect is the right development of the hysteretic rule. The literature related to hysteretic models is very rich. This is because, different structural systems develop different mechanisms when they are subjected to cyclic load and in most cases hysteretic models have been formed based on the behaviour of specific structural systems. However, all the proposed hysteretic models can be classified into two broad categories; the polygonal hysteretic models (PHM) and the smooth hysteretic models (SHM) (Sivaselvan & Reinhorn 2000; Reinhorn et al. 2009; Charalampakis 2009; Ray & Reinhorn 2014). A graphical representation of one loop for each of these two types of hysteretic models can be observed in the combined forced-displacement diagram of Figure 3.10.

3.2.1 Polygonal hysteretic models

In polygonal hysteretic models, every branch of the force displacement diagram follows a linear relationship, according to the time history response of the system. The simplest model of this category is the bilinear hysteretic model (Figure 2.3). A more advanced hysteretic model that accounts also for the effect of stiffness degra-

dation was developed by Clough and Johnston (1966). Takeda et al. (1970) proposed a rather complicated polygonal hysteretic model that considers both the effect of stiffness degradation and strength deterioration. A few years later, the hysteretic model of M. S. L. Roufaiel and Meyer (1987b) included also the pinching behaviour caused by load reversals.

Following these authors, the study of Park et al. (1988) suggested a polygonal hysteretic model that accounts for the stiffness degradation, the strength deterioration and the pinching effect; known as "the three parameter model". Each of those parameters, is linked to one of the aforementioned non-linear behaviours. The greatest innovation of this model is that the stiffness degradation of the unloading branch of the force-displacement diagram is encountered through a pivot point (as it is mention in the paragraph 2.4). A more general hysteretic rule, that can represent any of the aforementioned hysteretic models, was developed by Sivaselvan and Reinhorn (1999). Main attribute of this model is that, the stiffness degradation and the strength deterioration are specified by a backbone curve, typical of the structural system under investigation.

3.2.2 Smooth hysteretic models

The smooth hysteretic models, which employ non-linear formulations to capture the response of a system, seem to represent better the continuous changes of the loading branches during yielding (Ray & Reinhorn 2014). Moreover, the total stiffness of the smooth hysteretic models can be represented by an appropriate combination of component springs (reciprocal of structural elements). This decomposition of the whole model into sub-models results to the easier construction of algorithms for the implementation of the model. The first smooth hysteretic model was introduced by Bouc (1967) and extended by Wen (1976) and is known as the Bouc-Wen hysteretic model. Although it has been proven that this model possesses several deficiencies (Thyagarajan 1989; Charalampakis 2009), it is recognized that it sets the foundation for the development of advanced smooth hysteretic models.

In this particular study an enhanced smooth hysteretic model proposed by Ray and Reinhorn (2014) is employed for the investigation of the effects of strength hardening, stiffness degradation, strength deterioration and pinching on the response of non-linear systems. This model, which belongs to the category of smooth hysteretic models, is an extension of the models of Park et al. (1987), Sashi K Kunnath et al. (1997) and Sivaselvan & Reinhorn (2000) and simulates a rate independent hysteretic behaviour which can capture quite accurately the behaviour of ductile and brittle materials.

3.3 Hysteretic models

From the previous paragraphs, it becomes apparent that all the non-linear characteristics of the system are included in the restoring force ($F(t)$)of the system. This is achieved, on the one hand by updating the tangent stiffness at every time step according to the hysteretic model that has been chosen and on the other hand by decreasing directly the restoring force, when strength deterioration is considered.

3.3.1 Elastoplastic system

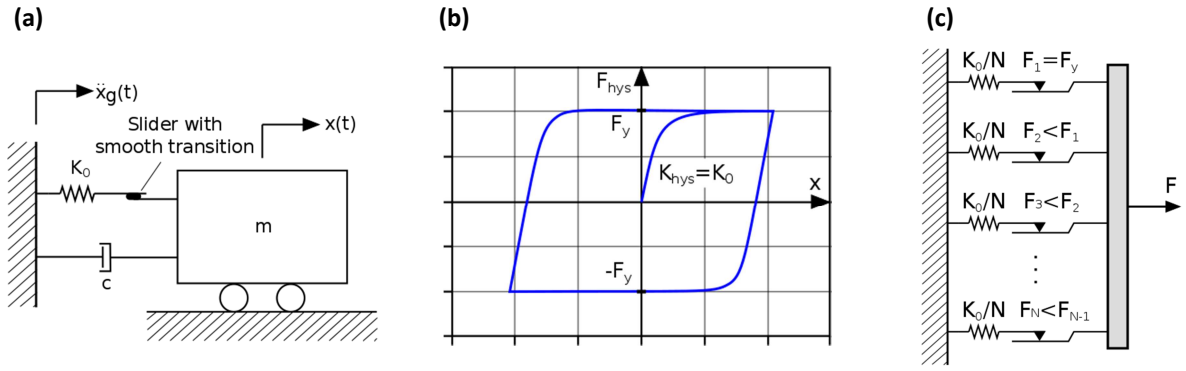

Figure 3.1. Development of (a) elastoplastic hysteretic model and (b) its response on the restoring force-displacement diagram. (c) Representation of hysteretic spring as N in parallel mechanical systems consisted of a spring and a slider in series.

The simplest hysteretic model and at the same time the basis for the rest of the hysteretic models is the elastic-perfectly plastic (or elastoplastic) hysteretic model. This type of hysteresis can be modeled by an elastic spring in series with a slider with smooth transition (Figure 3.1(a)). In general, the onset of a slider begins suddenly when the restoring force reaches a predefined value, usually the yield force of the system. A slider with smooth transition can be represented by a group of parallel mechanical systems, where each of them is consisted of a spring and a slider in series (Figure 3.1(c)) ((Sivaselvan 2013)). In that sense, a slider with smooth transition is activated before the predefined limit is reached, allowing a gradual transition to that limit. It should be noted that the combination of the spring and the slider with smooth transition is referred as hysteretic spring in this study and its response in the force-displacement diagram is illustrated in the Figure 3.1 (b).

The behaviour of the elastoplastic hysteretic model can be captured by the continuous change of the instantaneous tangent stiffness $K_{tangent}$ proposed by Sivaselvan and Reinhorn (2000) (Eq. (3.3)). In the relationship of the tangent stiffness (Eq.(3.3)), K_{hys}, F_{hys} and F_{hy} refer to the elastic stiffness of the hysteretic spring, the force of the hysteretic spring and the yield force of the hysteretic spring respectively. It is obvious that in the case of elastic-perfectly plastic non-degrading hysteretic system the elastic stiffness of the hysteretic spring is equal to the elastic stiffness of the overall system ($K_{hys}=K_0$).

$$k_{\text{tangent}} = k_{hys}\left[1-\left|\frac{F_{hys}}{F_{hy}}\right|^{N}\left(0.5+0.5sign\left(F_{hys}dx\right)\right)\right] \tag{3.3}$$

Furthermore, the exponent N of the Eq. (3.3) controls the level of smoothness of the transition between elastic and post-elastic branch. Large values of N ($N>10$) lead to steep transition, that approximates the bilinear behaviour, while small values ($2<N<10$) lead to a gradual smooth transition. When this variable is larger than ten, it can cause numerical instability in the solution (Ray & Reinhorn 2014). Meanwhile, small values ($N<3$) may lead to violation of the Drucker postulate of loop-closing (Thyagarajan 1989; Sivaselvan & Reinhorn 2000; Charalampakis 2009). For this reason, it is prudent to give N values in the range between five and ten. In this study, the variable N has a value of eight for all the hysteretic models.

Additionally, it has been noticed that when load reversal occurs in the force-displacement diagram, sudden transition is expected. This can be achieved through the *signum* function of Eq. (3.3). More specifically, when the *signum* product ($F_{hys}dx$) is equal to or greater than zero (i.e. loading branch), the *signum* function returns 1; while when the *signum* product is smaller than zero (i.e. unloading branch) it returns -1.

Moreover, in addition to the hysteretic spring, a viscous damper has been added to the model, in order to take into account the influence of the loading rate. For consistency reasons, a constant value of 2% has been chosen for the damping ratio of the dashpot of all the hysteretic models (i.e. the influence of different damping ratio is not considered in this study). The response (i.e. the maximum displacement, the residual displacement and the total hysteretic energy) of the elastoplastic model accommodates the basis with which the response of the rest of the hysteretic models is normalized.

3.3.2 Bilinear with strength hardening system

The only difference of a bilinear with strength hardening hysteretic system compared to the elastoplastic hysteretic system, is that in the former possesses a reserved strength after yielding, which refers to as strength hardening property. This behaviour can be modeled by adding a linear spring in parallel to the hysteretic spring (Figure 3.2). The level of strength hardening is controlled by the stiffness ratio (r_k), which represents the fraction between the pre-yield and the post-yield stiffness of the overall system. In the extreme case that the stiffness ratio is zero, the system performs elastoplastic behaviour, while when the stiffness ratio is unit the system behaves elastically.

An alternative way to represent the behaviour of the overall hysteretic model is by illustrating the behaviour of each type of spring of the system separately and subsequently combine these behaviours in the same fashion that the springs are combined (Figure 3.3). In this way, the formulation of the overall hysteretic system becomes simpler. For instance, in the case of a strength hardening hysteretic system, due to the fact that the hysteretic spring and the linear spring are in parallel, the overall stiffness in every time step is given by the summation of the stiffness of the hysteretic spring and the stiffness of the linear spring.

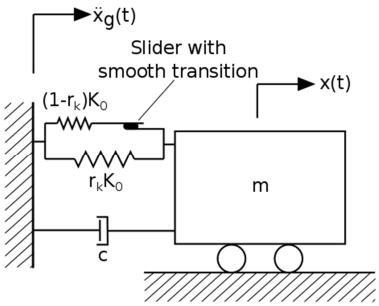

Figure 3.2. Bilinear model with strength hardening.

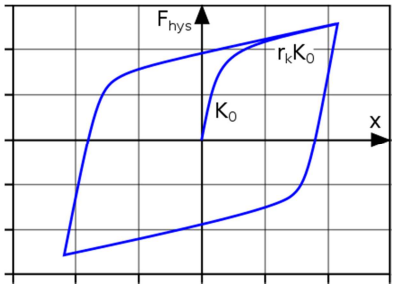

Figure 3.4. Response of bilinear model with strength hardening on the restoring force-displacement diagram.

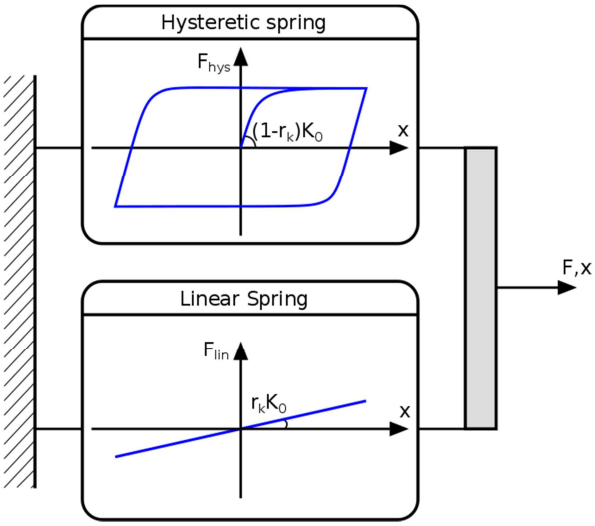

Figure 3.3. Behaviour of separate springs considered in a bilinear model with strength hardening

Therefore, the instantaneous tangent stiffness of the overall system can be computed by adding the stiffness of the linear spring in the relationship of the tangent stiffness of the elastoplastic hysteretic system given by the Eq. (3.3) (Eq. (3.4)). It should be noted that the elastic stiffness of the hysteretic spring of a bilinear system with strength hardening is equal to $K_{hys}=(1-r_k)K_0$, whereas the stiffness of the linear spring is equal to $K_{lin}=r_k K_0$. This is a choice which is made in order the elastic stiffness of the overall system to be K_0 (Figure 3.4)).

$$k_{\text{tangent}} = K_{lin} + k_{hys}\left[1-\left|\frac{F_{hys}}{F_{hy}}\right|^{N}\left(0.5+0.5sign\left(F_{hys}dx\right)\right)\right] \tag{3.4}$$

In this study three strength hardening levels are examined: (a) a low strength hardening level in which a stiffness ratio of r_k=20% is assigned, (b) a moderate strength hardening level in which a stiffness ratio of r_k=40% is assigned and (c) a high strength hardening level in which a stiffness ratio of r_k=80% is assigned.

3.3.3 Bilinear system with stiffness degradation

Stiffness degradation may be perceived as a gradual decrease of the elastic stiffness of the hysteretic spring ($K_{hys}=(1-R_k)K_0$). This behaviour is modeled accurately by the pivot rule, which is mentioned in the paragraph 2.4. This rule is implemented by the incorporation of the stiffness degradation factor R_k (Eq. (2.1)). However, the formula of this factor (Eq. (2.1)) is adjusted in order to consist of variables representative of the hysteretic spring as can be seen in Eq. (6.5).

$$R_k = \frac{F_i + aF_{hy}}{K_{hys}x_i + aF_{hy}} \tag{3.5}$$

This factor is updated at every time step and consequently multiplied by the stiffness of the hysteretic spring in order to decrease its value (Eq. (3.6)).

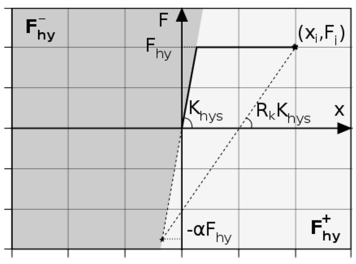

Figure 3.5. Pivot rule indicating the half planes of positive and negative yield force.

$$k_{\tan gent} = r_k K_0 + (1 - r_k) R_k K_0 \left[1 - \left| \frac{F_{hys}}{F_{hy}} \right|^N \left(0.5 + 0.5 sign\left(F_{hys} dx \right) \right) \right] \tag{3.6}$$

Additionally, it should be noted that the yield force in Eq. (3.5) is considered positive or negative depending on the half plane (defined by the initial elastic stiffness of the spring) in which the current state (x_i,F_i) lies (Figure 3.5).

Nevertheless, it has been observed (Reinhorn et al. 2009) that in addition to the degradation of the elastic stiffness of the hysteretic spring, degradation appears also in the linear spring that represents the post-yield stiffness. In this study, based on the formula suggested by Reinhorn et al. (2009), a one-parameter degradation model that accounts for the maximum displacement (x_{max}) is applied (Eq. (3.7)). The control parameter (η_1) takes values greater or equal to zero; with zero corresponding to non-degrading behaviour of the linear spring. Furthermore, in Eq. (3.7) $K_{lin,initial}$ refers to the initial value of the stiffness of the linear spring and x_{ult} refers to the ultimate displacement defined by monotonic load.

$$K_{lin} = K_{lin,initial} \left(1 - \eta_1 \frac{|x_{\max}|}{x_{ult}} \right) \tag{3.7}$$

In this study eight different models based on the stiffness degradation are formulated; with two varying levels of stiffness degradation of the pre-yield and of the post-yield stiffness. These levels are applied to elastoplastic model in one hand and to bilinear with moderate strength hardening model on the other hand.

3.3.4 Bilinear system with strength deterioration

Referring to the bilinear model of Figure 3.2, strength deterioration can be conceived as the gradual deterioration of the slider. While the slider deteriorates, the onset limit after which the slider starts to move, which is referred to as yield force, decreases. The level of decrease in every time step is controlled by the Eq. (2.2), based on the maximum displacement and the hysteretic energy. Due to the fact that the slider is part of the hysteretic spring, Eqs. (2.2) - (2.4) are modified in order the variables to be expressed according to the notation of the hysteretic spring.

$$F_{hy} = F_{hy0} \left(1 - \left(\frac{|x_{h,\max}|}{x_{h,ult}} \right)^{1/\beta_1} \right) \left(1 - \frac{\beta_2}{1 - \beta_2} \frac{EH}{EH_{ult}} \right) \tag{3.8}$$

$$EH = \int_0^{x_{hys}} F_{hys} \cdot dx - \frac{F_{hys}^2}{2(R_k - r_k) K_0} \tag{3.9}$$

$$EH_{ult} = \frac{F_{hy0} x_{h,y}}{2} + F_{hy0} \left(x_{h,ult} - x_{h,y} \right) \tag{3.10}$$

Strength degradation is eventually incorporated in the total hysteretic model by updating the yield force for every time step (F_{hy}) calculated by the Eq. (3.8), in order to determine the instantaneous tangent stiffness of the overall system expressed by the Eq. (3.6).

In this study eight different models based on the strength deterioration are formulated, with two varying levels of strength deterioration based on the maximum displacement and two varying levels of strength deterioration based on the hysteretic energy. These levels are applied to elastoplastic model in one hand and to bilinear with moderate strength hardening and moderate stiffness degradation model on the other hand.

3.3.5 Bilinear system with pinching

The formulation of the pinching effect is based purely on observations of laboratory tests that performed on elements of different materials. As a result, all the relationships that have been proposed (Baber & Noori 1985; Reinhorn et al. 2009; Ray & Reinhorn 2014) are based on phenomenological models. In the literature, the pinching behaviour is described by an imaginary spring (slip-lock spring) with zero stiffness for zero displacement and infinite stiffness when a particular displacement (x_s) is reached. This displacement is called slip (displacement) and it is equal to the difference between the maximum displacement (x_{max}) and the yield displace-

ment (x_y) of the overall system (Eq. (3.11)). Slip is zero if the system remains elastic and gradually increases depending on the maximum displacement. As a result, the level of the pinching effect also increases while the maximum displacement increases. The evolution of the stiffness, of the slip-lock spring, can be seen in the **Error! Reference source not found.**.

$$x_s = x_{\max} - x_y \geq 0 \tag{3.11}$$

When the slip-lock spring is attached in series with a hysteretic spring the pinching behaviour of an elasto-plastic hysteretic system can be captured. Additionally, when this combined system is attached in parallel with a linear spring (Figure 3.8), the response of a bilinear hysteretic system with stiffness hardening and pinching can be captured (**Error! Reference source not found.**).

As it is observed by Ray and Reinhorn (2014), the stiffness of the slip-lock spring resembles the tangent function (**Error! Reference source not found.**) and accordingly it can be formulated. Based on this assumption, the relationship between the force (F_{slip}) and the displacement (x_{slip}) of the slip-lock spring can be defined ((3.12)).

$$\frac{F_{slip}}{F_s} = \tan\left(\frac{x_{slip}}{x_s}\frac{\pi}{2}\right) \tag{3.12}$$

Due to the fact that the slip-lock spring is in series with the hysteretic spring, they essentially share the same force (F_{slip}=F_{hys}). The crack-closing force (F_s) that appears in the Eq. (3.12) is expressed as a fraction of the yield force of the hysteretic spring (F_{hy}) (Eq. (3.13)).

$$F_s = s_1 F_{hy} \tag{3.13}$$

Meanwhile, Ray and Reinhorn (2014) suggests that the slip (x_s) should be modified through the employment of an adjustment factor (s_2), because of uncertainties in the crack opening and the permeant deformations (Eq. (3.14)).

$$x_s = s_2\left(x_{\max} - x_y\right) \tag{3.14}$$

Furthermore, based on observations of laboratory tests, it has been noticed that the crack-closing force (F_s) and the slip (x_s) change non-linearly with respect to x_{max}, at large displacements. Therefore, it is suggested (Ray & Reinhorn (2014)) that instead of constant values the factors s_1 and s_2 should vary according to the Eq. (3.15) and Eq. (3.16). The degree of non-linear change of the crack-closing force (F_s) and the slip (x_s) is controlled by the variables s_{11} and s_{22}. In addition, s_{10} and s_{20} express the initial values of s_1 and s_2, whereas s_{1min} and s_{2max} express the minimum and the maximum values of s_1 and s_2 respectively.

$$s_1 = s_{10}\left(1 - s_{11}\frac{x_{\max}}{x_{ult}}\right) \geq s_{1\min} \geq 0 \tag{3.15}$$

$$s_2 = s_{20}\left(1 + s_{22}\frac{x_{\max}}{x_{ult}}\right) \leq s_{2\max} \leq 1 \tag{3.16}$$

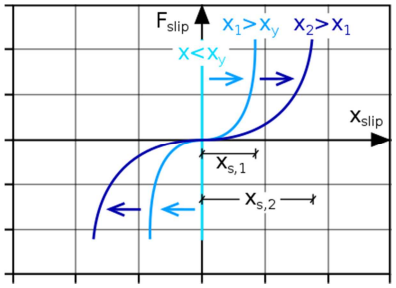

Figure 3.6. Evolution of the stiffness of the slip-lock spring with increasing slip displacement (x_s).

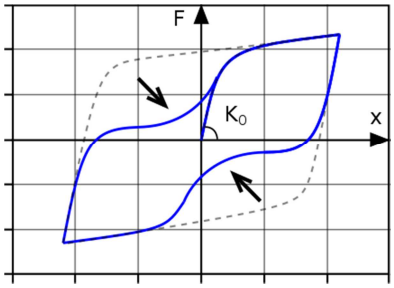

Figure 3.7. Response of bilinear hysteretic system with stiffness hardening and pinching in the force-displacement diagram.

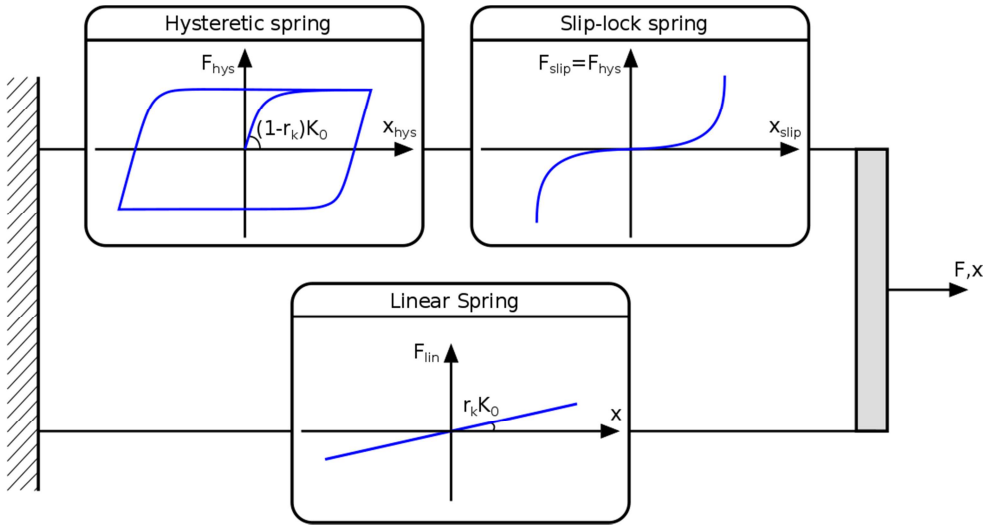

Figure 3.8. Behaviour of separate springs considered in a bilinear model with strength hardening and pinching.

The instantaneous tangent stiffness of the slip-lock spring is obtained through the derivative of the force of the slip-lock spring (F_{slip}) (Eq. (3.12)) with respect to the displacement of the slip-lock spring (x_{slip}) (Eq. (3.17)).

$$K_{slip} = \frac{dF_{slip}}{dx_{slip}} = \frac{F_s}{x_s}\frac{\pi}{2}\left(1+\left(\frac{F_{slip}}{F_s}\right)^2\right) \tag{3.17}$$

Due to the fact that the slip-lock spring and the hysteretic spring are in series, their combined stiffness ($K_{hys,slip}$) is given by the Eq. (3.18). Moreover, if the strength hardening is also considered in the hysteretic model, the tangent stiffness of the linear spring (K_{lin}), which is attached in parallel, is added to the Eq. (3.18) (Eq. (6.5)). The behaviour of the separate springs, along with the way that they are combined to capture the overall response of a hysteretic system with strength hardening and pinching is illustrated in the **Figure 3.8**.

$$K_{hys,slip} = \frac{K_{hys}K_{slip}}{K_{hys}+K_{slip}} \tag{3.18}$$

$$K_{hys,slip,lin} = \frac{K_{hys}K_{slip}}{K_{hys}+K_{slip}} + K_{lin} \tag{3.19}$$

In this study four different models based on the pinching are formulated, which consider a moderate and a high level of pinching effect applied to elastoplastic model on one hand and to bilinear with moderate strength hardening, moderate stiffness degradation and moderate strength deterioration model on the other hand.

3.4 Method of solution

The last few years, several researchers (Caughey 1960; Miller & Butler 1988; Pratap et al. 1994; Pratap & Mukherjee 1994; Wang 1996; Liu 2000; Liu & Huang 2004; Kalmár-Nagy & Shekhawat 2009; Bayat et al. 2010; Bayat et al. 2011; Bayat & Pakar 2013) have suggested analytical solutions for the calculation of the response of bilinear systems subjected to harmonic load. However, in the case of more advanced non-linear systems, or in the case of arbitrarily varying with time excitation (e.g. earthquake motion), no solution has been proposed by means of analytical methods. In these cases, the response is defined through numerical integration methods.

In this study, Newmark-β numerical integration method is used, because it is the most commonly used for problems in structural dynamics. This method computes the solution at the $i+1$ time step, based on equilibrium condition at the $i+1$ time step. It is an implicit numerical integration method, in which the restoring force at the $i+1$ step (F_{i+1}) is a function of the unknown displacement at the same step (x_{i+1}). For this reason, an iterative method is needed to guarantee convergence of the solution. For this study, the Newton-Raphson iterative procedure is employed, through which the tangent stiffness of the system is updated in every iteration until the convergence criterion is fulfilled. The calculation of the tangent stiffness and the restoring force in each

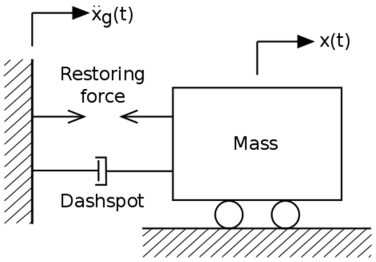

Figure 3.9. Model of generalized single degree of freedom non-linear system.

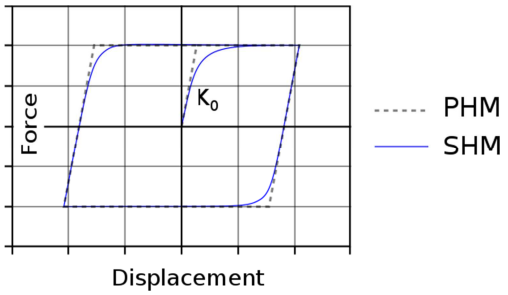

Figure 3.10. Polygonal hysteretic model (PHM) versus Smooth hysteretic model (SHM).

step depend on the values of the previous step and follows rules that originate from the choice of the hysteretic model.

The MATLAB scrips through which these methods are implemented can be found in the Appendix A

3.5 Development of models

For this study a total of 22 different hysteretic models are developed. The parameters[2] that have been chosen for the calibration of these models can be seen in the Table 1. They have been chosen in such a way that the several non-linear behaviours are examined: (1) separately and (2) combined. Those models are idealized hysteretic models are and in that sense, they do not explicitly correspond to real structures.

In addition to these models, a separate model has been calibrated in such a way that fits the force-displacement diagram of a pushover test (Ravenshorst et al. 2016). The pushover laboratory test was performed by Delft university of technology in a masonry assemblage. The loading cycles can be seen in Figure 3.11, while the hysteresis loops are presentenced in Figure 3.12. Through impact test, the first natural frequency of the assemblage in the direction that the load is applied, before the beginning of the pushover test has been determined equal to f = 4.05Hz; therefore, the initial natural period of the structure is T = 0.25s. Furthermore, the initial elastic stiffness is evaluated equal to k = 15.5kN/mm through the two first loading quarter-cycles of the pushover test, assuming that no substantial damage has occurred to the structure. Based on the initial natural period and the initial elastic stiffness, the mass of the equivalent SDoF system can be estimated:

$$T = 2\pi\sqrt{\frac{m}{k}} \Rightarrow m = \frac{T^2}{4\pi^2}k = \frac{0.25^2}{4\pi^2}15500000 \Rightarrow m = 24.560\text{kg} \tag{3.20}$$

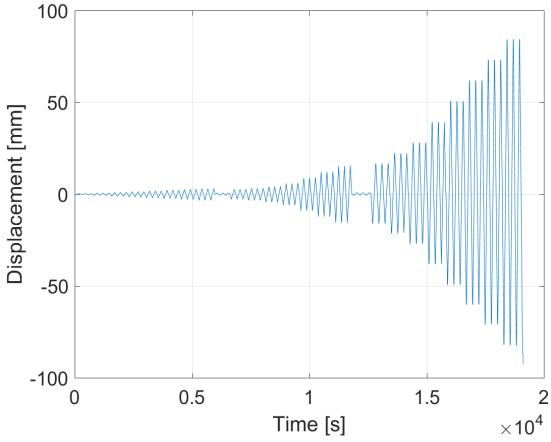

Figure 3.11. Loading cycles for pushover test of masonry assemblage.

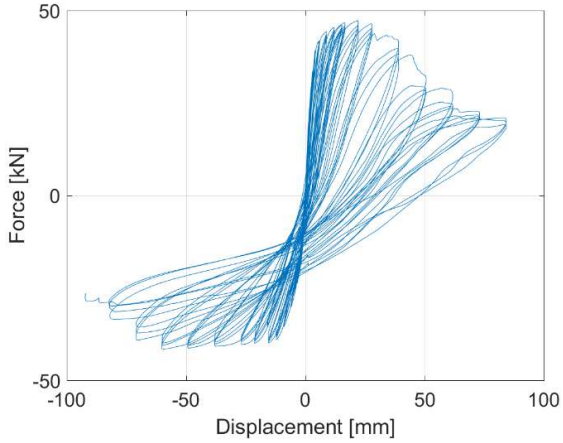

Figure 3.12. Hysteresis loops of pushover test of masonry assemblage.

[2] The role of each parameter is explained in the paragraph that corresponds to each non-linear behavior, in section 3.3.

	Model	r_k	α	η_1	β_1	β_2	s_{11}	s_{22}	s_{10}	s_{20}	s_{1min}	s_{2max}
1.	*Elastoplastic*	0	-	-	-	-	-	-	-	-	-	-
2.	*Moderate strength hardening*	0.2	-	-	-	-	-	-	-	-	-	-
3.	*High strength hardening*	0.4	-	-	-	-	-	-	-	-	-	-
4.	*Extreme strength hardening*	0.8	-	-	-	-	-	-	-	-	-	-
5.	*Elastoplastic with low stiffness degradation*	0	20	-	-	-	-	-	-	-	-	-
6.	*Elastoplastic with high stiffness degradation*	0	4	-	-	-	-	-	-	-	-	-
7.	*Moderate strength hardening & low stiffness degradation*	0.2	20	0.1	-	-	-	-	-	-	-	-
8.	*Moderate strength hardening & moderate stiffness degradation*	0.2	20	0.6	-	-	-	-	-	-	-	-
9.	*Moderate strength hardening & moderate stiffness degradation*	0.2	4	0.1	-	-	-	-	-	-	-	-
10.	*Moderate strength hardening & high stiffness degradation*	0.2	4	0.6	-	-	-	-	-	-	-	-
11.	*Elastoplastic with low strength deterioration*	0	-	-	0.1	0.1	-	-	-	-	-	-
12.	*Elastoplastic with moderate strength deterioration*	0	-	-	0.1	0.5	-	-	-	-	-	-
13.	*Elastoplastic with moderate strength deterioration*	0	-	-	0.5	0.1	-	-	-	-	-	-
14.	*Elastoplast. with high strength deterioration*	0	-	-	0.5	0.5	-	-	-	-	-	-
15.	*Moderate strength hardening & moderate stiffness degradation & low strength deterioration*	0.2	10	0.2	0.1	0.1	-	-	-	-	-	-
16.	*Moderate strength hardening & moderate stiffness degradation & moderate strength deterioration*	0.2	10	0.2	0.1	0.5	-	-	-	-	-	-
17.	*Moderate strength hardening & moderate stiffness degradation & moderate strength deterioration*	0.2	10	0.2	0.5	0.1	-	-	-	-	-	-
18.	*Moderate strength hardening & moderate stiffness degradation & high strength deterioration*	0.2	10	0.2	0.5	0.5	-	-	-	-	-	-
19.	*Elastoplast. with low pinching*	0	-	-	-	-	1.5	1.5	0.6	0.3	0.2	0.8
20.	*Elastoplast. with high pinching*	0	-	-	-	-	4	4	0.3	0.6	0.05	1
21.	*Moderate strength hardening & moderate stiffness degradation & moderate strength deterioration & low pinching*	0.2	10	0.2	0.2	0.2	1.5	1.5	0.6	0.3	0.2	0.8
22.	*Moderate strength hardening & moderate stiffness degradation & moderate strength deterioration & high pinching*	0.2	10	0.2	0.2	0.2	4	4	0.3	0.6	0.05	1

Table 1. Selection of parameters for the calibration of the hysteretic models.

The rest of the parameters for the calibration of the model are chosen through an automatic iterative procedure according to a script that the author build which performs 10^9 different combinations. The values that give the best fit to the laboratory test are presented in the Table 2, while the hysteresis loops of the calibrated model subjected to the same loading cycles as the pushover test of the masonry assemblage are illustrated in Figure 3.13 for comparison with the hysteresis loops of the laboratory test.

Parameters	Value
Initial stiffness (k_0)	15.5 kN/mm
Mass (m)	24560 kg
Initial yield force (F_{y0})	58 kN
Stiffness ratio (r_k)	0.022
Stiffness degradation (α), (η_1)	1.6, 2.74
Strength deterioration (β_1), (β_2)	0.25, 0.38
Pinching (s_1), (s_2), (s_{11}), (s_{22}), (s_{1min}), (s_{2max})	0.63, 0.39, 1.95, 1.95, 0.1, 0.95

Table 2. Calibration parameters to fit the pushover laboratory test.

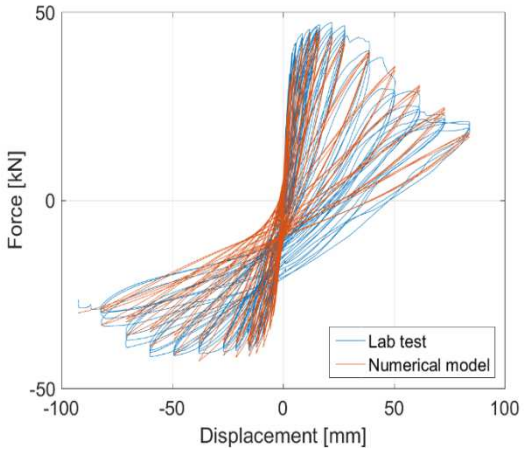

Figure 3.13. Comparison of hysteresis loops from laboratory test and from the calibrated SDoF model.

4 Earthquake ground motions

In this study, the total of 22 different hysteretic models, that are presented in section 3.3, are subjected to 167 different earthquake motions. 160 of these ground motions are obtained through the database of Pacific earthquake engineering research center (PEER), selected in such a way that they satisfy the following requirements: (a) they are recorded on accelerographic stations in which enough information is given regarding the geotechnical conditions, so that the soil can be classified in the appropriate site class according to Eurocode 8; (b) they are recorded on free field stations or on the first floor of low-rise buildings; (c) the magnitude of the recorded earthquakes is larger than 3.5; (d) the distance from the fault rapture plane to the accelerographic station is less than 10km (i.e. shallow events); (e) the maximum useable period, as a result of the signal processing[3], is at least 4 sec. A detailed list of all the ground motions which are used in this study can be seen in the Appendix C.

Despite the fact that the study of the response of non-linear systems with regard to the total sample of ground motions may already lead to valuable observations, the ground motions are divided into different ensembles, for the reasons are explained in the following paragraph.

4.1 Ensemble of ground motions

The response of an inelastic system subjected to a ground motion is a very complex phenomenon, affected by the choice of the hysteretic model and by the characteristics of the input ground motion. It is very probable that some of the characteristics of the ground motion affect more than others the inelastic response of the system. This, opinion has been already expressed in earlier studies by Rahnama and Krawinkler (1993) and by Ruiz-García and Miranda (2006) who examined the influence of the soft soil on the response of several hysteretic mondels and by Ruiz-García and Miranda (2003 and 2006) who examined the influence of the earthquake magnitude and the influence of the distance to the source on the response of several hysteretic mondels.

However, such influences may altogether disappear when the response is averaged for the total ensemble of the ground motions. Therefore, the total ensemble of the ground motions is divided into different groups with common characteristics and subsequently the response of the systems is averaged for each group separately. More specifically, the ground motions are separated into: (a) two categories based on their magnitude, (b) two categories based on their significant duration, (c) three categories based on the soil conditions, (d) one more group which consists of signals that resembles the ground motions in Groningen.

4.1.1 Classification based on earthquake magnitude

The earthquake magnitude is the most commonly used parameter for the characterization of an earthquake event. It is related to the energy which is released in the earthquake source and it is measured in several scales. Most of the accelerograph stations, define the magnitude in terms of: the local magnitude (M_L), usually referred to as "Richter magnitude", the surface-wave magnitude (M_s), the body-wave magnitude (M_b) and the moment magnitude (M_w) (L.Kramer 1997; Kramer & Stewart 2004; Chopra 2012; Akkar 2014).

In this particular study, the magnitude of the earthquakes is expressed in moment magnitude. A distinction of the ground motions is made depending on whether their magnitude is larger or smaller than 5.5, based on the limit that the Eurocode 8 has set. The group of the moderate earthquakes, which have magnitude lower than five (M_w<5.5), is consisted of 66 ground motions, while the group of the strong earthquakes, which have magnitude larger than five (M_w>5.5) is consisted of 94 ground motions.

4.1.2 Classification based on significant duration

In the literature, there is a large number of studies that proposed different indices for the measurement of the duration of a ground motion (Bommer & Martinez-Pereira 1999). Most of them are based either on the concept of the bracketed duration or on the concept of the significant duration. The bracketed duration is described as the total time elapsed between the first and the last excursion of a specified level of acceleration,

[3] The cut-off frequency of the high-pass filter applied to these signals is smaller than 0.25Hz (f <0.25Hz or T>4s).

whereas the significant duration represents the time interval between the moments at which a specified percentage of wave energy is released. In this study, the significant duration $t_{5\text{-}95}$ is chosen to represent the duration of the ground motion. This measure, which is developed by Trifunac & Brady (1975), accumulates the time between the moments where 5% and 95% of the total Arias intensity is attained.

Based on the significant duration $t_{5\text{-}95}$, the total ensemble is divided into two groups. The first group contains 65 ground motions with significant duration shorter than 10s, while the second group contains 95 ground motions with duration longer than 10s.

4.1.3 Classification based on soil class

The importance of the soil conditions in the earthquake engineering is well recognized by several studies and seismic design codes. In most of the design codes the classification of the soil is based on the average shear-wave velocity at a depth between 0 and 30 meters (Vs_{30}). Following the provisions of the Eurocode 8, regarding the soil classification, three different groups of ground motions are formed. The first group corresponds to the ground types A and B, which refer to rock or very stiff soil with Vs_{30} >360m/s and consists of 81 ground motions. The second group corresponds to the ground type C, which refers to stiff soil with 180<Vs_{30} <360m/s and consists of 76 ground motions. The third group corresponds to the ground type D, which refers to soft soil with Vs_{30} <180m/s and consists of 3 ground motions.

4.1.4 Signals similar to Groningen area

Additionally to the previous 160 ground motions, an ensemble of seven ground motions that resembles the ground motions that appear in the area of Groningen has been collected for this study. This is because the earthquakes in Groningen as induced, shallow, with short duration and low magnitude earthquakes possess different characteristics from the other 160 ground motions that are examined her.

For the production of these signals the following procedure was followed:

- Signals that were spectrally that have been matched to a uniform hazard spectrum at -350 m, (published by (KNMI 2016)) were collected by Deltares.
- Deltares performed calculations of site response between 350 m and 30 m depth.
- The signals at 30m depth were provided to Witteveen+Bos by Deltares.
- Witteveen+Bos derived the surface signals.

The ground acceleration time-histories of these seven signals can be seen in the Appendix C.

Magnitude \ Soil	A&B	C	D
M_w<5	41	19	0
M_w>5	40	57	3

Table 3. Distribution of ground motions in terms of magnitude and soil class.

Magnitude \ Duration	$t_{5\%\text{-}95\%}$<10s	$t_{5\%\text{-}95\%}$>10s
M_w<5	53	7
M_w>5	42	58

Table 4. Distribution of ground motions in terms of Magnitude and significant duration.

Duration \ Soil	A&B	C	D
$t_{5\%\text{-}95\%}$<10s	53	41	1
$t_{5\%\text{-}95\%}$>10s	28	35	2

Table 5. Distribution of ground motions in terms of significant duration and soil class.

Mechanism	Normal	Reverse	Reverse Oblique	Strike slip
	11	21	14	114

Table 6. Distribution of ground motions in terms of the generation mechanism of the earthquake.

5 Response parameters of engineering interest

In this chapter an extensive overview of proposed in the literature damage indices takes place. The purpose of this investigation is to give a better understanding of the response parameters that may play a key role on the damage of a structural system. In a subsequent chapter, those response parameters are calculated for a set of earthquake ground motions applied on various inelastic systems and their values are compared to the ones calculated for the elastoplastic system.

Figure 5.1. Classification of damage indices

5.1 Classification of damage indices

Main goal of most of the current design procedures is the safety against collapse (Fajfar 1992). More specifically the inelastic design spectra in the existing design codes are given according to uniform ductility levels, which however, represent only the collapse limit state. A more useful design procedure would allow the designers to design according to a preferable damage limit other than the collapse limit state (Bracci et al. 1989).

This is called performance based design and the damage index is the tool that specifies the level of the performance of a structure that is subjected to an earthquake. The damage index is always normalized and takes values that range between 0 and 1; with 0 the structure remains in the elastic region and no damage occurs, while with 1 the state of collapse has been reached. A damage parameter that do not follow the previous rule, it is a damage variable (or measure) and not a damage index (Cosenza & Manfredi 2000). A performance based design can be applied not only for the design of new structures but also for the evaluation of existing ones. More specifically, given a design earthquake and a desirable performance level, the design of a new structure can be performed. On the other hand, given the characteristics of an existing structure and a possible upcoming earthquake, the performance level of the existing structure can be determined.

The idea of quantifying the state of damage of a structure by a single number on a predefined scale is very attractive due to its simplicity. However, the development of such an index is extremely complex, because it should be applicable to different structural systems, quantifying stages from the initiation of the first crack until the total collapse of the structure. Two types of approaches are usually followed in the formulation of damage indices; empirical and theoretical approaches. The empirical damage models, are based on statistical analyses of observed damages of different structural systems after the occurrence of an earthquake. Despite the fact that a procedure like this entails a high degree of subjectivity, it provides useful information for the general performance of various structural systems. In contrast, theoretical damage models can be more rational, but due to the fact that they consider the seismic response of a structural system based on its characteristics, they involve extra degrees of complexity (Ghobarah et al. 1999).

Several comprehensive review works of existing damage indices have been carried out by various authors (Rodriguez Gomez & S. 1990; Kappos 1997; Ghobarah et al. 1999; Cosenza & Manfredi 2000; Rodriguez & Padilla 2009; Velde 2010; Sinha & Shiradhonkar 2012; Nyarko et al. 2014). A collection of damages indices which have been presented in the above studies combined with additional damages indices is given in the following paragraphs; where their performance is discussed and critically evaluated.

5.1.1 Local damage indices

The damage indices are classified as local damage indices and global damage indices depending on whether they quantify the damage state of individual members or of the entire building. The local damage indices are further classified regarding their ability to capture the accumulation of the inelastic energy. In this sense the damage indices are divided into cumulative and non-cumulative damage indices. Additionally, the local damage indices are classified as deformation-based damage indices, stiffness-based damage indices, energy-based damage indices and combined damage indices.

5.1.1.1 Non-cumulative damage indices

Non-cumulative damage indices do not explicitly account for the time history of the seismic response of a structure, but instead they consider the maximum value of a response parameter that appear in the time history response. This response parameter, usually is deformation-based, stiffness-based or combined.

5.1.1.1.1 Deformation based damage indices

- *Ductility ratio and damage index DM*

The ductility ratio is a quantity that expresses the ratio between the maximum deformation (x_{max}) and the yield deformation (x_y) of a system (Eq. (5.1)) (Newmark & Emilio 1971). It is widely used in the seismic design procedures for the calculation of the inelastic response spectra. Alternatively, the ductility ratio can be expressed as the ratio between the maximum curvature (φ_{max}) and the yield curvature (φ_y) (Eq. (5.2)), or the ratio between the maximum rotation (θ_{max}) and the yield rotation (θ_y) (Eq. (5.3)).

$$\mu(x) = \frac{x_{\max}}{x_y} \tag{5.1}$$

$$\mu(\varphi) = \frac{\varphi_{\max}}{\varphi_y} \tag{5.2}$$

$$\mu(\theta) = \frac{\theta_{\max}}{\theta_y} \tag{5.3}$$

The ductility ratio itself is a damage variable and not a damage index, because it does not include characteristics of the capacity of the structure. The adoption of the ductility as a damage index, is achieved by the Eq. (5.4) (Powell & Allahabad 1988). This equation implies that failure occurs when the ductility demand (μ) exceeds the ductility capacity of the structural system, which is determined through experiments under monotonic load (μ_u). In the case that the ductility demand is smaller or equal to one the damage index is smaller or equal to zero and the system will remain undamaged. On the other hand, if the ductility demand is equal to the ductility capacity the damage index is 1 and collapse will occur.

$$DM = \frac{\mu - 1}{\mu_u - 1} = \begin{cases} 0, & if \quad \mu < 1 \\ DM, & if \quad 1 \le \mu \le \mu_u \\ 1, & if \quad \mu > \mu_u \end{cases} \tag{5.4}$$

According to the definition of this damage index, it is evident that the collapse of the structural system is expected for the maximum plastic displacement, independently of the number of plastic cycles and the amount of energy dissipated during the inelastic excursion. For that reason a large number of earlier studies (Fajfar 1992; Fajfar & Krawinkler 1997; Rodriguez & Aristizabal 1999; Bojórquez & Ruiz 2004; Teran-gilmore et al. 2005; Hancock & Bommer 2006; Bojorquez et al. 2010) prove that the performance of structures subjected to long duration ground motions cannot be adequately characterized through the ductility ratio alone.

- *Inter-story drift*

The inter-storey drift (ID) expresses the maximum relative deformation between two consecutive storeys (x^{i+1}-x^i) normalized by the storey height (H) (Eq. (5.5)).

$$ID = \frac{x^{i+1} - x^i}{H} \tag{5.5}$$

In 1981, Sozen M. suggested the calibration of this variable, in order to be able to express the percentage of damage of a structure (D) through the Eq. (5.6).

$$D = 50\,ID \text{ (in percentage)} - 25 \tag{5.6}$$

Through the analysis of tests on structural elements and small-scale structures it is shown that for inter-storey drift smaller than one per cent, non-structural elements may be damaged, while for inter-storey drift larger than four per cent, irreparable damage of structural elements or even collapse will occur (Velde 2010). Collapse has been observed (Roufaiel & Meyer 1982) for inter-storey drift larger than six per cent.

Due to the fact that the maximum inter-storey drift does not account for the cumulative damage caused by plastic deformations, collapse is expected to occur when a predefined limit of inter-storey drift is exceeded. However, this predefined limit should vary for structures with different ductility ratio, because the maximum deformation of the collapse stage is related to the ductility capacity (Ghobarah et al. 1999). Through this remark, it becomes apparent that the limits expressed above are questionable and the inter-storey drift damage index, as defined by Sozen, (Eq. (5.6)) is unreliable.

- *Maximum permanent drift*

By replacing the maximum relative deformation by the permanent deformation caused by seismic loading, the index ID of the previous paragraph is transformed to maximum permanent drift. Stephens and Yao (1987) defined the values of maximum permeant drift that correspond to four structural damage levels. More specifically, if the permanent drift is zero and the inter-stotey drift does not exceed one per cent, the structure is safe,

while if the permanent drift is 0.5 per cent or one per cent the structure is lightly damaged or damaged respectively. Furthermore, if at the end of the excursion aperiodic motion appears at the top storey the structure is heavily damaged. Same as in the case of the inter-storey drift, this measure does not account for the different levels of ductility that exist in different structural systems.

5.1.1.1.2 Stiffness based damage indices

- *Stiffness ratio*

The stiffness ratio represents the initial elastic stiffness divided by the reduced secant stiffness (Lybas & Sozen 1977). The term secant stiffness describes the slope of the line that connects the point of origin with the maximum displacement response in the force displacement diagram. Strictly speaking, the stiffness ratio does not describe a damage index but a damage variable. However, it is mentioned here because a lot of future researchers got inspired by this measure.

- *Flexural damage ratio and Modified flexural damage ratio*

Based on the idea of the stiffness ratio, Banon et al. (1981) proposed the flexural damage ratio (FDR). This damage variable is given by the Eq. (5.7), where M_u and φ_u indicate the ultimate bending moment as a result of pushover analysis and its corresponding curvature, while M_{max} and φ_{max} are the maximum bending moment due to seismic load and its corresponding curvature. It is worth mentioning that it has been observed a very strong relationship between the flexural damage ratio and the damage indices based on the maximum inelastic deformation. As a matter of fact, it has been proven (Banon & Veneziano 1982) that the correlation coefficient between the flexural damage ratio and the ductility ratio is 0.95.

$$FDR = \frac{M_u \varphi_{\max}}{M_{\max} \varphi_u} \tag{5.7}$$

Quantification of the intermediate damage stages takes place through calibration of the flexural damage ratio against experimentally observed structural damage due to earthquake in the field or through tests in the laboratory. However, due to the differences in the characteristics of the expected earthquakes (duration, frequency content, magnitude etc.) and the ones used for the calibration process, the application of this damage variable requires caution.

Examining Eq. (5.7), it is clear that flexural damage ratio does not vary between zero and one, therefore it cannot be employed as a damage index. For this reason, Roufaiel and Meyer (1987) subtracted from both the numerator and the denominator of Eq. (5.7) the quantity (φ_y / M_y), which is equal to one divided by the initial elastic stiffness, resulting to the modified flexural damage ratio (Eq. (5.8)).

$$MFDR = \frac{\frac{\varphi_{\max}}{M_{\max}} - \frac{\varphi_y}{M_y}}{\frac{\varphi_u}{M_u} - \frac{\varphi_y}{M_y}} \tag{5.8}$$

- *Slope ratio*

Slightly different from the stiffness ratio, the slope ratio is defined as the ratio between the slope of the loading and the slope of the unloading branch of the force-displacement diagram. This measure implies that damage occurs due to degradation of stiffness during a seismic loading. Laboratory tests (Toussi & Yao 1983) have shown that (in contrast to the definition of damage index given at the beginning of this chapter) a structure will remain undamaged when the slope ratio is equal to 1 and it is severely damaged when the slope ratio is smaller than 0.2.

5.1.1.1.3 Combined non-cumulative damage index

- *Deformation Damage*

In 1989, Bracci et al. proposed a combined damage index in order to express the damage level in terms of the maximum inelastic displacement and the stiffness degradation. The formula that is suggested is given by the Eq. (5.9).

$$D_I = \frac{x_{\max} - \frac{F_{\max}}{k_{\max}}}{x_u - \frac{F_u}{k_u}} \tag{5.9}$$

Where: $x_{\max}$: maximum displacement (or curvature) response due to earthquake loading,

x_u : ultimate displacement (or curvature) for monotonic loading,

$F_{\max}$: force (or moment) at maximum displacement (or curvature) response due to earthquake loading,

F_u : force (or moment) at ultimate displacement (or curvature) for monotonic loading,

$k_{\max}$: stiffness of the unloading branch at the maximum displacement (or curvature).

k_u : Stiffness of the unloading branch at the ultimate displacement (or curvature)

Similar to the aforementioned non-cumulative damage indices, this damage index cannot capture the accumulation of inelastic energy of a structure subjected to an earthquake and therefore attention should be paid when it is used.

5.1.1.2 Cumulative damage indices

The application of cumulative damage models is a more rational choice for the evaluation of damage states of structures subjected to earthquakes. This is because they quantify the damage by taking into account the time history of the response. In that sense, they are able to describe the evolution of damage over time. The damage level is measured either by accumulating the plastic deformations or by employing a term related to the hysteretic energy dissipated throughout the whole excursion. Shortcoming of the cumulative damage indices is their inability to predict the collapse caused by a single excessively large deformation.

5.1.1.2.1 Deformation based damage indices

- *Normalized cumulative rotation*

In 1982 Banon and Veneziano proposed a damage index (Eq. (5.10)) which is expressed by the accumulation of plastic rotations of every half inelastic cycle (φ_{max} - φ_y), normalized by the ultimate rotation determined through monotonic loading (φ_u).

$$NCR = \frac{\sum_{i=1}^{N} \left| \varphi_{\max,i} - \varphi_y \right|}{\varphi_u} \tag{5.10}$$

Despite the fact that this is a relatively easy-to-compute index, its application is limited due to lack of calibrated values that correspond to different damage states.

- *Normalized cumulative plastic deformation*

Based on the hypothesis of failure of small axially-loaded mild-steel specimens due to low-cycle fatigue (Yao & Munse 1962), Stephens and Yao (1987) developed a damage index (Eq. (5.11)) that accounts for the accumulation of plastic deformation; with the vision to be applied on different structural systems subjected to various cyclic loads. In Eq. (5.11) Δx_i^+ indicates the deformation increment from the maximum negative to the maximum positive displacement of the i cycle, while $\Delta x_{f,i}$ is the deformation increment from the maximum negative displacement of the i cycle to the displacement of failure defined by one-cycle test. The exponent (1-br) accounts for the fatigue damage, where b is a deformation ratio coefficient. The variable r represents the relative deformation ratio, defined as the deformation increment from the maximum negative to the maximum positive displacement (Δx_i^+) divided by the deformation increment from the maximum positive to the maximum negative displacement (Δx_i^-) of the i cycle (Eq. (5.12)).

$$D = \sum_{i=1}^{n} \left(\frac{\Delta x_i^+}{\Delta x_{f,i}} \right)^{1-br} \tag{5.11}$$

$$r = \frac{\Delta x_i^+}{\Delta x_i^-} \tag{5.12}$$

In an attempt to simplify the aforementioned damage function, constant value of the fatigue exponent (*1-br*) is suggested equal to 1.77 (Stephens & Yao 1987) and the normalization factor $\Delta x_{f,i}$ is taken equal to 10% of the floor height. It should be noted that these values are established on the basis of laboratory tests on reinforced concrete structural components, therefore their direct application to different structures contains large uncertainty.

- *Cumulative cyclic inelastic deformation*

Cumulative cyclic inelastic deformation is a damage model proposed by Wang and Shah (1987), in which the accumulation of damage depends on the maximum displacement, experienced by the structure in every loading cycle. The dependency is captured by the cyclic loading parameter β (Eq. (5.13)) which indicates the sum of the maximum displacements in each cycle (x_i) divided by the ultimate displacement determined through monotonic loading test (x_u) and multiplied by a constant (C) which is less than 1.

$$\beta = C \sum_{i=1}^{n} \frac{x_i}{x_u} \tag{5.13}$$

The damage index is given by an exponential form (Eq. (5.14)) in which the coefficient η is determined from experimental data.

$$D = \frac{e^{\eta\beta} - 1}{e^{\eta} - 1} \tag{5.14}$$

It is noted that this damage index is very sensitive to the choice of the constants C and η, which are related to the member design properties. Unless a relationship is established between these constants and the design properties, the method is difficult to be applied in more general cases (Wang & Shah 1987). In the case of a well-reinforced members the constants C and η is recommended (Sreekala et al. 2011) to have values of 0.1 and 1 respectively.

- *Cumulative displacement ductility*

Based on the concept of ductility ratio, the cumulative displacement ductility (Park 1988) represents the sum of the displacement ductility of cycles with reversed loading (Eq. (5.15))

$$\Sigma\mu = \sum_{i=1}^{n} \left(\frac{x_{\max,i}}{x_y} \right) \tag{5.15}$$

This variable should be used with caution on damage assessment of structures. This is because, smaller number of loading cycles with higher ductility per cycle may result in different damage state compared to bigger number of loading cycles with lower ductility per cycle, although they appear to have the same cumulative displacement ductility. For instance, 16 cycles with displacement ductility μ=1 in each direction will cause significantly less damage than 2 cycles with displacement ductility μ=8 in each direction, even if in both cases the cumulative displacement ductility is $\Sigma\mu$=32) (Park 1988).

- *Low-cycle fatigue model*

Based on the assumption that the structural members under cyclic load follow a rule similar to the Manson-Coffin relationship (a relationship between plastic strain and low-cycle fatigue), Jeong and Iwan (1988) developed an index for the estimation of the damage level of structures subjected to seismic load. The relationship in Eq. (5.16) shows that the number of cycles (N) that leads to failure at a given ductility ratio (μ) to the power of an empirical constant (s), is a positive constant (C), which can be determined through laboratory tests.

$$N\mu^s = C \tag{5.16}$$

By using the Miner's rule, (that assumes that the damage accumulation is a linear function of the number of cycles of constant amplitude cyclic loading) the incremental damage caused by n_i cycles of ductility ratio μ_i is given by:

$$D_i = \frac{n_i}{N_i} = \frac{n_i \mu_i^s}{C} \tag{5.17}$$

By assuming that the damage is independent of the sequence of application of the loading cycles during the excursion, the total damage is given by the Eq. (5.18).

$$D = \sum_{i=1} D_i = \sum_{i=1} \frac{n_i \mu_i^s}{C} \tag{5.18}$$

Although this damage index is very attractive due to its simplicity, Jeong and Iwan (1988) recognised that it should be used only for a crude estimation of the actual structural damage, due to the assumptions that are involved.

- *Cumulative plastic rotation damage index that incorporates the primary and follower cycles concept*

Inspired by an energy-based damage index (Kratzig et al. 1989), Mehanny and Deierlein (2001) developed a damage index that tracks the cumulative inelastic deformations. The damage index, which is described by Eq. (5.19), consists of the primary half cycle (PHC) inelastic rotation (θ_{PHC}), the sum of the follower half cycle (FHC) inelastic rotations (θ_{FHC}) and the ultimate inelastic rotation defined by monotonic loading test (θ_u).

The term primary half cycle (PHC) refers to the half-cycle that corresponds to the maximum inelastic rotation until the n^{th} cycle, whereas, the term follower half cycle (FHC) refers to the inelastic rotation of the rest of the half-cycles. PHC and FHC can be updated in every half cycle, giving the opportunity to determine the damage level of the structure at the corresponding moment. The exponents α and β are coefficients that were calibrated through tests for different structural systems, depending on whether the maximum rotation or the accumulation of inelastic rotations contributes more on the structural damage of the structural system.

$$D_\theta = \frac{(\theta_{PHC})^\alpha + \left(\sum_{i=1}^{n} \theta_{FHC,i}\right)^\beta}{(\theta_u)^\alpha + \left(\sum_{i=1}^{n} \theta_{FHC,i}\right)^\beta} \tag{5.19}$$

The damage index is calculated separately for the positive rotations (D_θ^+) and for the negative rotations (D_θ^-) through the Eq. (5.19). The two components are combined in a single damage index (Eq. (5.20)), in which γ represents a third calibrated coefficient.

$$D = \sqrt[\gamma]{\left(D_\theta^+\right)^\gamma + \left(D_\theta^-\right)^\gamma} \tag{5.20}$$

5.1.1.2.2 Energy based damage indices

Damage indices that account only for the accumulation of energy, implicitly accept that each structure has the capacity to dissipate a given amount of energy. When this amount of energy is exceeded the structure is expected to collapse.

- *Work damage index*

Gosain et al. (1977) adopting the theory expressed above, proposed a damage index that accumulates the work produced in every cycle i for which the force is larger than 75% of the yield force, normalized by the work done when the yield point is reached (Eq. (5.21)). The work produced in each cycle is given by the product of the maximum force of each cycle (F_i) multiplied by the corresponding displacement (x_i). Meanwhile, the work done when the yield point is reached is given by the product of the yield force (F_y) multiplied by the yield displacement (x_y).

$$D_E = \sum_{i=1}^{n} \frac{F_i x_i}{F_y x_y}; \qquad F_i / F_y \geq 0.75 \tag{5.21}$$

It is clear that the approximation of the inelastic dissipated energy with the product of the inelastic force times the inelastic displacement is a rather rough assumption. Therefore, this damage index in most cases is inappropriate.

- *Energy dissipation index*

In 1986 Darwin and Nmai, searching for a more realistic measure for the quantification of the performance of an actual structural member, they proposed the energy dissipation index (Eq. (5.22)). This index describes the ratio between the total energy dissipation capacity of a beam (E_d) (calculated analytically or defined through cyclic loading tests) and the elastic energy stored in the beam at yield. The latter quantity can be approximated by half of the product of the yield force times the yield displacement ($0.5F_y x_y$).

$$D_i = \frac{E_d}{\frac{1}{2} F_y x_y} \tag{5.22}$$

- *Energy dissipation index that incorporates the primary and follower cycles concept*

Another, more complex, energy-based damage index (Eq. (5.23)) has been developed by Kratzig et al. (1989). The method is based on the concept of primary half cycle (PHC) and follower half cycles (FHC), which has been addressed in a previous paragraph. Primary half cycle (PHC) is the one whose dissipated energy is greater compared to the previous half cycles and the corresponding dissipated energy is noted as E_{PHC}. The half cycles that have dissipated energy smaller than primary half cycle are accordingly denoted as follower half cycles (FHC) and the corresponding dissipated energy is noted as E_{FHC}. Additionally, the variable E_f in Eq. (5.23) indicates the total energy absorbed through a monotonic test that leads to failure.

$$D = \frac{\sum_{i=1}^{n} E_{PHC,i} + \sum_{i=1}^{n} E_{FHC,i}}{E_f + \sum_{i=1}^{n} E_{FHC,i}} \tag{5.23}$$

The damage index should be calculated separately for the positive half-cycles (D^+) and for the negative half-cycles (D^-) through the Eq. (5.23). The two components should be combined in an overall damage index (Eq. (5.24)).

$$D = D^+ + D^- - D^+ D^- \tag{5.24}$$

This damage index is able to quantify damage caused by a big number of low-amplitude cycles, as well as damage caused by a single high-amplitude cycle. This means that it considers not only fatigue-type damage, but also damage due to large deformation.

5.1.1.3 Combined damage indices

The combined damage indices are considered as the most rational among the local damage indices, because they characterize the damage state of structures in terms of deformations and accumulation of energy (Velde 2010). This is because, it has been recognized that both cumulative and non-cumulative effects contribute to the damage and possibly to the failure of structures.

- *Park & Ang (1985)*

Probably, the most well-known combined damage index (Eq. (5.24)), which has a substantial influence on various studies, is proposed by Park and Ang (1985). This damage index is defined by the linear combination of the maximum displacement (x_{max}) normalized by the ultimate displacement determined by monotonic loading (x_u) and the dissipated energy (E) normalized by the product of the yield force (F_y) multiplied by the ultimate displacement determined by monotonic loading (x_u). Additionally, the term which accounts for the accumulation of energy is multiplied by a coefficient that accounts for the strength deterioration (β).

$$DI_{PA} = \frac{x_{\max}}{x_u} + \beta \frac{\int dE}{F_y x_u} \tag{5.25}$$

Despite of its wide use, this damage index appears to have some shortcomings, which have been pointed out by various authors (Ghobarah 2001; Bozorgnia & Bertero 2002; Mihaiță 2013) aiming to its improvement. More specifically, the strength deterioration coefficient (β) is difficult to be determined because the methodology is not well defined. Furthermore, the linear combination of the deformation-based term and the energy-based term in such a highly non-linear problem is questionable. Additionally, in the case that a structure experiences only elastic response, the damage index should be equal to zero. However, DI_{PA} will be greater than zero because the integral of the $\int dE$ of the Eq. (5.25) accounts also for the elastic energy. Meanwhile, a structure that experiences a deformation equal to the ultimate deformation in the first loading cycle it is expected to collapse and the damage index to be equal to unity. Nevertheless, by observing the Eq. (5.25) it is clear that the DI_{PA} will be greater than unity due to accumulation of the energy. In the following paragraphs, a number of damage indices suggested by authors who tried to correct these shortcomings will be presented.

- *Chai et al. (1995)*

An attempt for the improvement of the Park and Ang damage factor was made by Chai et al., who proposed to subtract from the dissipated energy of Eq. (5.25), the inelastic energy dissipated by the structure under monotonic loading at deformation equal to x_{max} (E_{mon}). In this way, the authors present a damage index (Eq. (5.26)) that is equal to one when the structure experiences deformation equal to the ultimate deformation in the first loading cycle. Evidently, the strength deterioration parameter (β) needs to be calibrated again and that is the reason that in Eq. (5.26) it is denoted as β^*.

$$DI_{Ch} = \frac{x_{\max}}{x_u} + \beta^* \frac{\int dE - E_{mon}}{F_y x_u} \tag{5.26}$$

- *Bozorgnia & Bertero (2002)*

Furthermore, in 2002 Bozorgnia and Bertero made a step further to the correction of the imperfections detected in the Park and Ang damage index (DI_{PA}), by introducing an improved cumulative damage index (Eq. (5.28)). The first difference between this index and the DI_{PA} is the replacement of the deformation quantities by ductility ratios (Eq. (5.27)).

The displacement ductility (μ), defined as the ratio between the maximum displacement due to cyclic load (x_{max}) divided by the yield displacement (x_y). The elastic displacement ductility (μ_e), which is one in case of inelastic behaviour and equal to the maximum elastic displacement (x_e) divided by yield displacement (x_y) when the structure experiences only elastic response. The monotonic displacement ductility capacity (μ_u), that represents the ultimate displacement defined by monotonic loading (x_u), divided by the yield displacement (x_y).

$$\mu = \frac{x_{\max}}{x_y} \qquad \mu_e = \frac{x_e}{x_y} \qquad \mu_u = \frac{x_u}{x_y} \tag{5.27}$$

The second difference refers to the fact that the dissipated energy, which in DI_{PA} accounts also for the dissipation due to viscous damping, is replaced by the hysteretic energy (E_H), which accounts for the dissipated energy only due to inelastic deformations. The third difference is associated with the replacement of the product $F_y d_u$ by the hysteretic energy capacity under monotonically increasing loading ($E_{H,u}$). Lastly, the strength deterioration parameter (β) has been replaced by a constant (α) which takes values in a range between zero and one and its estimation is a result of comparisons between DI_{PA} and DI_{BB} for a variety of structural systems and ground motions.

$$DI_{BB} = (1-\alpha)\frac{\mu - \mu_e}{\mu_u - 1} + \alpha \frac{E_H / E_{Hu}}{\mu_u - 1} \tag{5.28}$$

By examining the damage index proposed by these authors (Eq. (5.28)) it can be seen that when the response remains elastic ($\mu=\mu_e$ and $E_H=0$) the damage index is indeed zero. Meanwhile, if the ultimate displacement appears in the first cycle ($x_{max}=x_u$, $E_H=E_{H,u}$ and $\mu_e=1$), the damage index is unity. Those two remarks summarize the level of improvement of the Park and Ang damage index.

In the same direction, various researchers (Nishigaki & Mizuhata 1983; Chung et al. 1987; Kunnath et al. 1990; Niu & Ren 1996; Sashi K. Kunnath et al. 1997; He et al. 2014) suggested slightly different damage indices; main-

ly by varying the constant multiplier of the energy term or by introducing different exponents for the deformation term and the energy term.

- *Colombo & Negro (2005)*

In 2005 Colombo and Negro, proposed a more generalized damage index, which is able to capture the behaviour of brittle and ductile structural members, under seismic load, within the same formulation (Eq. (5.29)). This index is linked to the reduction of the capacity of a structural member and it reaches unity when the structural strength drops to zero. The damage is consisted of three functions, with their associated weighting factors (β_1, β_2, β_3). The first function ($f(\beta_1,\mu)$) corresponds to the maximum deformation experienced throughout the whole excursion, while the other two are related to the energy dissipation in ductile ($f(\beta_2,\int dE_{duct}$)) and in brittle ($f(\beta_3,\int dE_{br}$)) structural elements respectively.

$$D_{CN} = 1 - f(\beta_1,\mu)\cdot f\left(\beta_2,\int dE_{duct}\right)\cdot f\left(\beta_3,\int dE_{br}\right) \tag{5.29}$$

The analytical expressions of these functions are given by the Eq. (5.30)-(5.32). The deformation-based function (Eq. (5.30)) consists of the maximum ductility demand (μ_{max}), the ultimate ductility capacity (μ_u) of the structural element and the parameter β_1, that accounts for the hardening/softening effects. The energy-based function for ductile behaviour (Eq. (5.31)) attempts to describe the descending branch of the hysteresis loop and it incorporates the dissipated energy ($\int dE$), the maximum hysteretic energy (E_u^*) and the parameter β_2 that identifies the point that the capacity starts to decrease. The brittle behaviour is captured by an exponential function (Eq. (5.32)) of the dissipated energy ($\int dE$) normalized by the maximum hysteretic energy (E_u^*). The exponentiality, represents the rapid progress of damage of a brittle structural element under cyclic load. The rate of the strength deterioration is captured by the parameter β_3.

$$f(\beta_1,\mu) = \left(1 - \frac{\mu_{\max}}{\mu_u}\right)^{1/\beta_1} \tag{5.30}$$

$$f\left(\beta_2,\int dE_{duct}\right) = 0.5\left[1 - \tanh\left(\beta_2\frac{\int dE}{E_u^*} - \pi\right)\right] \tag{5.31}$$

$$f\left(\beta_3,\int dE_{br}\right) = \exp\left(-\beta_3\frac{\int dE}{E_u^*}\right) \tag{5.32}$$

The damage index of Colombo and Negro has been characterized (Mirzaaghabeik & Vosoughifar 2015) as the most advanced and complete, due to the fact that it is based on the material fracture theory; therefore it is independent of the material used in the structure.

5.1.2 Global damage indices

Global damage indices are intended for the quantification of the damage of a structure as a whole. It has been pointed out (Kappos 1997; Ghobarah et al. 1999) that global damage indices are less accurate and it is advised to be used only as crude estimates of structural performance during a seismic event. The global damage indices can be calculated directly from global factors or through weighted combination of local damage defined for a number of structural elements.

5.1.2.1 Global damage indices in terms of global parameters

Global damage indices determined by global parameters can be divided into two categories those that are related to deformation and those that are related to the softening of structures subjected to cyclic load.

5.1.2.1.1 Deformation-based index

In 1987, Roufaiel and Meyer proposed an index that defines the overall level of damage of reinforced concrete frames. The damage index (Eq. (5.33)) is a function of the maximum roof displacement ($x_{roof,max}$), the roof displacement at which the first member in the frame yields ($x_{roof,y}$) and the roof displacement at which the frame is expected to fail ($x_{roof,u}$). For this approach, it is assumed that the frame will deflect in the first mode and failure is expected due to excessive roof displacements.

$$GDP = \frac{x_{roof,\max} - x_{roof,y}}{x_{roof,u} - x_{roof,y}} \tag{5.33}$$

5.1.2.1.2 Softening-based indices

Assessment of the time-history response of structures subjected to seismic load shows a significant softening of the structure after a specific number of cycles. Based on this observation, Di Pasquale and Camak developed two damage indices; the maximum softening and the final softening damage index.

- *Maximum softening*

The first damage index (Eq. (5.34)) (Di Pasquale & Camak 1987), is based on the evolution of the fundamental period during an earthquake event and it depends on the combined effect of the stiffness degradation and plastic deformation. It consists of a ratio between the initial period of the structure (T_{inital}) and the structural period that corresponds to the maximum softening (T_{max}). The determination of the maximum softening requires the calculation of the total history response.

$$DI_{S,\max} = 1 - \frac{T_{initial}}{T_{\max}} \tag{5.34}$$

This damage index focuses only on the overall behaviour of the structure and does not provide any information about the damage of individual structural members.

- *Final softening*

The second damage index (Di Pasquale & Camak 1989) employs the natural period that corresponds to the final softening (T_{final}) instead of the maximum softening (T_{max}) (Eq. (5.35)). A direct advantage of this index is that it can be defined from the initial period and the final period of the structure, determined by a vibration test in the field after the earthquake event.

$$DI_{S,final} = 1 - \left(\frac{T_{initial}}{T_{final}} \right)^2 \tag{5.35}$$

One drawback of this damage index is that information that concern the structural element damage or the storey damage are neglected. Furthermore, it is noted that the stiffness of a structure in a loading position differ from the stiffness in the zero-load position and therefore the determination of only the final period may not be accurate.

Based on this damage index and on the fact that the square of the natural period is directly related to the stiffness of a structural system, Ghobarah et al. (1999) proposed a damage index by replacing the fundamental period terms, by parameters of stiffness (Eq. (5.36)).

$$DI_K = 1 - \frac{K_{initial}}{K_{final}} \tag{5.36}$$

5.1.2.2 Weighted averages of member damage indices

- *Weighted by local dissipated energy*

In 1989 Seidel et al. developed a global damage model (Eq. (5.37)) based on the local damage index of Park and Ang ($DI_{PA,i}$) by introducing weighting factors. Those factors are related to the energy dissipated by the i^{th} structural member (E_i) normalized by the energy dissipated by all the members (N) during a seismic load $\sum_{j=1}^{N} E_j$. In that sense, higher weightage corresponds to more heavily damaged elements.

$$D_{total} = \sum_{i=1}^{N} \frac{E_i}{\sum_{j=1}^{N} E_j} DI_{PA,i} \tag{5.37}$$

- *Weighted by tributary gravity load*

The local damage index proposed by Bracci et al. (1989), it can also be employed for the evaluation of the damage of the total structure by incorporating an importance factor that involves the gravity load of each member

(W_i) normalized by the total gravity load of the structure $\sum_{j=1}^{N} W_j$ (Eq. (5.38)). The parameter m is employed to assign an additional degree of sensitivity to elements that are more important for the stability of the structure (e.g. column components are more important than beams (Bracci et al. 1989)).

$$D_{total} = \frac{\sum_{i=1}^{N} \frac{W_i}{\sum_{j=1}^{N} W_i} DI_i^{m+1}}{\sum_{i=1}^{N} \frac{W_i}{\sum_{j=1}^{N} W_i} DI_i^{m}} \tag{5.38}$$

Both weighted models can be expressed in the level of the whole structure if the damage of the element i is replaced by the damage of the story. Additionally, it has been stated (Kappos 1997; Sinha & Shiradhonkar 2012) that both types of weighted factors tend to give higher importance to members of lower storeys. Although this is conceptually correct, ignores that failure of a soft storey typically leads to failure of the whole structure.

5.2 Selection of response parameters

The initial idea of this study was to investigate the influence of the strength hardening, stiffness degradation strength deterioration and pinching, with respect to the most efficient damage index. However, recognizing the complexity that the damages indices entail, it is considered more preferable to evaluate only individual response parameters and not their combination. Considering that in this study several inelastic effects of systems subjected to cyclic load are examined separately, while the ground motions are also divided according to various characteristics, the right choice of the most appropriate response parameters can lead to very clear conclusions.

The literature rereview of the paragraph 5.1, plays a key role on the identification of the more important response parameters, in terms of their connection to the structural damage. By examining the most well-known damage indices it becomes apparent that some response parameters appear more often than others. These response parameters are the maximum inelastic displacement and the hysteretic energy. On the one hand, the maximum inelastic displacement represents the damage that may occur due to extensively large deformations. On the other hand, the hysteretic energy represents the damage that may occur due to the accumulation of the inelastic energy, caused by cyclic loading. Both of them, are considered very critical and they will be the first two response parameters which will be evaluated in this study.

On top of that, the residual displacement is decided to be an additional response parameter, inspired by the concept of the maximum residual drift. Moreover, this response parameter is considered by several authors (Macrae & Kawashima 1997; Yazgan 2010; Bojórquez & Ruiz-García 2011) to play a key role in the performance of structural systems. Finally, it was decided the dissipated energy and the input energy to be examined as response parameters as well.

6 Study results

In this study two types of results are presented. The first one can be characterized as specific with practical interest. This is because it refers to a single model that is calibrated in section 3.5 to fit the pushover test of the masonry assemblage, which was performed in the Delft university of technology. This calibrated model is subjected to an ensemble of seven different ground motions that resembles the ground motions of Groningen (Appendix C). The resulting forces and displacement of this model are compared to the ones that are calculated through the Nederlandse praktijkrichtlijn (NPR 9998) in order to find out if substantial differences appear.

The second type of results is more generic with scientific interest. This is because it evaluates the response of a large number of SDoF hysteretic systems subjected to a large number of ground motions. The response calculated by these systems is compared to the response calculated by elastoplastic hysteretic systems, in order to draw valuable conclusions regarding the influence of non-linear effects on the seismic response of SDoF systems.

6.1 Single calibrated model

6.1.1 Response spectrum method (NPR 9998)

By assuming that the soil conditions are normal, the elastic design forces are calculated based on the section 3.2.2.2.2 of the NPR 9998 as follows:

Firstly, the natural period and the level of damping ratio of the structure have to be estimated. The natural period can be calculated if the mass and the elastic stiffness of the system are estimated. The elastic stiffness will be graphically approximated through the backbone curve of the pushover test in such a way, that the curve is idealized by an elastoplastic force-displacement relationship. The yield force of the elastoplastic curve is assumed to be equal to the maximum force of the backbone curve. The equivalent elastic stiffness is calculated by aiming to equate the Area 1 with the Area 2 of the Figure 6.1 and Figure 6.2.

Following this procedure, the equivalent elastic stiffness of the elastoplastic force-displacement relationship in the positive side can be approximated $K_{equivalent,1}$=6kN/mm, whereas in the negative side is $K_{equivalent,2}$=3.8kN/mm. Both values will be employed to calculate two different elastic periods, in order to observe what are the differences in the response mesures based on the response spectrum method. The two elastic periods are equal to T_1=0.4s and T_2=0.5s respectively.

Additionally, a damping ratio equal to 5% is chosen. Furthermore, the peak ground acceleration of the seven ground motions that are examined in this section should be determined. It should be mentioned that in order the response spectrum to be consistent with the group of ground motions, the importance factor k_{ag}, which is normally given in tables of the design code, is chosen in such a way that the acceleration of the response spectrum for natural period T=0 to be equal to the peak ground acceleration ($S_a(T=0)=pga$).

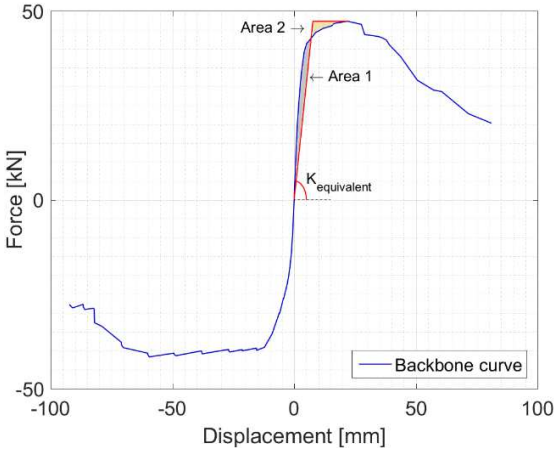

Figure 6.1. Backbone curve of pushover test for masonry assemblage with equivalent stiffness on the positive side.

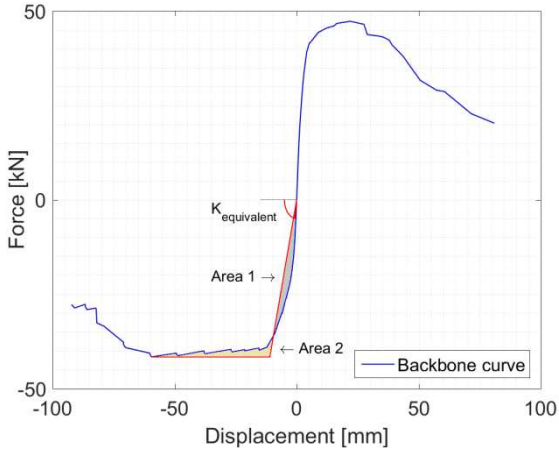

Figure 6.2. Backbone curve of pushover test for masonry assemblage with equivalent stiffness on the negative side.

Due to the fact that the NPR9998 is still under development, the formulas for the calculations are not revealed in this study. However, the calculated values of the parameters are presented in the Table 7. The design forces have been calculated by multiplying the mass (m) of the system by the ordinate of the design response spectrum ($S_d(T)$).

Parameter	Signal 1	Signal 2	Signal 3	Signal 4	Signal 5	Signal 6	Signal 7
pga (g)	0.213	0.203	0.203	0.177	0.185	0.215	0.217
S_S	0.440	0.409	0.409	0.333	0.356	0.445	0.455
S_1	0.131	0.122	0.122	0.099	0.106	0.132	0.135
F_a	1.454	1.491	1.491	1.593	1.560	1.449	1.438
F_v	2.266	2.278	2.278	2.308	2.299	2.264	2.260
S_{MS}	0.641	0.610	0.610	0.531	0.556	0.645	0.654
S_{M1}	0.297	0.277	0.277	0.229	0.244	0.300	0.305
T_C (s)	0.681	0.674	0.674	0.656	0.662	0.682	0.683
T_B (s)	0.136	0.135	0.135	0.131	0.132	0.136	0.137
T_1 (s)	0.40	0.40	0.40	0.40	0.40	0.40	0.40
T_2 (s)	0.50	0.50	0.50	0.50	0.50	0.50	0.50
m (kg)	24560	24560	24560	24560	24560	24560	24560
q	2.00	2.00	2.00	2.00	2.00	2.00	2.00
$S_e(T_1)$	0.641	0.610	0.610	0.531	0.556	0.645	0.654
$S_e(T_2)$	0.641	0.610	0.610	0.531	0.556	0.645	0.654
$S_d(T_1)$	0.320	0.305	0.305	0.266	0.278	0.322	0.327
$S_d(T_2)$	0.320	0.305	0.305	0.266	0.278	0.322	0.327
Design force (N)	77629 77629	73901 73901	73905 73905	64383 64383	67383 67383	78159 78159	79256 79256
Displacement (mm)	25.47 39.79	24.24 37.88	24.25 37.88	21.12 33.00	22.11 34.54	25.64 40.06	26.00 40.62

Table 7. Calculation of design forces and maximum displacements through response spectrum method.

Where:

S_s : is the input spectral acceleration for short periods.
S_1 : is the input spectral acceleration for long periods.
F_a : is the site coefficient for short periods.
F_v : is the site coefficient for long period.
S_{MS} : is the design spectral acceleration for short periods.
S_{M1} : is the design spectral acceleration for long periods.
T_B : is the lower limit of the periods for which the spectral acceleration is constant, in s.
T_C : is the upper limit of the periods for which the spectral acceleration is constant, in s.
T : is the fundamental period of a linear single degree of freedom system.
m : is the mass of the single degree of freedom system.
q : is the dimensionless behaviour factor that decreases the ordinates of the elastic spectrum.
$S_e(T)$: is the elastic response spectrum, in g.
$S_d(T)$: is the design response spectrum of ductile constructions, in g.

The bahaviour factor q controls the degree of the decrease of the elastic forces and it depends on the material and the type of the structure. For masonries, the behavior factor takes vales between 1.5 and 2 and in this study a behavior factor equal to 2 is chosen. It should be mentioned that in NPR 9998 a higher reduction compared to these limits is also accepted, based on non-linear pushover analysis, but this is beyond the scope of the thesis.

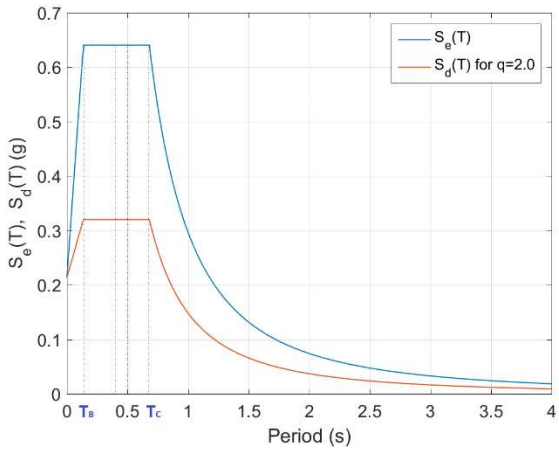

Figure 6.3. Elastic $(S_e(T))$ and design $(S_d(T))$ response spectrum according to NPR 9998 for ground motion with pga=0.21g.

According to NPR 9998, when linear analysis is performed the displacements induced by the design seismic action shall be calculated by multiplying the elastic deformations of the structural system by the behaviour factor q_d which is employed to decrease elastic forces (Eq. (6.1)):

$$d_s = q_d \cdot d_e \tag{6.1}$$

Where:

d_s : is the displacement of a point of the structural system induced by the design seismic action.

q_d : is the displacement behaviour factor, assumed equal to q unless otherwise specified.

d_e : is the displacement of the same point of the structural system, as determined by a linear analysis based the design response spectrum (Eq. (6.2)).

$$d_e = S_d(T) \cdot \left(\frac{T}{2\pi}\right)^2 \tag{6.2}$$

It can be noticed (Table 7) that the design forces for both estimated natural periods are the same. The reason for this is that both periods belong to the plateau of the design spectrum (Figure 6.3); the horizontal part of the design spectrum between T_B and T_C. In contrast, the estimated displacements differ for the two natural periods, because they have been estimated through the Eq. (6.2), in which it is obvious that they are a function of the natural period.

6.1.2 Time history analysis of calibrated SDoF model

In this section the results of the maximum forces and the maximum displacements of the SDoF model which is calibrated in section 3.5 and is subjected to an ensemble of seven ground motions similar to the ones in Groningen are presented (Table 8). The method of the solution of a SDoF system subjected to ground motion is described in the section 3.4.

Parameter	Signal 1	Signal 2	Signal 3	Signal 4	Signal 5	Signal 6	Signal 7
Max force (N)	58722	68564	68586	60561	65171	57688	72296
Max Displacement (mm)	29.71	34.61	30.03	21.68	33.05	24.11	45.43

Table 8. Maximum forces and maximum displacements calculated through time-history analysis.

6.1.3 Comparison

By comparing the maximum forces which are estimated by the response spectrum method with those calculated by the time history analysis of the calibrated SDoF system (Figure 6.4), it can be observed that in general they are overestimated by the former method. This overestimation varies from 6% to 35 % depending on the characteristics of the ground motion. By considering that the response spectrum method is a simplified method

that allows a fast estimation of a structure subjected to earthquake load and taking into account that the over-estimation of the results is on the safe side, the deviations can be acceptable.

However, when the maximum displacements are examined it can be noticed that there are large differences of the results when they are calculated by those two methods of analysis. These differences, vary significantly from signal to signal and they depend on the choice of the natural period of the structure. In the case that the system is represented by the natural period T_1=0.4s, the displacement is underestimated for the six ground motions. This difference may be up to 75% less compared to the displacement calculated through the time-history analysis of the calibrated SDoF system for the ground motion of the seventh signal. In contrast, if the system is represented by natural period T_2=0.5s, the response spectrum method overestimates the maximum displacement calculated through the time-history analysis of the calibrated SDoF system for six of the signals. However, even for this natural period the response spectrum method underestimates the displacement response when the system is subjected to the seventh ground motion.

One possible reason for the underestimation of the maximum displacements by the response spectrum method of the NPR compared to the maximum displacements calculated through the time-history analysis of the calibrated SDoF system, is the fact that the former method does not account for the permanent displacements that may appear after a structure enters the non-linear regime. In contrast this phenomenon is present in the latter method of analysis.

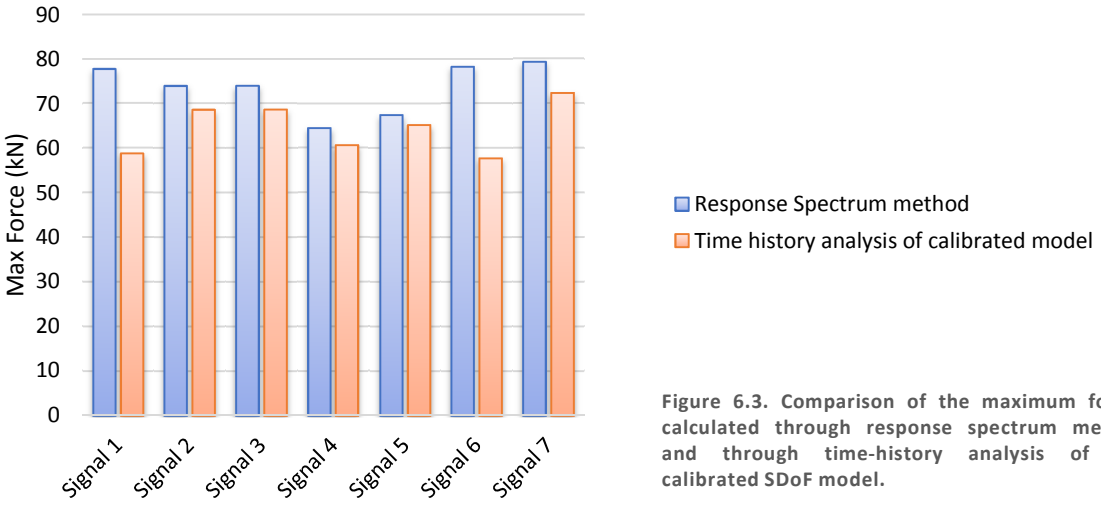

Figure 6.3. Comparison of the maximum forces calculated through response spectrum method and through time-history analysis of the calibrated SDoF model.

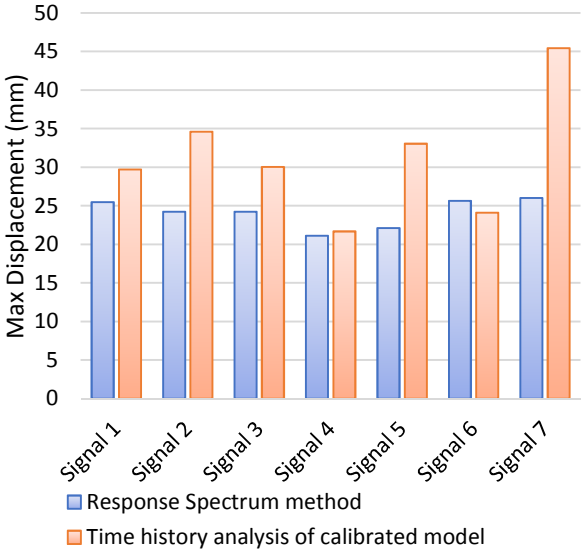

Figure 6.4. Comparison of the maximum displacements calculated through response spectrum method (T_1=0.4s) and through time-history analysis of the calibrated SDoF model.

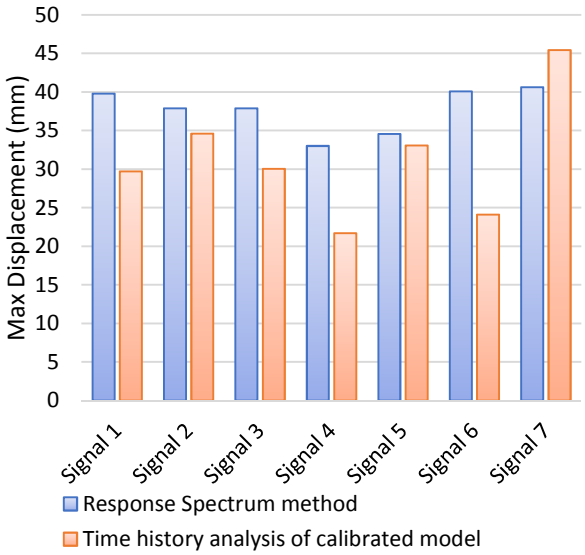

Figure 6.5. Comparison of the maximum displacements calculated through response spectrum method (T_1=0.5s) and through time-history analysis of the calibrated SDoF model.

6.2 Sensitivity analysis

In this section, the degree of the influence of strength hardening, stiffness degradation, strength deterioration and pinching on several response parameters of systems subjected to ground motions, is evaluated. In order to do that 4116 idealized SDoF systems are developed. These systems are developed based on the 21 hysteretic models (model 2 – model 22) of Table 1. For each model 196 different systems have been constructed with varying period (T = 0.04s – 1.0s, with a time step of 0.02s) and varying yield force. The yield force has been normalized by the maximum force of the corresponding elastic system. Four different ratios of yield force divided by maximum elastic force are examined ($F_y/F_{el,max}$ = 1, 0.75, 0.5, 0.25). When the ratio is equal to unity the system is practically elastic and when the ratio is decreasing, we enter more into the non-linear regime. Let us call these systems "advanced", in order to distinguish them from the elastoplastic systems, once they incorporate enhanced non-linear behaviours.

These advanced systems are subjected to an ensemble of 167 different ground motions in order to evaluate:

- the maximum displacements,
- the residual displacements (permanent displacement of the system at the end of the excursion),
- the total hysteretic energy (energy dissipated inelastically by the system),
- the total energy dissipated by the viscous damper,
- the total input energy (energy imparted to the system by the ground motion; which at the end of the excursion is equal to the total of the energy dissipated by the viscous damper and the hysteretic energy),
- the ratio of the hysteretic energy divided by the input energy.

Subsequently, these results are compared with the corresponding elastoplastic systems. In order to be consistent in the comparisons, every elastoplastic system is chosen to have the same elastic period and to be able to acquire the same maximum force as the advanced system with which is compared to. In order to achieve this, the following steps are taking place:

1. The elastic period (T_{el}) of a SDoF elastic system is chosen and the elastic system is subjected to a ground motion.
2. Through the elastic analysis of the SDoF system the maximum elastic force ($F_{el,max}$) is calculated.
3. A non-linear system is developed with the same elastic period (T_{el}), with yield force equal to $F_y = F_{el,max}$ or $F_y = 0.75F_{el,max}$ or $F_y = 0.5F_{el,max}$ or $F_y = 0.25\ F_{el,max}$ and non-linear parameters according to one of the models (model 2 – model 22) of Table 1.
4. This system is subjected to the same ground motion and the six response parameters that are mentioned in the bullets above are calculated.
5. At the same time the maximum force ($F_{inel,max}$) of the same non-linear system is calculated.
6. An elastoplastic system with the same elastic period (T_{el}) and yield force equal to $F'_y = F_{inel,max}$ is developed.
7. The elastoplastic system is subjected to the same ground motion and the six response parameters that are mentioned in the bullets above are calculated.
8. Each response parameter calculated by the elastoplastic system is divided by the respective response parameter calculated by the advanced non-linear system.

These steps have been chosen by the author in order the resulting elastoplastic system to correspond to the way that a backbone curve of a laboratory test is idealized by an elastoplastic force-displacement relationship, according to the design codes (Figure 6.1).

The ratios that are produced on the last step of the previous procedure, indicate whether the response is overestimated or underestimated by the elastoplastic model, compared to each of the 21 hysteretic models. In that sense, it is feasible to evaluate what is the influence of strength hardening, stiffness degradation, strength deterioration and pinching on the response of a system.

The ratios of the results are presented in the form of contour plots, with respect to the initial elastic period of the system and the yield force of the advanced systems divided by the maximum elastic force ($F_y/F_{el,max}$). The color bar of the contour plots indicates that:

- When the color is blue, the elastoplastic model underestimates the results compared to the results of the advanced models.
- When the color is white, there is perfect match between the results of the elastoplastic model and the results of the advanced models.
- When the color is yellow to red, the elastoplastic model overestimates the results compared to the results of the advanced models

Additionally, a complementary diagram that presents the Fourier spectrum of the input ground motion signals with respect to the period has been incorporated (orange line), in order to give a better understanding of the fluctuations that appear in the contour plots. This last diagram is employed in order to reveal the dynamics behind the results.

The four non-linear behaviours that are investigated in this study are presented one by one in the following paragraphs, where their influence to the response parameters is discussed. More emphasis is put on the results of the maximum displacement, while when significant differences appear in the energies or the residual displacements these are also mentioned. In general, in the following sections the results that correspond to the group of long duration ground motions will be presented. When it is judged beneficial, these results are compared to the results of other groups of ground motions or individual signals. The reader can find the plots of the six response parameters calculated from the 21 hysteretic models as mean values of the 167 earthquakes in the Appendix B.

6.2.1 Strength hardening

Firstly, the case in which the strength hardening effect is incorporated to the system is examined. Through the Figure 6.7 - Figure 6.9 it can be noticed that when the stiffness ratio is increasing, the differences between the elastoplastic model and the models that incorporate the strength hardening effect are fade out. This observation, which in the beginning seems paradoxical, is due to the choice to set the yield force of the elastoplastic systems equal to the maximum force that appears in the advanced systems subjected to the same ground motion.

This effect can be explained through an example in terms of statics. If it is assumed that a system with stiffness ratio r_k = 0.2 and initial stiffness K_0 is subjected to a load two times larger than the systems yield force (F = $2F_y$), the system will deform:

$$x_{r_k=0.2} = \frac{F_y}{K_0} + \frac{F_y}{r_k K_0} = \frac{F_y}{K_0} + \frac{F_y}{0.2K_0} = \frac{1.2F_y}{0.2K_0} = 6\frac{F_y}{K_0} \tag{6.3}$$

If we set the yield force of the elastoplastic system equal to F = $2F_y$ (this is what it has been done in this study), the elastoplastic system subjected to the same load F = $2F_y$ will deform:

$$x_{r_k=0} = \frac{2F_y}{K_0} \tag{6.4}$$

It is obvious that the elastoplastic system seems to underestimate the displacement, because it remains elastic. If instead the stiffness ratio was chosen equal to r_k = 0.8, then the system would have deformed:

$$x_{r_k=0.8} = \frac{F_y}{K_0} + \frac{F_y}{r_k K_0} = \frac{F_y}{K_0} + \frac{F_y}{0.8K_0} = \frac{1.8F_y}{0.8K_0} = 2.25\frac{F_y}{K_0} \tag{6.5}$$

Which, indicates that the difference with the elastoplastic system is much smaller.

This behaviour, of course applies when the system is subjected to static load. This fact seems to be more relevant for systems with very short eigen-period (T_n << 0.1s), at least for the mean response of the systems subjected to long period earthquakes (Figure 6.7). The reason might be that in these systems the maximum displacement is governed by the stiffness of the spring, due to the fact that most of the energy of the signal (judging by the Fourier spectrum of the signal) appears in periods T > 0.1s. This phenomenon becomes more apparent when the yield force becomes smaller, because we enter more into the non-linear regime.

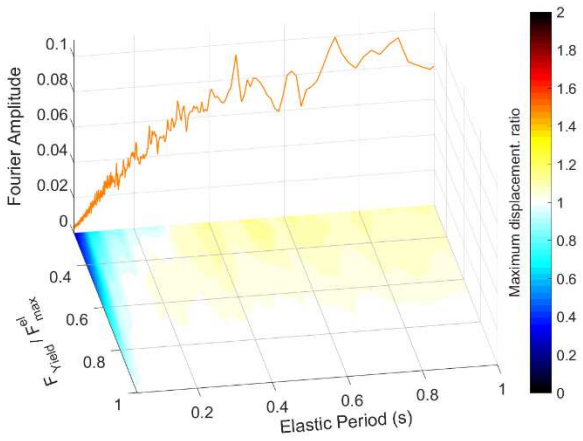

Figure 6.7. Maximum displacement ratios for stiffness ratio r_k=0.2 subjected to long duration earthquakes.

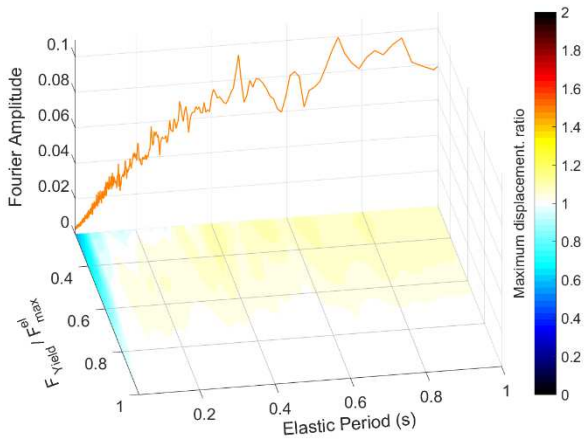

Figure 6.8. Maximum displacement ratios for stiffness ratio r_k=0.4 subjected to long duration earthquakes.

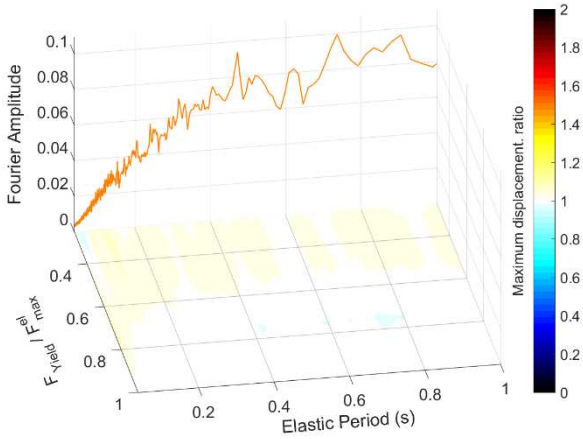

Figure 6.9. Maximum displacement ratios for stiffness ratio r_k=0.8 subjected to long duration earthquakes.

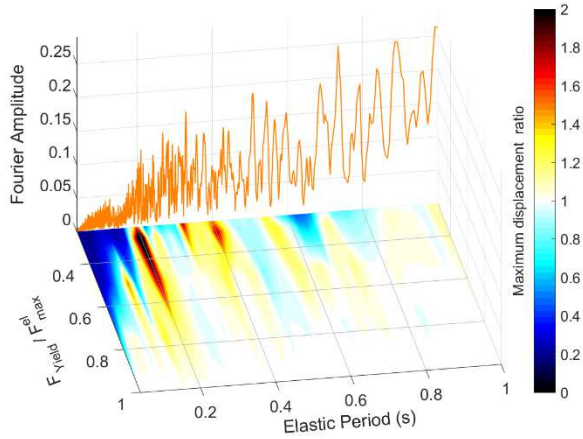

Figure 6.10. Maximum displacement ratios for stiffness ratio r_k=0.2 subjected to ground motion, record sequence no. 1551 (Table 9).

By observing the Figure 6.7 it can be seen that whether the maximum displacement response is overestimated or underestimated by the elastoplastic system depends on the frequency content of the ground motion. More specifically, for the periods close to the peaks of Fourier amplitude the elastoplastic system seems to overestimate the response (yellow color in the contour plot); whereas, for the periods that are far from the peaks of the Fourier amplitude elastoplastic system seems to underestimate the response (blue color in the contour plot). This differences, are more apparent when the maximum displacement response is examined with respect to a single ground motion (Figure 6.10).

By examining the residual displacements, it can be noticed that they are overestimated to a large degree by the elastoplastic model. Due to the fact that the same color bar is used for every result for consistency reasons, it cannot be seen clearly how large this overestimation is, but it is mentioned that the ratio in the case of the sys-

tems in Figure 6.11 it can reach as high values as 10. It should be underlined that, despite the fact that the residual displacements have been recognized as a very reliable measure for the quantification of the performance level of a structure subjected to earthquake load, it is not possible to be predicted approximately. This is because the residual displacements are highly sensitive to the time history of the displacement response. More specifically, this response measure depends on the number, the sequence and the direction of the large and the small displacements, of the displacement response time-history.

When the hysteretic energy (Figure 6.12) is examined it is quiet peculiar the fact that for the case of low strength hardening (r_k=0.2) it is underestimated in the whole range of periods, despite the fact that the displacements were overestimated by the elastoplastic model for small yield force and periods T > 0.25s. Accord-

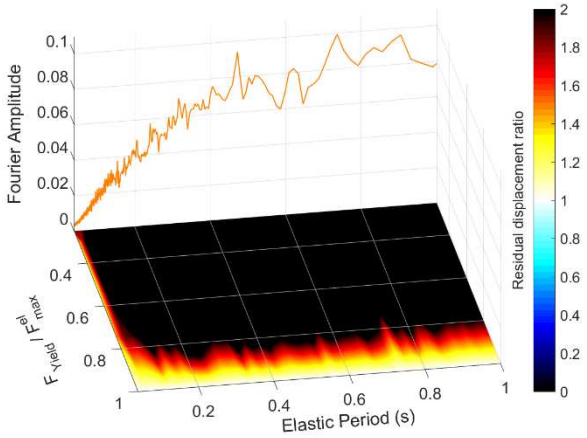

Figure 6.11. Residual displacement ratios for stiffness ratio r_k=0.2 subjected to long duration earthquakes.

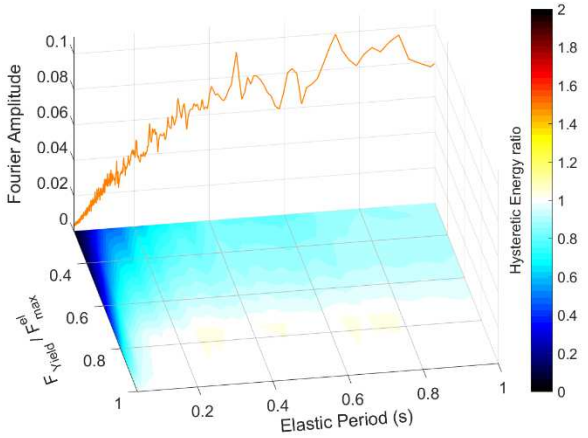

Figure 6.12. Hysteretic energy ratios for stiffness ratio r_k=0.2 subjected to long duration earthquakes.

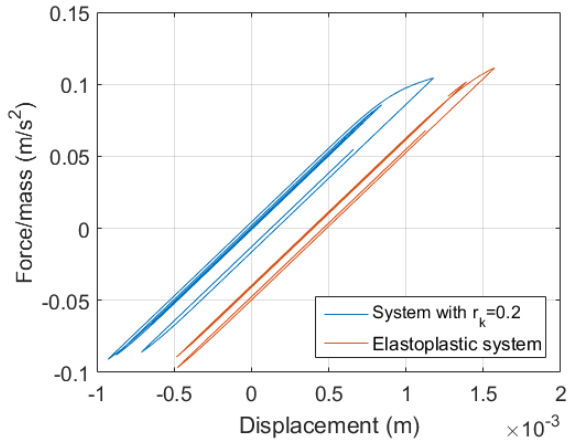

Figure 6.13. Hysteresis loops of an elastoplastic system and a system with r_k=0.2, with T=0.84s and F_y/F^{el}_{max}.for the last 60% of the total loading cycles of the ground motion with record sequence no. 1106 (Table 9).

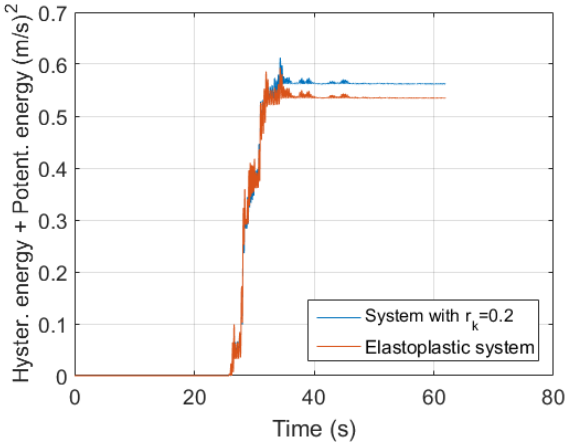

Figure 6.14. Time-history of the sum of the hysteretic energy and the potential energy of an elastoplastic system and a system with r_k=0.2, with T=0.84s and F_y/F^{el}_{max}.subjected to the ground motion with record sequence no. 1106 (Table 9).

ing to this, the hysteretic energy would be also expected to be overestimated by the elastoplastic model for the same region in the contour plot. This behaviour can be explained by examining the last 60% of loading cycles of a SDoF system that was developed based on this model (model 2) and it has natural period T = 0.84s and F_y/F^{el}_{max} = 0.25 (Figure 6.13).

In this figure, it can be noticed that the last hysteresis loops[4] of the elastoplastic model are much smaller than the ones of the model that incorporates some degree of strength hardening. This is due to the reason that the elastoplastic model results to large residual displacements and in the last cycles it is prone to oscillate around these displacements, while the model that incorporates strength hardening tends to return closer to the initial position. This phenomenon results to smaller cycles at the end of the excursion for the elastoplastic model. This behavior can be also noticed in the time history that presents the energy of the spring (hysteretic energy and potential energy) (Figure 6.14).

6.2.2 Stiffness degradation

When the stiffness degradation behavior is investigated independently from the strength hardening (Figure 6.15, Figure 6.16) it is noticed that the differences between the maximum displacement calculated by the elastoplastic model and the models that incorporate stiffness degradation are not very large. However, if another group of ground motions is examined (Figure 6.17, Figure 6.18), large overestimations of the maximum

[4] The accumulation of the area of the hysteresis loops results to the hysteretic energy.

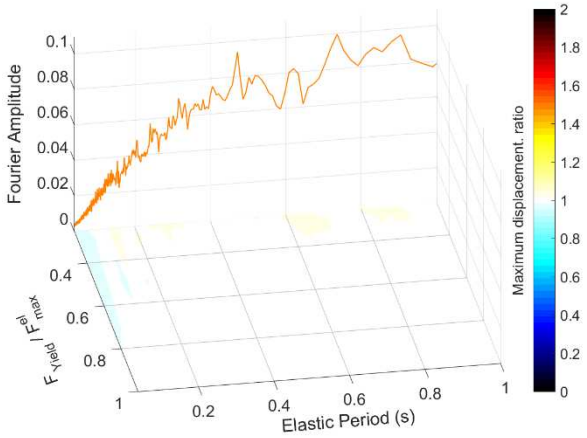

Figure 6.15. Maximum displacement ratios for systems with low degree of stiffness degradation (model 5 Table 1) subjected to long duration earthquakes.

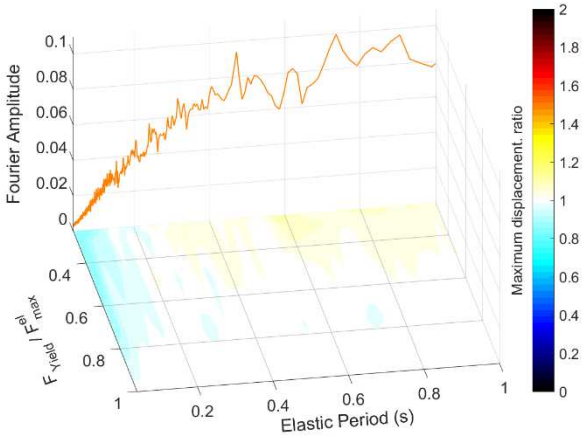

Figure 6.16. Maximum displacement ratios for systems with high degree of stiffness degradation (model 6 Table 1) subjected to long duration earthquakes.

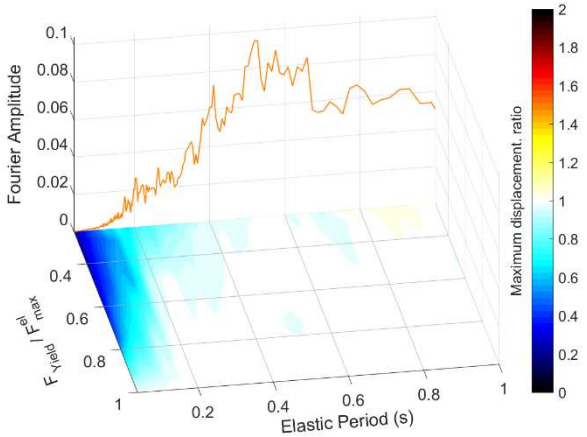

Figure 6.17. Maximum displacement ratios for systems with low degree of stiffness degradation (model 5 Table 1) subjected to the group of earthquakes similar to Groningen.

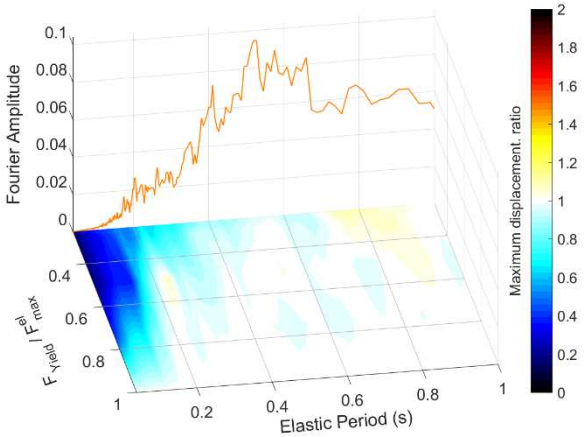

Figure 6.18. Maximum displacement ratios for systems with high degree of stiffness degradation (model 6 Table 1) subjected to the group of earthquakes similar to Groningen.

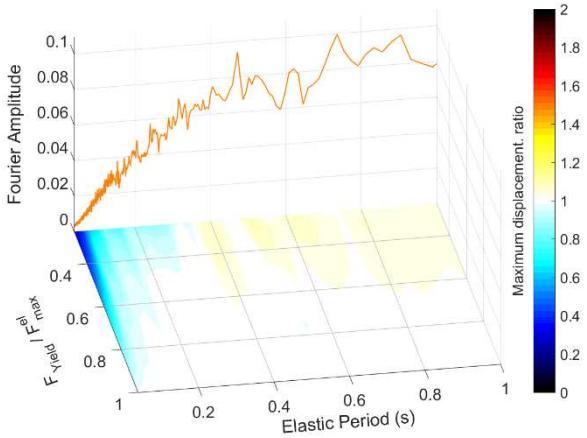

Figure 6.19. Maximum displacement ratios for systems with low degree of stiffness degradation and stiffness ratio r_k=0.2 (model 7 Table 1) subjected to long duration earthquakes.

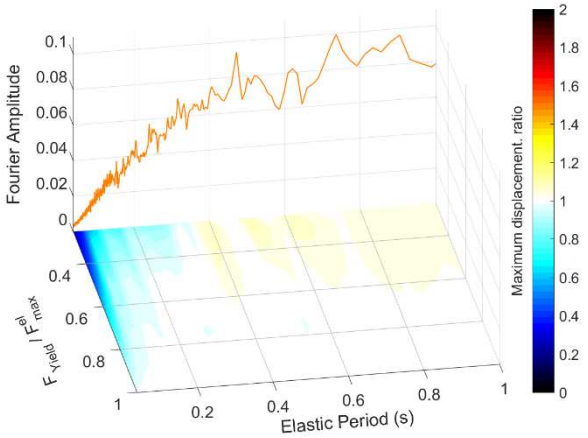

Figure 6.20. Maximum displacement ratios for systems with high degree of stiffness degradation and stiffness ratio r_k=0.2 (model 10 Table 1) subjected to long duration earthquakes.

displacement response can be noticed. For this scenario, the most severe case seems to be the group of ground motions that are similar to the earthquakes in Groningen. This behavior was expected, but it seems that it is more apparent when the most of the energy of the signal is concentrated to a small period range, and the eigen-period of the system, is much smaller than the aforementioned range of periods.

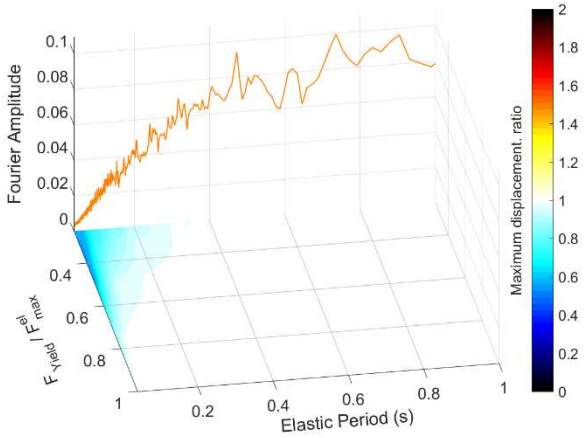

Figure 6.21. Maximum displacement ratios for systems with low degree of strength deterioration (model 11 Table 1) subjected to long duration earthquakes.

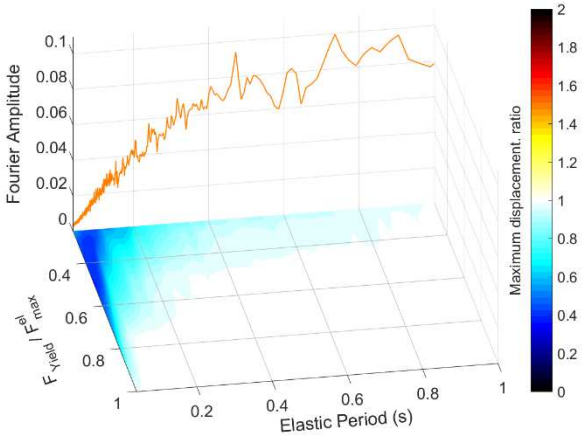

Figure 6.22. Maximum displacement ratios for systems with high degree of strength deterioration (model 14 Table 1) subjected to long duration earthquakes.

The ground motions are far from a sinusoidal load, but in cases like in the Groningen ground motions, where most of the peaks of the Fourier amplitude seem to appear in periods T > 0.3s, it might not be far from reality to admit that for structures with short eigen-periods (T_n << 0.2s) the maximum response is governed by the stiffness of the system. Given that fact and due to the reason that stiffness degradation results to smaller stiffness after a number of loading cycles the reason that the maximum displacements are underestimated by the elastoplastic system (whose stiffness is not decreasing) can be explained.

Additionally, when the stiffness degradation is examined in addition to the strength hardening (Figure 6.21, Figure 6.22), both effects are combined resulting to larger underestimation of the maximum displacement response in the short period range (T < 0.25s).

6.2.3 Strength deterioration

When the strength deterioration is examined independently from the other non-linear behaviours (Figure 6.21, Figure 6.22), it becomes apparent that the for short periods and low ratios of yield force divided by maximum elastic force ($F_y/F_{el,max}$) the maximum displacement is underestimated by the elastoplastic model. The degree of underestimation is increasing when higher level of strength deterioration is present (Figure 6.22). Similarly, when the level of strength deterioration increases, the range of periods on which the maximum displacement is underestimated also increases.

The reason that strength deterioration seems to play a more important role in short period structures is due to the fact that the strength deterioration is perceived and modelled as a quasi-static concept. More specifically, regardless the fact that the strength degradation accounts for the loading cycles in terms of the amplitude and the number of displacements, it does not account for the rate that the load is applied to the structure. In that sense, when a structure has eigen-period much shorter than the range of periods where most of the energy of the signals appears (according to the Fourier spectrum of the signal) the maximum displacement is governed by spring force and the phenomenon becomes more static. Therefore, the strength deterioration as a quasi-static behavior becomes more apparent.

When the strength deterioration is examined in addition to the non-linear behaviours of stiffness hardening and stiffness degradation (Figure 6.22, Figure 6.23), all the effects are combined but it is still obvious that in short period structures the response is underestimated by the elastoplastic model for the reason that is mentioned above. This behaviour can be very important when the Fourier spectrum resembles the group of ground motions which are similar to the earthquakes in Groningen (Figure 6.25, Figure 6.26). This is not only because the degree of overestimation is larger, but also because the range of the natural periods that are affected by the strength deterioration behavior is twice as big as in the case of ground motions of long duration earthquakes. The reason for this is the same as in the case that stiffness degradation behavior is examined.

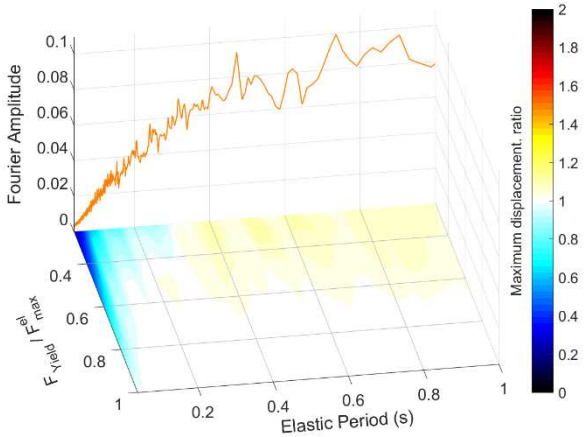

Figure 6.23. Maximum displacement ratios for systems with low degree of strength deterioration in addition to strength hardening and stiffness degradation (model 15 Table 1) subjected to long duration earthquakes.

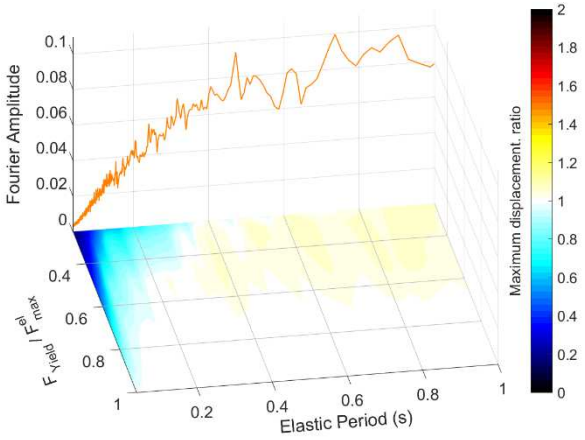

Figure 6.24. Maximum displacement ratios for systems with high degree of strength deterioration in addition to strength hardening and stiffness degradation (model 18 Table 1) subjected to long duration earthquakes.

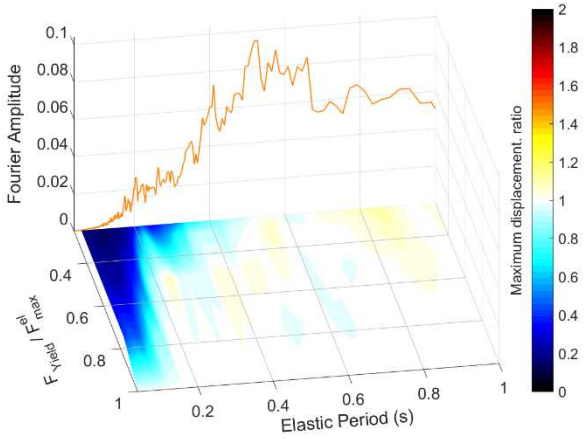

Figure 6.25. Maximum displacement ratios for systems with low degree of strength deterioration in addition to strength hardening and stiffness degradation (model 15 Table 1) subjected to the group of earthquakes similar to Groningen.

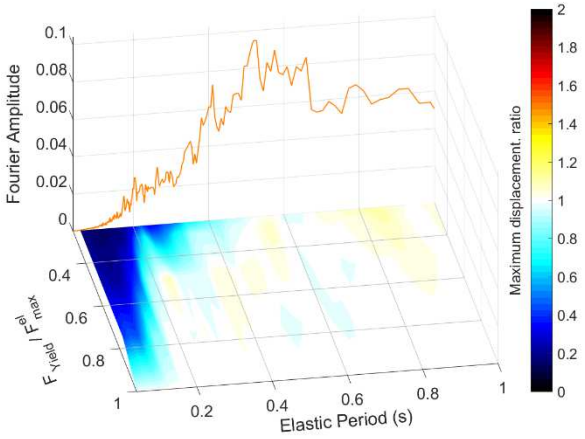

Figure 6.26. Maximum displacement ratios for systems with high degree of strength deterioration in addition to strength hardening and stiffness degradation (model 18 Table 1) subjected to the group of earthquakes similar to Groningen.

6.2.4 Pinching

By observing the maximum displacements calculated by systems that incorporate the pinching behaviour, with or without combining it with the rest of the non-linear behaviours (Figure 6.27 - Figure 6.28), it is clear that they are underestimated by the elastoplastic model. The maximum displacements are underestimated even more by the elastoplastic model when the pitching effect is stronger. This behavior is not surprising, due to the fact that the pinching effect is caused due to decrease of the stiffness to very low levels around the point of origin. This gives the opportunity to the structure to move back to the position that it was half-cycle before when the load reverses. Further increase of the load, displaces the structure even more in every cycle.

For the reasons that mentioned in previous section, it can be explained the fact that the underestimation of the maximum displacements is larger when the phenomenon is less dynamic (short period structures).

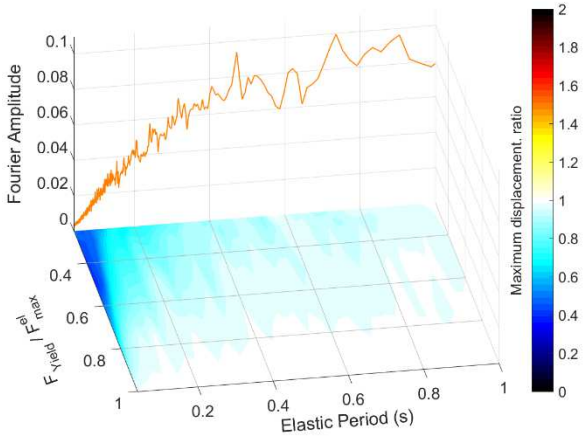

Figure 6.27. Maximum displacement ratios for systems with low pinching effect (model 19 Table 1) subjected to long duration earthquakes.

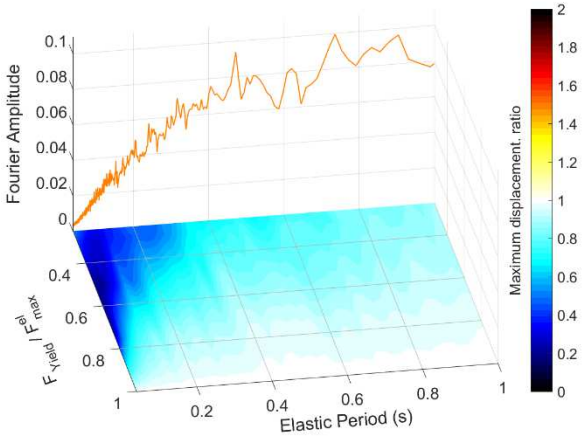

Figure 6.28. Maximum displacement ratios for systems with high pinching effect (model 20 Table 1) subjected to long duration earthquakes.

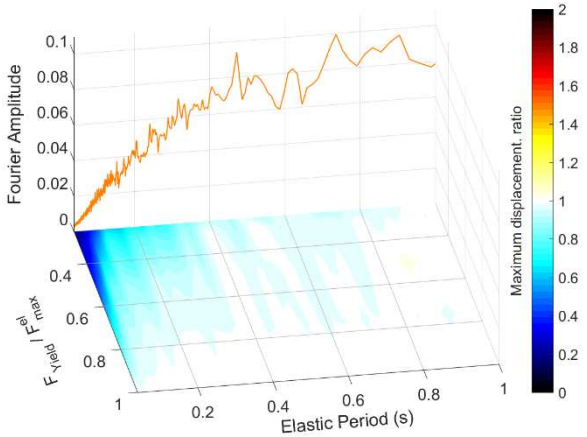

Figure 6.29. Maximum displacement ratios for systems with low pinching effect in addition to strength hardening, stiffness degradation and strength deterioration (model 21 Table 1) subjected to long duration earthquakes.

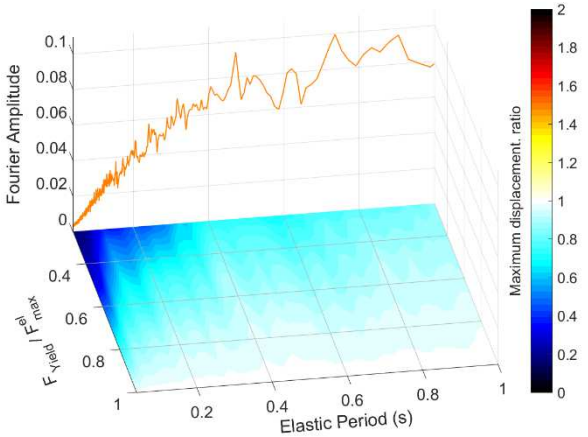

Figure 6.30. Maximum displacement ratios for systems with high pinching effect in addition to strength hardening, stiffness degradation and strength deterioration (model 22 Table 1) subjected to long duration earthquakes.

7 Conclusions and recommendations

In this study the non-linear behaviours of strength hardening, stiffness degradation, strength deterioration and pinching on the seismic response of SDoF systems is investigated. This investigation is performed in terms of:

- a calibration of a SDoF system to fit the pushover test of a real structure and
- a sensitivity analysis of 5145 different hysteretic systems.

Main goal of the first part of the investigation is to figure out whether or not there are shortcomings in the response spectrum method of the design code NPR 9998 regarding the calculation of maximum displacements. For this reason, the calibrated system is subjected to seven ground motions that resemble the ground motions in the area of Groningen in order to evaluate its response, based on a time-history analysis of a SDoF non-linear system. In parallel, the response of the same structure is estimated through the linear inelastic response spectrum analysis method that is proposed by the NPR 9998. The comparison of the results showed that

- Regarding the maximum forces, the linear inelastic response spectrum analysis in general overestimates the values which were calculated by the time-history analysis. This overestimation varies from 6% to 35%. Based on the fact that this is an approximated method and due to the reason that overestimation of the design forces is from the safe side, these deviations are acceptable.
- Regarding the maximum displacements, the linear inelastic response spectrum analysis in some cases overestimates and in other cases underestimates the values that were calculated by the time-history analysis. These differences depend on the choice of the eigen-period of the structure and the peak ground acceleration. This observation makes the adequacy of the linear inelastic response spectrum analysis method for the calculation of the maximum displacements questionable. It is worth mentioning, that the linear inelastic response spectrum analysis method does not account for the permanent displacements and that is already a reason for the deviations compared to the time-history analysis.

Main goal of the second part of the investigation is to figure out the influence of the non-linear behaviours, which were mentioned above, on idealized systems. This type of investigation reveals the tendency of some non-linear behaviours to affect more than others some response parameters. The influence of the non-linear behaviours is examined in comparison to the resulting response of equivalent elastoplastic systems. The elastoplastic systems have been developed in such a way that their force-displacement relationship envelopes the maximum force of the models that incorporate non-linear effects. This method resembles the approach that has been followed for the development of the behavior factor q which is employed by the linear inelastic response spectrum analysis method in order to calculate the design forces. Therefore, the results of this study may be valuable for the development of a more rational factor for the calculation of the design forces and displacements.

In contrast with previous studies in this investigation the results are interpreted in the spectrum of dynamics, by incorporating a complementary diagram of the Fourier spectrum of the input signal. The more important results of this investigation can be summarized to the following:

- The behavior that seems to affect the most the maximum acceleration response is the pinching effect.
- The residual displacements in general are overestimated to a large degree by the elastoplastic model.
- Regarding the maximum displacements, their overestimation or underestimation by the elastoplastic system seems to depend highly on the frequency content of the signal.
- In this work, it is observed that for short-period structures the elastoplastic model underestimates the maximum displacement response, compared to models that incorporate strength hardening or stiffness degradation or strength deterioration or pinching or combination of these effects.
- This phenomenon seems to be more apparent when the energy of the signal is concentrated in small range of periods and the eigen-period of the system is much smaller than the mean period of this range. An example such a ground motion is given by the group of the seven signals that are similar to the ground motions of the area of Groningen.

Taking into consideration these observations it becomes apparent that great care should be paid when the maximum displacements are estimated by the linear inelastic response spectrum method of the design codes. In addition, great care should be also paid when an elastoplastic model is used; because it may be assumed that it is safe to employ such a model but in this study, it has been proven that depending on the input signal and on the structural period this maybe not be the case.

Furthermore, in this study it is shown that regarding the maximum displacement response further investigation is needed for the seismic response of buildings in Groningen. This is not only because most of the buildings in that area have short eigen-period, but also because of the frequency content of the ground motions that were recorded in the area. This combination has been shown in this study that leads to the largest underestimation of the displacements by the elastoplastic model.

While this thesis was conducted a lot of questions has been raised. For some of them the answer is given by the results but for others the answer hasn't been given yet. Following, some of the questions are formed in terms of recommendations for further work.

Firstly, most the biggest part of these study is based on idealized models. It is believed that the results will be more valuable if the analyses are performed in terms of a large number of models that are calibrated in order to fit the force-displacement diagrams of pushover tests that have been performed on several types of structures. Subsequently these models can be subjected to several ground motions and their response will be evaluated in comparison with an elastoplastic model.

Additionally, it has been mentioned that the hysteretic model which is used in this study is rate independent. The load rate is taken into account by the viscosity. The first question that arises is to what extend is it accurate to accept that only the viscosity can responsible for the rate that the load is applied. Secondly, how rational is to assume that the viscous damper has a constant damping coefficient throughout the total excursion, when non-linearity is examined. It is suggested a model that incorporates gradual change on the viscosity of the system to be incorporated in a future model.

Furthermore, it would be very beneficial if a similar study would be performed in a shaking table of a laboratory in which several structures with short eigen-periods ($T < 0.25$s) would be loaded by signals that resembles the signals of Groningen in order to measure their response. At the same time the response would be calculated by an elastoplastic model with the same characteristics subjected to similar load. Though this it could be shown if the remarks of this study can be validated or contradicted.

Finally, in this study it has been assumed that the models are isotropic. This means that initially they had the same yield force and elastic stiffness in every direction, whereas the laws according to which the stiffness degradation, the strength deterioration and the pinching effect evolve are also independent of the direction. Due to the fact, that the real structures deviate from this model, it is advisable to investigate this behavior as well.

Appendices

A MATLAB codes

A.1 Newmark beta method and Newton-Raphson iterations

```
%-------------------------------------------------------------------------
% Newmark beta method for the solution of inelastic SDoF system subjected
% to ground motion. (c) Apostolos Bougioukos
%-------------------------------------------------------------------------
%   The location that the ground motion time-history is saved
file = dir ('Signals');
filea = ['Signals\', file(ii).name];
fileID = fopen(filea);
%   Calls function that reads the ground motion signal and returns:
%   NPTS: total number of samples in the signal
%   Dt: time interval between samples
%   recordings: the values of the samples
[NPTS,Dt,recordings] = fnc_Strong_motion(fileID);
%   External force
F_external = m*recordings;
%   Elastic period of system
periods =  1;
%   yield force of the system
fy =       1;
%   Damping ratio of the system
ksi =      0.02;
%   Unit mass
m = 1;
%   Calculation of yield displacement
uy= (periods)^2*fy/(4*pi()^2*m);
%   Calculation of elastic stiffness
k = fy/uy;
%   Calculation of damping coefficient
c = ksi*2*sqrt(m*k);
%   Calculation of omega
omega_n = sqrt(k/m);
%   Parameters of Newmark beta method
gamma = 1/2;
beta = 1/6;
%   Initial conditions
x(1) = 0; u(1) = 0; x_max = 0;
%-------------------------------------------------------------------------
%                         Initial calculations
%-------------------------------------------------------------------------
% Define the function of the resisting force fs of the inelastic system.
% Calculate a(1) acceleration at t=0.
% alpha1, alpha2, alpha3: Are terms of the expression of the residual
%   force. These terms remain constant in every time step.
kT(1) = k;
fs(1) = kT(1)*x(1);
t = (0:NPTS-1)*Dt;
a(1) = -recordings(1);
alpha1 = 1 / ( beta * Dt ^ 2 ) * m + gamma / ( beta * Dt ) * c;
alpha2 = 1 / ( beta * Dt ) * m + ( gamma / beta - 1 ) * c;
alpha3 = ( 1 / ( 2 * beta ) - 1 ) * m + Dt * ...
         ( gamma / ( 2 * beta ) - 1 ) * c;
```

```
%-------------------------------------------------------------------------
%                 Calculations for each time instant.
%-------------------------------------------------------------------------
% In the expression of the residual force we have terms that do not change
%   from iteration to iteration. These terms are collected and put into the
%   expression named p_unchanged.
% i represents the time instants.
% R is the residual force which is changing in every iteration.
% Dx is the change in displacement from iteration to iteration. Initially
%   we give a value of 1 in order not to converge before the first
%   iteration occurs.
% j represents the iteration.
% The iterations will continue till convergence occurs.
% Convergence criteria (one of them should be fulfilled):
%   1) Residual force less than a tolerance eR (in a range 10^-3 to 10^-8).
%   2) Change in displacement less than a tolerance eu (in a range 10^-3 to
%   10^-8).
%   3) Incremental work done by the residual force acting through the
%   change in displacement less than a tolerance ew (near to computer
%   tolerance).
eR = 10^-3;
eu = 10^-3;
ew = 10^-5;
i = 0;
while i < NPTS-1
    i = i + 1;
    x(i+1)      = x(i);
    u(i+1)      = u(i);
    a(i+1)      = a(i);
    fs(i+1)     = fs(i);
    kT(i+1)     = kT(i);
    p_unchanged(i+1) = - recordings(i+1) + alpha1 * x(i) + ...
                         alpha2 * u(i) + alpha3 * a(i);
    R(i+1) = 0.01;
%-------------------------------------------------------------------------
%       Calculation for each iteration, Newton-Ramphson iterations
%-------------------------------------------------------------------------
    while  (abs(R(i+1)) > eR) ;
        R(i+1) = p_unchanged(i+1) - fs(i+1) - alpha1 * x(i+1);
        kT_hat(i+1) = kT(i+1) + alpha1;
        Dx(i) = R(i+1) / kT_hat(i+1);
        x(i+1) = x(i+1) + Dx(i);
        du = x(i+1) - x(i);
        % This fuction returns the tangent stiffness and restoring force in
        % each iteration based on the hysteretic system we have chosen.
        % This part of the code will remain hidden but it may be
        % distributed uppon request.
        [kT(i+1), fs] = fnc_Tangent_stiff( fs(i+1), x(i+1), du, k);
        %-----------------------------------------------------------------
        %    Calculation of total velocity and relative acceleration
        %-----------------------------------------------------------------
        u(i+1) = gamma / ( beta * Dt ) *( x(i+1) - x(i) ) + ...
                ( 1 - gamma / beta ) * u(i) + Dt *...
                ( 1 - gamma /( 2 * beta ) ) * a(i);
        a(i+1) = 1 / ( beta * Dt ^ 2 ) * ( x (i+1) - x(i) ) - ...
                 1 / ( beta * Dt ) * u(i) - ...
                ( 1 / ( 2 * beta ) - 1 ) * a(i);
    End
```

```
%-------------------------------------------------------------------------
% Calculations total acceleration
%-------------------------------------------------------------------------
    a_tot(i+1) = recordings(i+1) +a (i+1);
end
```

A.2 Function that reads ground motion files

```
%-------------------------------------------------------------------------
% This script has been created ((c) Apostolos Bougioukos) in order to read
% ground motion files in the format that are extracted from PEER ground
% motion database.
%-------------------------------------------------------------------------
% This is a function that loads the file of the recordings from the main
%  code as it has been downloaded from PEER, and returns the external
%  exerted by the strong motion to the SDOF system.
%  It keeps the text of the file in different cell and the data in a
%  vector.
% Input of the function are:
%  The name of the file of recordings, fileID.
%  The mass of the system, m.
% Output of the function are:
%  The Number of the records, NPTS [#].
%  The time interval, Dt [sec].
%  And the vector of the external force [N], versus time.
%-------------------------------------------------------------------------
% The force versus time is simply calculated multiplying the ground motion
%  acceleration [m/s^2] with the mass m [kg] of the system.
%  If the acceleration is given in G we multiply it with 9.81m/s^2.
% In that case that the file is downloaded through the PEER database is
% always in g
%-------------------------------------------------------------------------
function [NPTS,Dt,recordings] = Strong_motion_normalised(fileID)
tline='';
for k=1:4
    tline = [tline, fgets(fileID)];
end
NPTS = str2double(regexp(tline, '(?<=NPTS=[^0-9]*)[0-9]*', 'match'));
Dt = str2double(regexp(tline, '(?<=DT=[^0-9]*)[0-9]*\.?[0-9]+', 'match'));
C_data = textscan(fileID,'%f %f %f %f %f');
not = mod(NPTS,5);
if not > 0
    Nrows = fix(NPTS/5) + 1;
else
    Nrows = fix(NPTS/5);
end
i = 1;
recordings = zeros(1,Nrows*5);
for row = 1:Nrows
    for col = 1:5
        if isnan(C_data{1,col}(row,1))
        else
            recordings(i) = C_data{1,col}(row,1)* 9.81;
            i=i+1;
        end
    end
end
NPTS = length(recordings);
fclose(fileID);
```

A.3 Fourier and power spectra

```
% ------------------------------------------------------------------------
%   Calculates and plots the Fourier and the Power spectrum of a signal
%   (in periods) (c) Apostolos Bougioukos
% ------------------------------------------------------------------------
file = dir ('Signals');
filea = ['Signals\', file(ii).name];
fileID = fopen(filea);
[NPTS,Dt,recordings] = Strong_motion_normalised(fileID);
%   Calculate the root mean square
RMSAcc = rms(recordings)/9.81;
%   Calculation of Fourier Amplitude through FFT
Fourier = abs(fft((recordings*Dt/9.81),NPTS));
%   Calculation of Power Amplitude
Power = Fourier.^2/(pi()*Dt*NPTS*RMSAcc^2);
%   Total time T_0 of the signal
T_0 = (NPTS)*Dt;
f_0 = 1/T_0;
for j=0:NPTS-1
   if j>=0 && j<=NPTS/2
       f(j+1) = j*f_0;
   elseif j>NPTS/2 && j<=NPTS-1
       f(j+1) = -(NPTS-j)*f_0;
   end
   T(j+1) = 1/f(j+1);
end
T_Fourier   = T(1:NPTS/2);
Fourier_SP  = Fourier(1:NPTS/2);
T_Power     = T(1:NPTS/2);
Power_SP    = Power(1:NPTS/2);
Figure
plot(T_Fourier, Fourier_SP)
Figure
plot(T_Power, Power_SP)
```

A.4 Inelastic response

Several scripts that control the non-linear behaviour of the inelastic systems have been built by the author of this study. Each one incorporates different non-linear effects. None of these scripts will be presented here, but may be distributed upon request.

B Plots

In order to avoid a very extensive appendix, ratios of the 6 response parameters calculated for the 21 models are presented as mean values of the total group of 167 ground motions. In the case that the 9 ground motion groups would be presented here a total of 1134 plots should have been presented. However, the author of this study can provide the reader with the plots upon request.

The ratios of the 6 response parameters:

- Maximum displacements,
- Residual displacements,
- Total hysteretic energy,
- Total dissipated energy,
- Total input energy,
- Fraction of the hysteretic energy divided by the input energy,

are presented in the following 21 pages, where each page represents one of the hysteretic models that are presented in Table 1. It is reminded, that the contour plots present the ratios of the resulted response parameters of the elastoplastic model normalized by the respective response calculated by the other

- *Model 2 (Moderate strength hardening)*

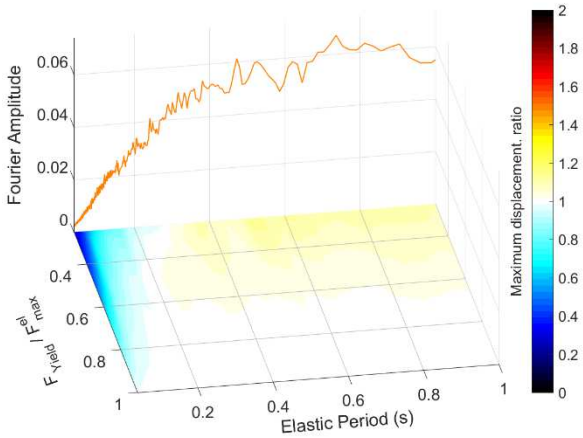

Figure 0.1. Mean maximum displacement ratios for the hysteretic model 2, subjected to all the ground motions.

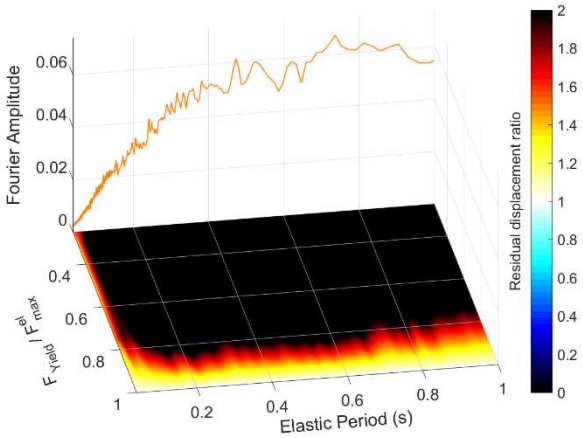

Figure 0.2. Mean residual displacement ratios for the hysteretic model 2, subjected to all the ground motions.

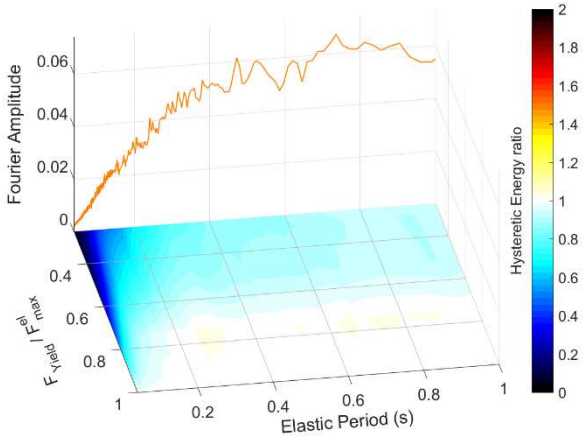

Figure 0.3. Mean total hysteretic energy ratios for the hysteretic model 2, subjected to all the ground motions.

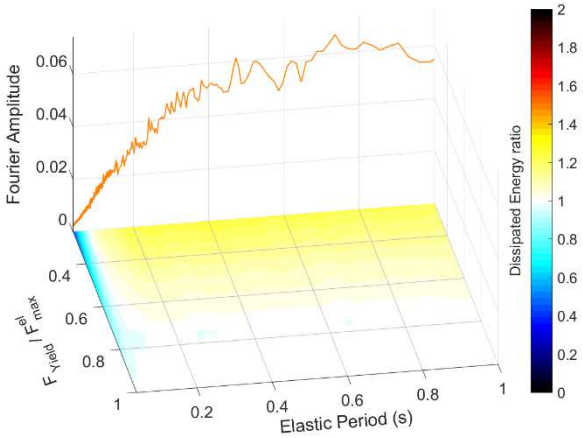

Figure 0.4. Mean total dissipated energy ratios for the hysteretic model 2, subjected to all the ground motions.

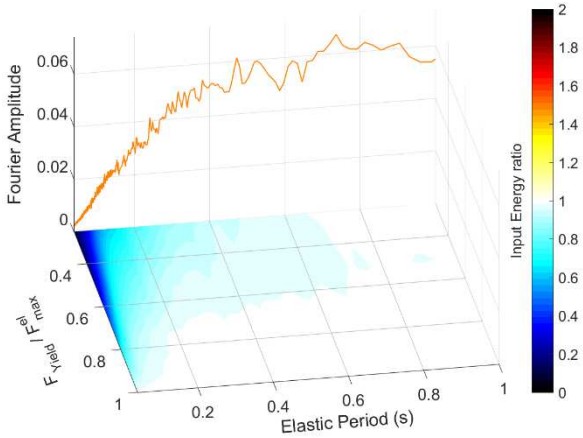

Figure 0.5. Mean total input energy ratios for the hysteretic model 2, subjected to all the ground motions.

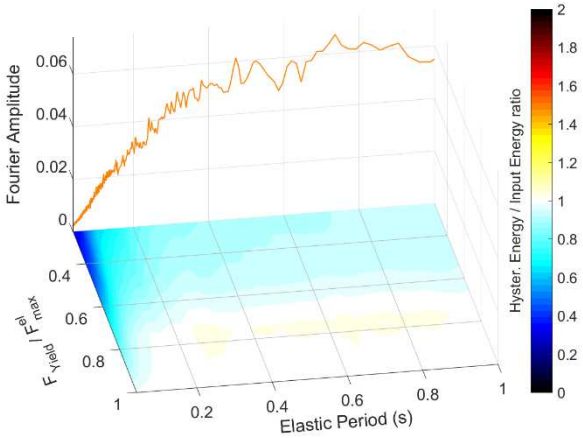

Figure 0.6. Mean ratios of the fractions of the hysteretic energy divided by the input energy for the hysteretic model 2, subjected to all the ground motions.

- *Model 3 (High strength hardening)*

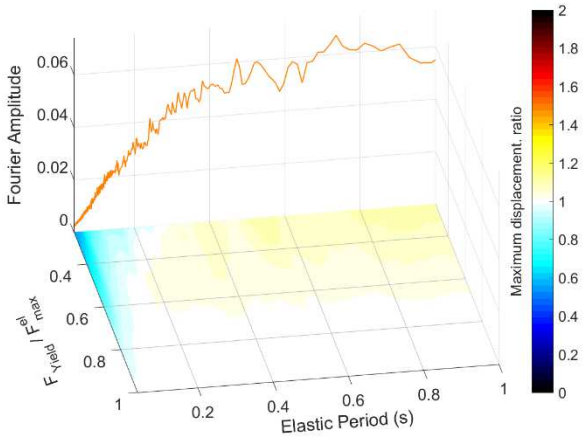

Figure 0.7. Mean maximum displacement ratios for the hysteretic model 3, subjected to all the ground motions.

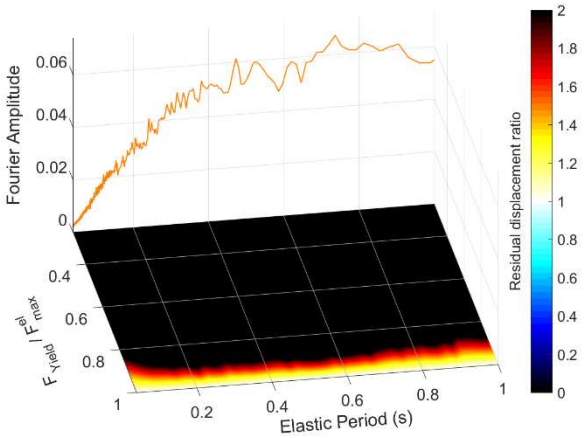

Figure 0.8. Mean residual displacement ratios for the hysteretic model 3, subjected to all the ground motions.

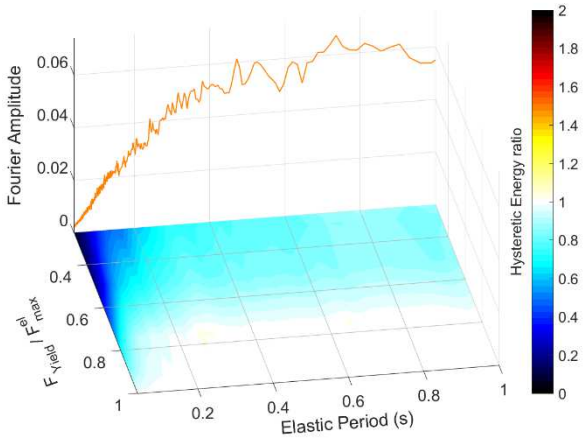

Figure 0.9. Mean total hysteretic energy ratios for the hysteretic model 3, subjected to all the ground motions.

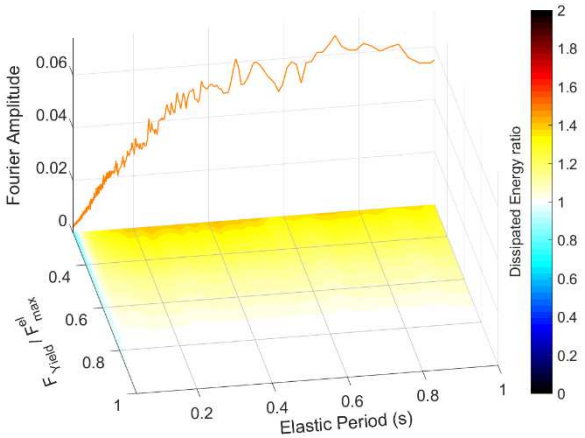

Figure 0.10. Mean total dissipated energy ratios for the hysteretic model 3, subjected to all the ground motions.

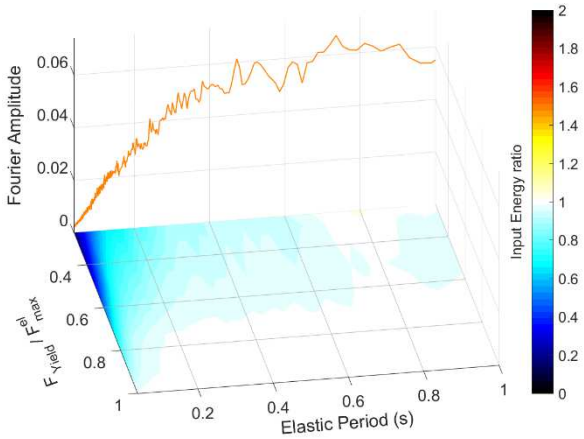

Figure 0.11. Mean total input energy ratios for the hysteretic model 3, subjected to all the ground motions.

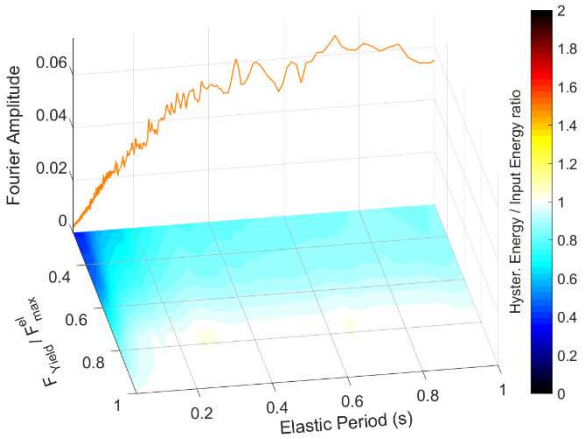

Figure 0.12. Mean ratios of the fractions of the hysteretic energy divided by the input energy for the hysteretic model 3, subjected to all the ground motions.

- *Model 4 (Extreme strength hardening)*

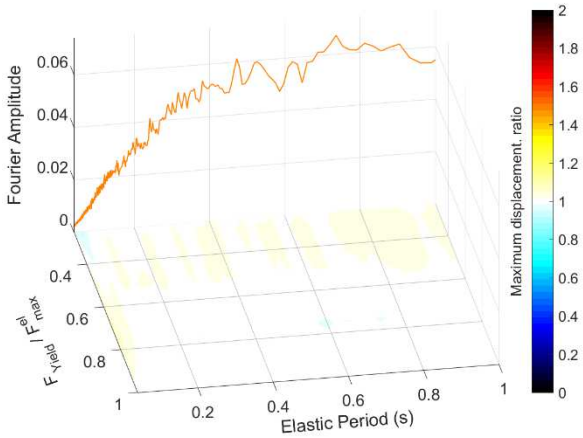

Figure 0.13. Mean maximum displacement ratios for the hysteretic model 4, subjected to all the ground motions.

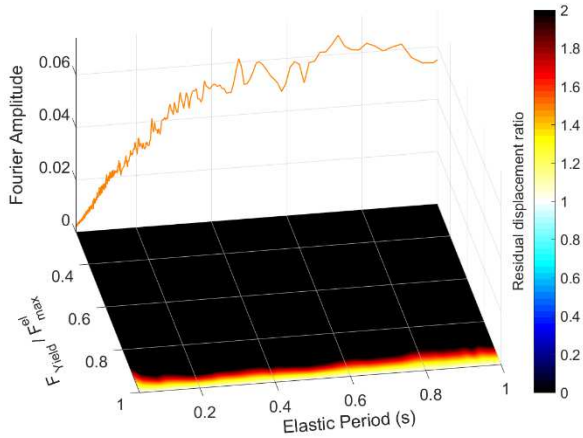

Figure 0.14. Mean residual displacement ratios for the hysteretic model 4, subjected to all the ground motions.

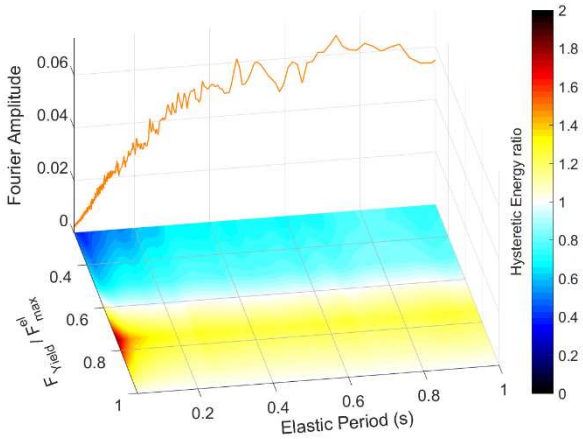

Figure 0.15. Mean total hysteretic energy ratios for the hysteretic model 4, subjected to all the ground motions.

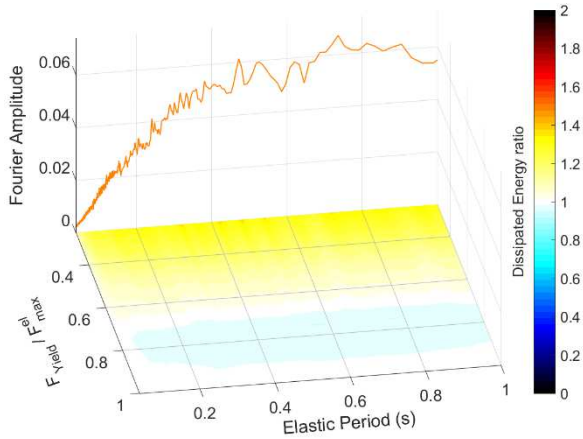

Figure 0.16. Mean total dissipated energy ratios for the hysteretic model 4, subjected to all the ground motions.

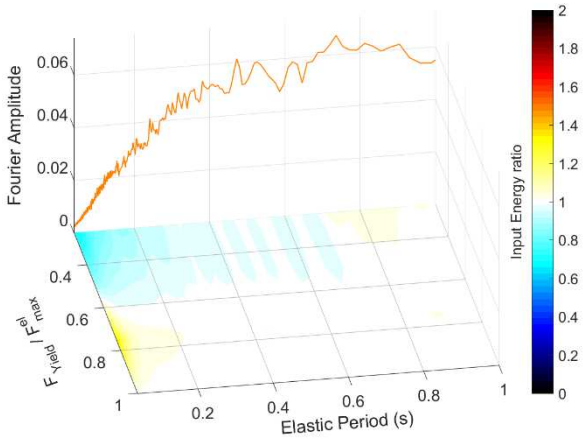

Figure 0.17. Mean total input energy ratios for the hysteretic model 4, subjected to all the ground motions.

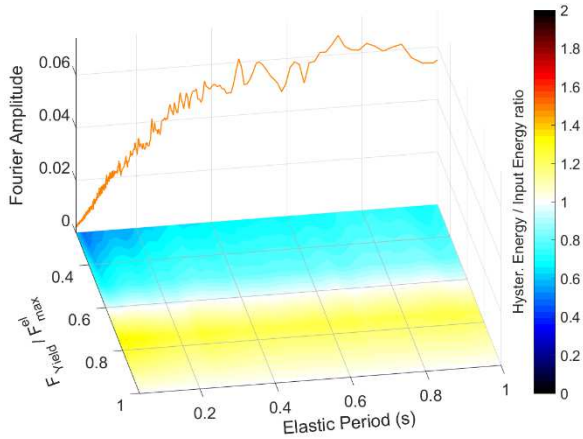

Figure 0.18. Mean ratios of the fractions of the hysteretic energy divided by the input energy for the hysteretic model 4, subjected to all the ground motions.

- *Model 5 (Elastoplastic with low stiffness degradation)*

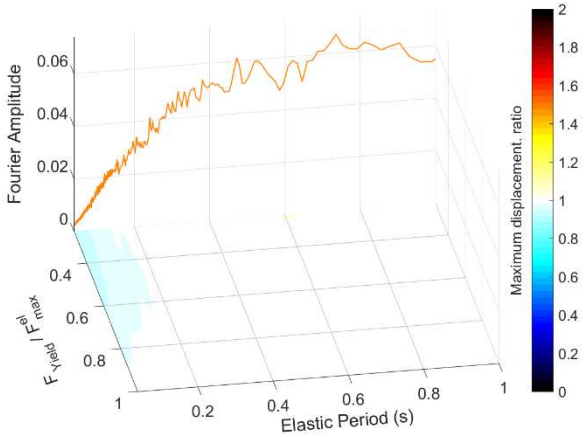

Figure 0.19. Mean maximum displacement ratios for the hysteretic model 5, subjected to all the ground motions.

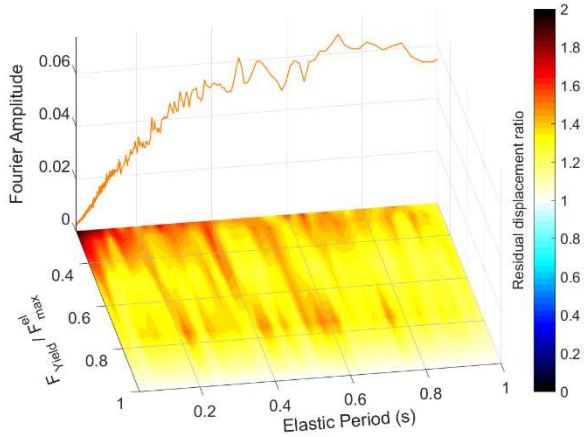

Figure 0.20. Mean residual displacement ratios for the hysteretic model 5, subjected to all the ground motions.

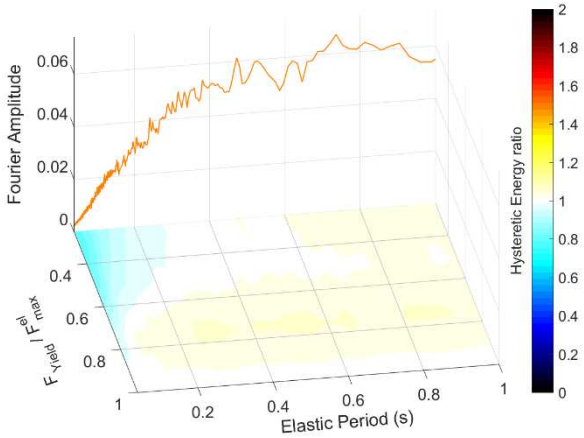

Figure 0.21. Mean total hysteretic energy ratios for the hysteretic model 5, subjected to all the ground motions.

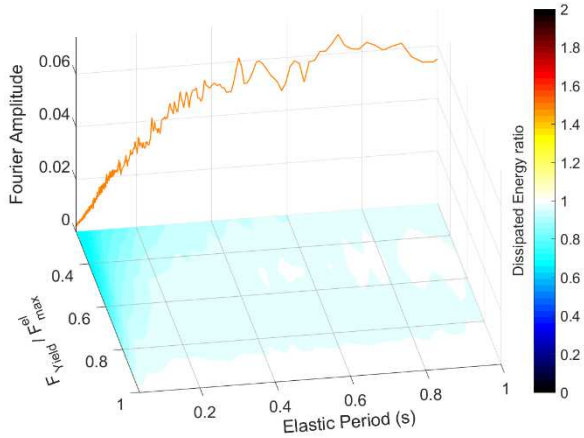

Figure 0.22. Mean total dissipated energy ratios for the hysteretic model 5, subjected to all the ground motions.

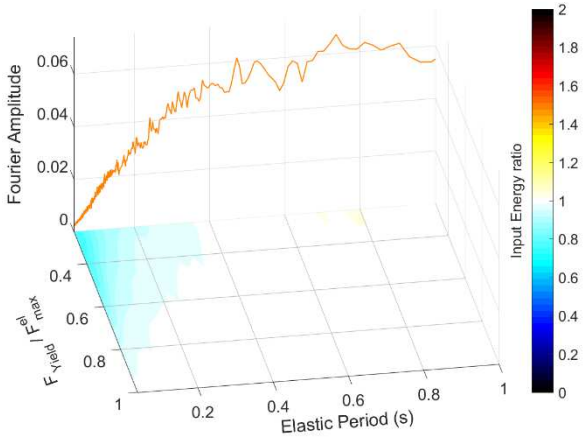

Figure 0.23. Mean total input energy ratios for the hysteretic model 5, subjected to all the ground motions.

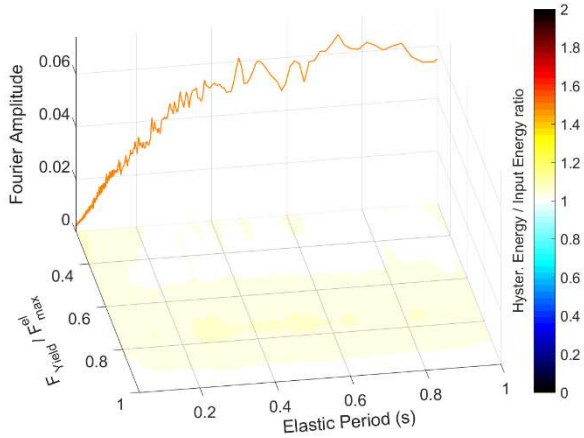

Figure 0.24. Mean ratios of the fractions of the hysteretic energy divided by the input energy for the hysteretic model 5, subjected to all the ground motions.

- *Model 6 (Elastoplastic with high stiffness degradation)*

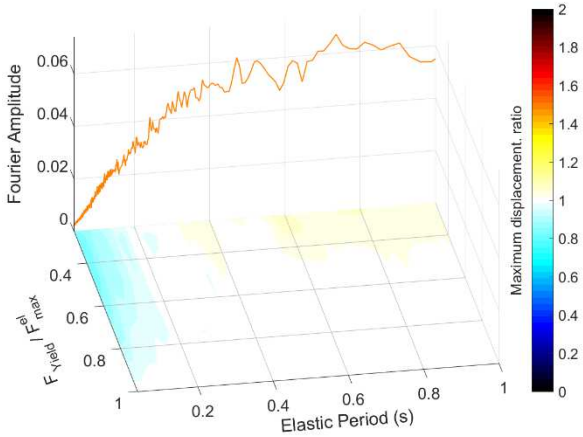

Figure 0.25. Mean maximum displacement ratios for the hysteretic model 6, subjected to all the ground motions.

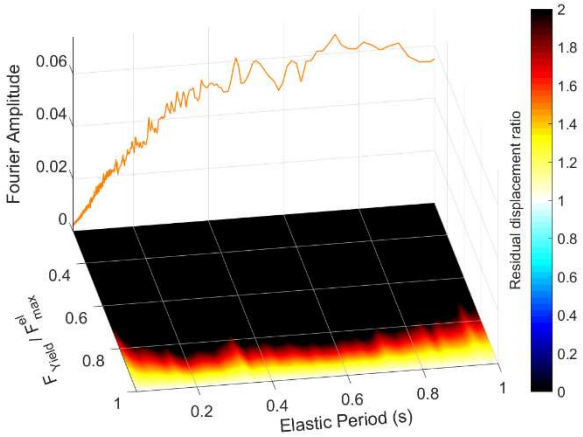

Figure 0.26. Mean residual displacement ratios for the hysteretic model 6, subjected to all the ground motions.

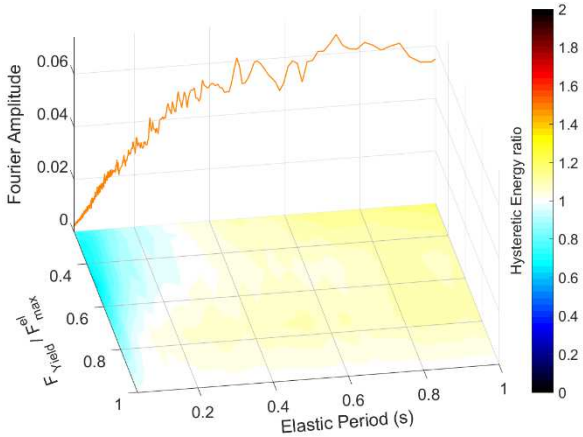

Figure 0.27. Mean total hysteretic energy ratios for the hysteretic model 6, subjected to all the ground motions.

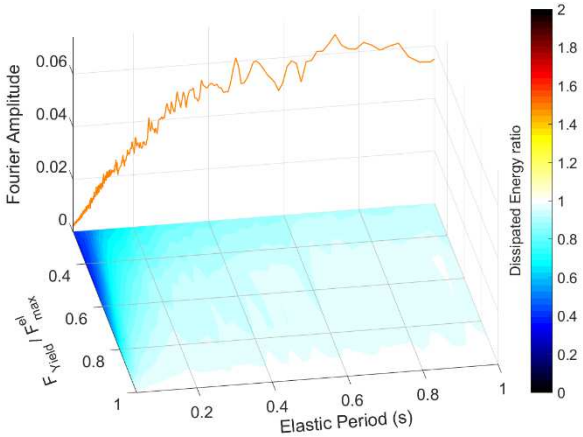

Figure 0.28. Mean total dissipated energy ratios for the hysteretic model 6, subjected to all the ground motions.

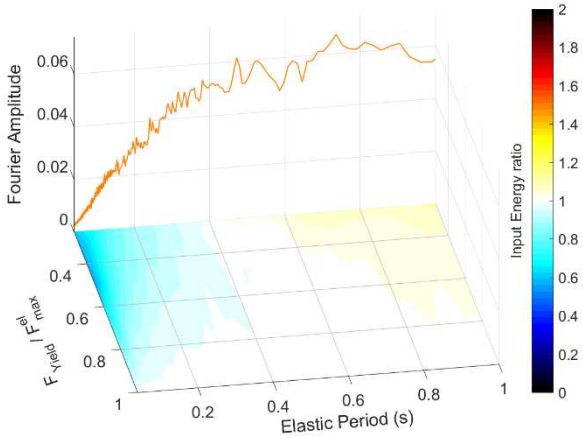

Figure 0.29. Mean total input energy ratios for the hysteretic model 6, subjected to all the ground motions.

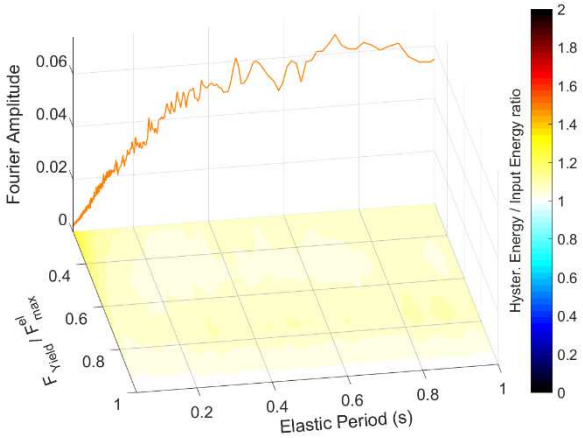

Figure 0.30. Mean ratios of the fractions of the hysteretic energy divided by the input energy for the hysteretic model 6, subjected to all the ground motions.

- *Model 7 (Strength hardening with low stiffness degradation)*

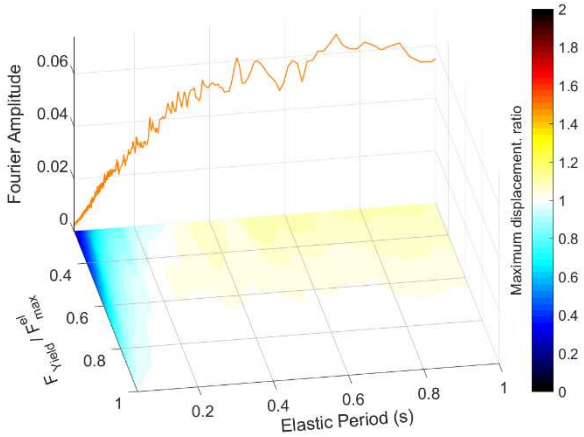

Figure 0.31. Mean maximum displacement ratios for the hysteretic model 7, subjected to all the ground motions.

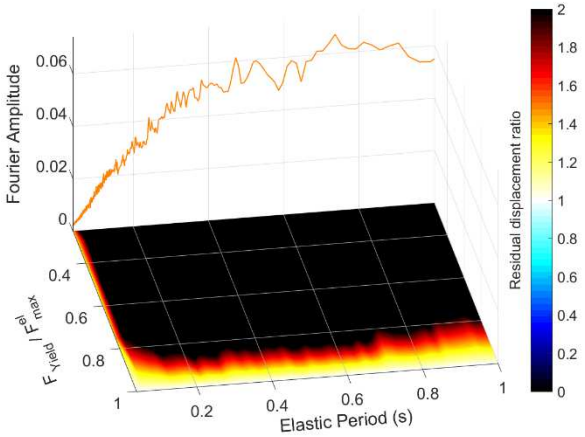

Figure 0.32. Mean residual displacement ratios for the hysteretic model 7, subjected to all the ground motions.

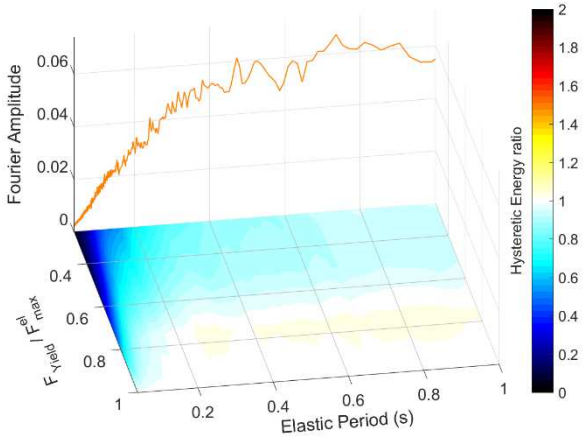

Figure 0.33. Mean total hysteretic energy ratios for the hysteretic model 7, subjected to all the ground motions.

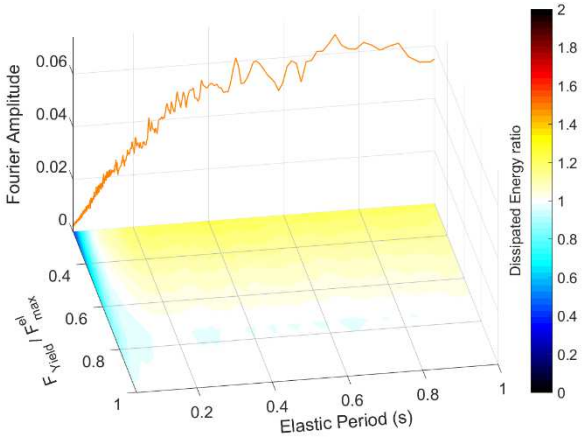

Figure 0.34. Mean total dissipated energy ratios for the hysteretic model 7, subjected to all the ground motions.

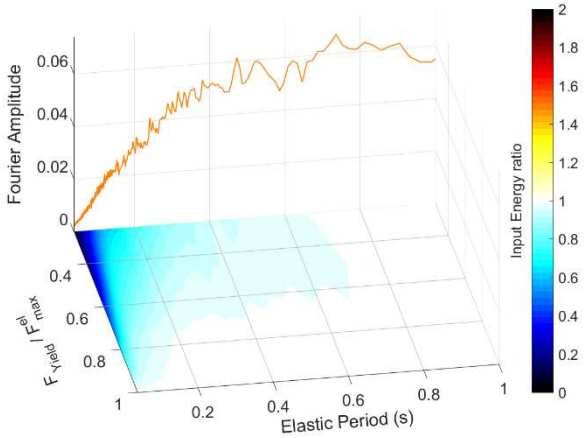

Figure 0.35. Mean total input energy ratios for the hysteretic model 7, subjected to all the ground motions.

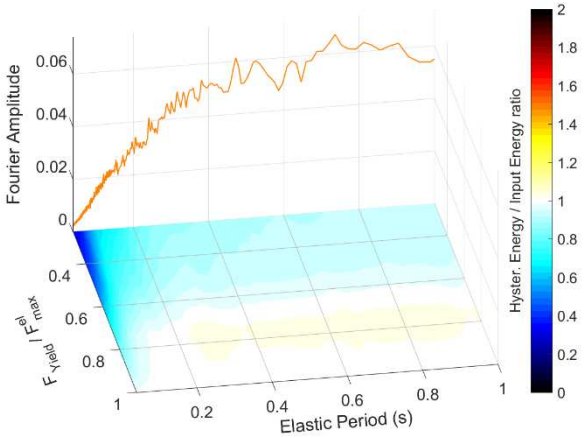

Figure 0.36. Mean ratios of the fractions of the hysteretic energy divided by the input energy for the hysteretic model 7, subjected to all the ground motions.

- *Model 8 (Strength hardening with moderate stiffness degradation)*

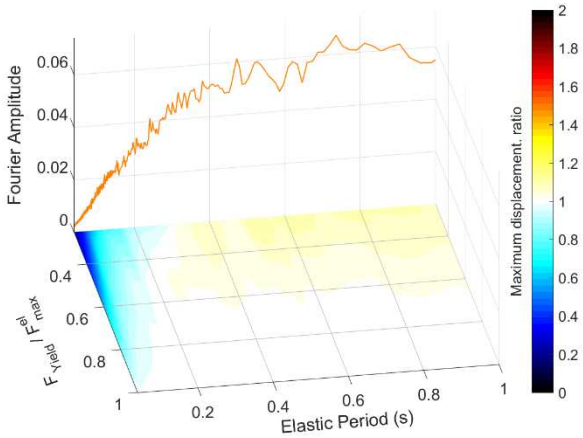

Figure 0.37. Mean maximum displacement ratios for the hysteretic model 8, subjected to all the ground motions.

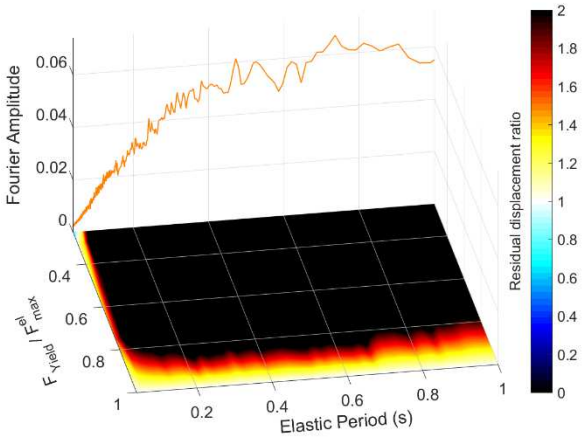

Figure 0.38. Mean residual displacement ratios for the hysteretic model 8, subjected to all the ground motions.

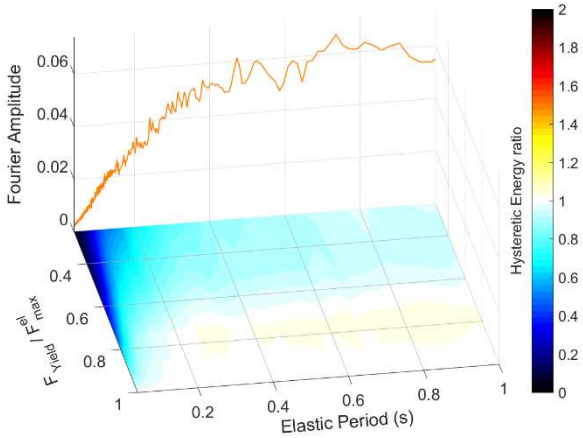

Figure 0.39. Mean total hysteretic energy ratios for the hysteretic model 8, subjected to all the ground motions.

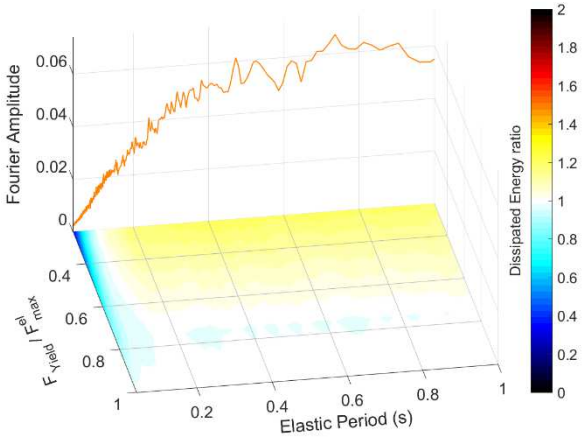

Figure 0.40. Mean total dissipated energy ratios for the hysteretic model 8, subjected to all the ground motions.

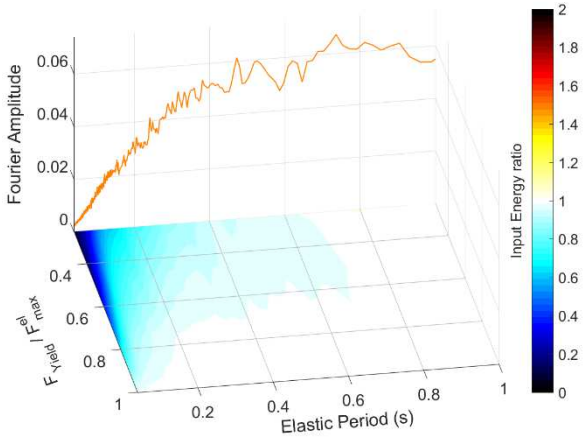

Figure 0.41. Mean total input energy ratios for the hysteretic model 8, subjected to all the ground motions.

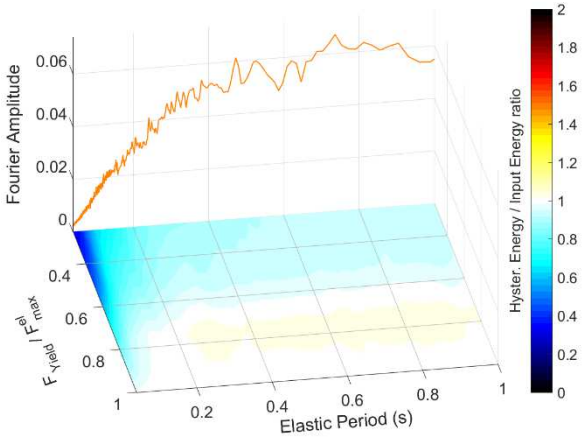

Figure 0.42. Mean ratios of the fractions of the hysteretic energy divided by the input energy for the hysteretic model 8, subjected to all the ground motions.

- *Model 9 (Strength hardening with moderate stiffness degradation)*

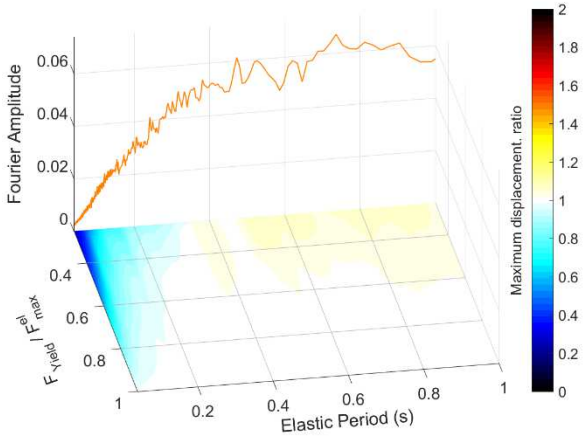

Figure 0.43. Mean maximum displacement ratios for the hysteretic model 9, subjected to all the ground motions.

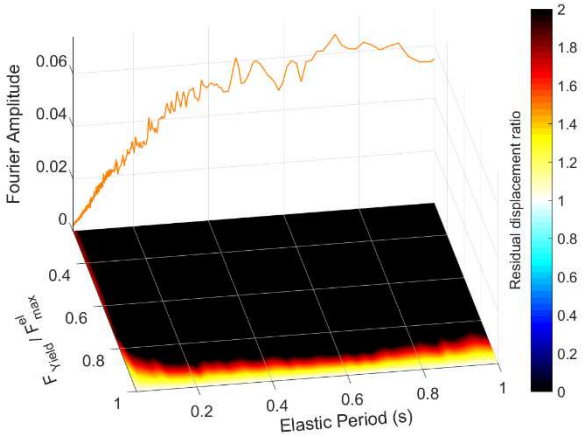

Figure 0.44. Mean residual displacement ratios for the hysteretic model 9, subjected to all the ground motions.

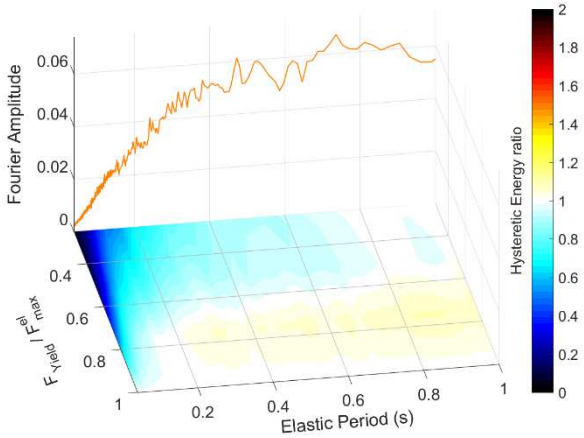

Figure 0.45. Mean total hysteretic energy ratios for the hysteretic model 9, subjected to all the ground motions.

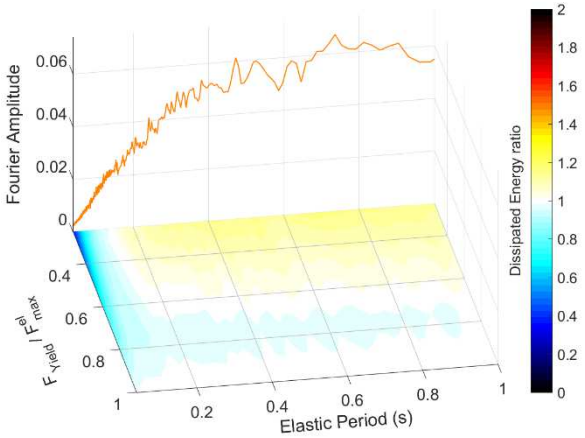

Figure 0.46. Mean total dissipated energy ratios for the hysteretic model 9, subjected to all the ground motions.

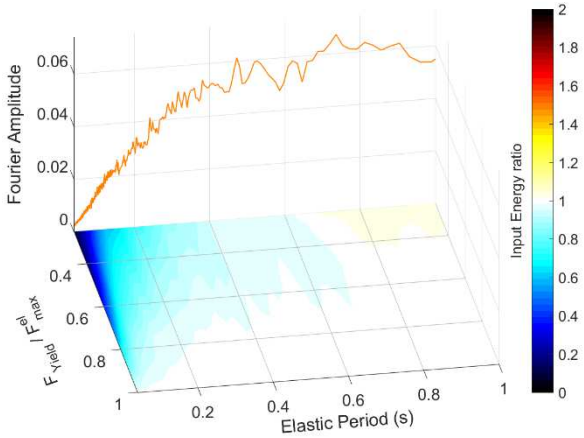

Figure 0.47. Mean total input energy ratios for the hysteretic model 9, subjected to all the ground motions.

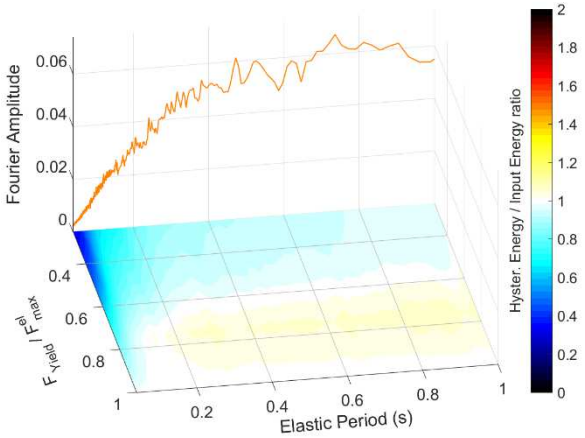

Figure 0.48. Mean ratios of the fractions of the hysteretic energy divided by the input energy for the hysteretic model 9, subjected to all the ground motions.

- *Model 10 (Strength hardening with high stiffness degradation)*

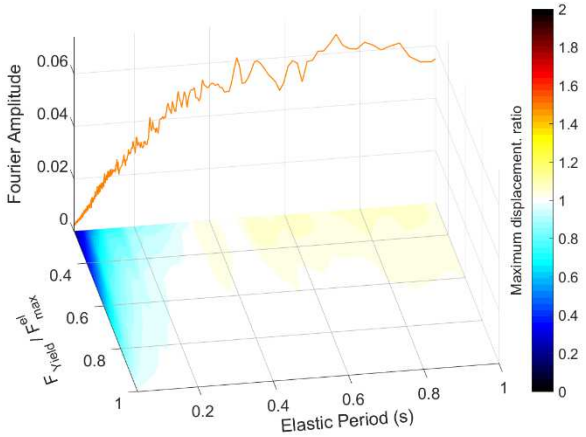

Figure 0.49. Mean maximum displacement ratios for the hysteretic model 10, subjected to all the ground motions.

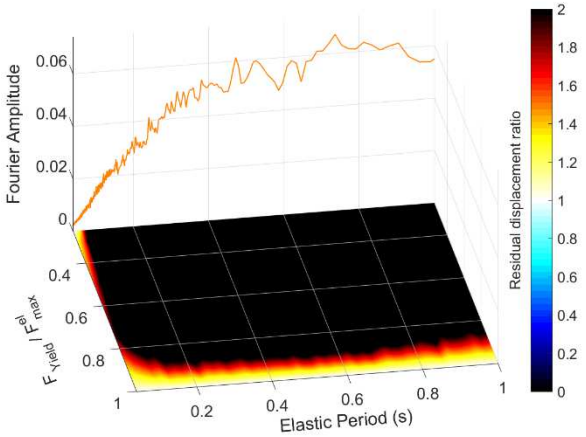

Figure 0.50. Mean residual displacement ratios for the hysteretic model 10, subjected to all the ground motions.

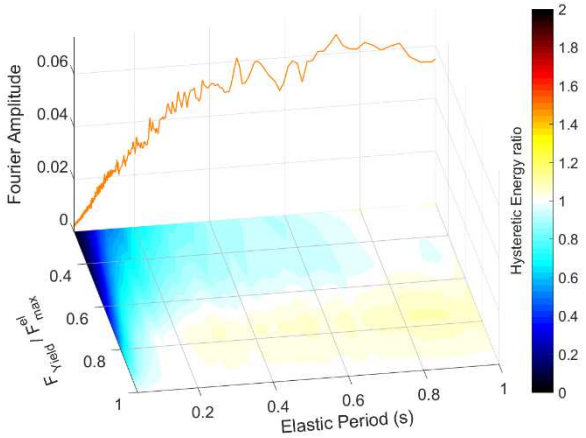

Figure 0.51. Mean total hysteretic energy ratios for the hysteretic model 10, subjected to all the ground motions.

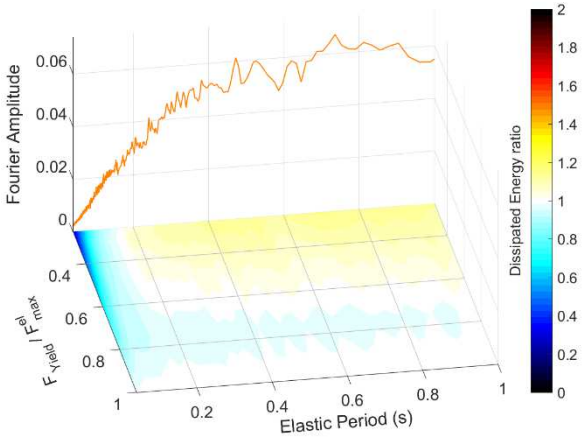

Figure 0.52. Mean total dissipated energy ratios for the hysteretic model 10, subjected to all the ground motions.

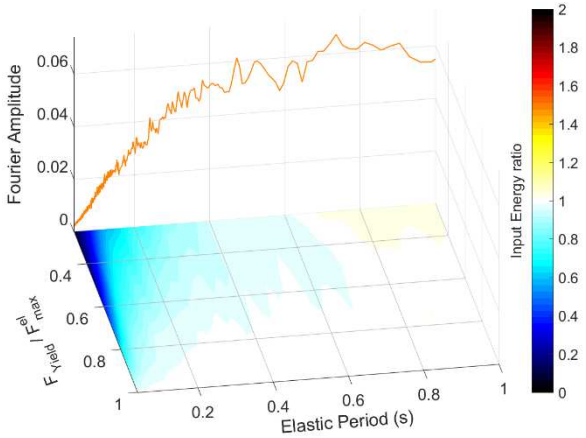

Figure 0.53. Mean total input energy ratios for the hysteretic model 10, subjected to all the ground motions.

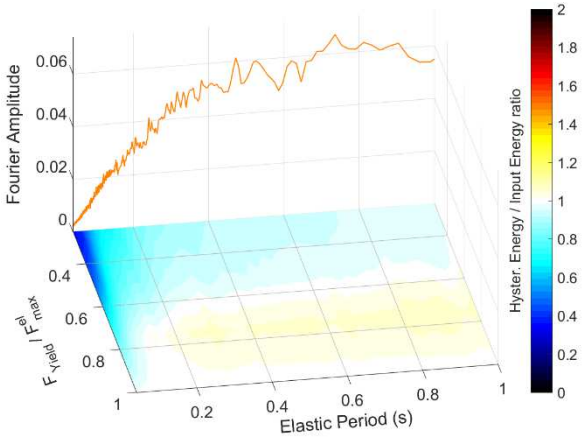

Figure 0.54. Mean ratios of the fractions of the hysteretic energy divided by the input energy for the hysteretic model 10, subjected to all the ground motions.

- *Model 11 (Elastoplastic with low strength deterioration)*

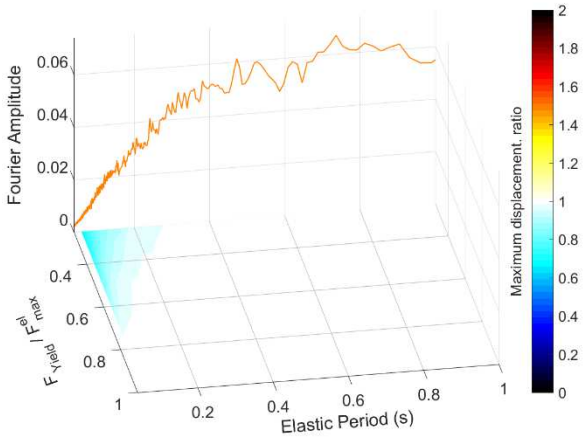

Figure 0.55. Mean maximum displacement ratios for the hysteretic model 11, subjected to all the ground motions.

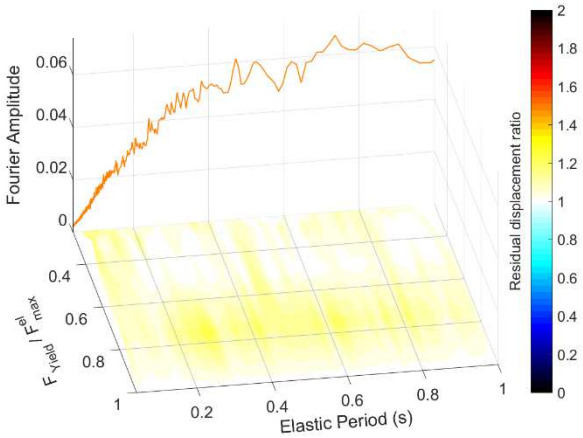

Figure 0.56. Mean residual displacement ratios for the hysteretic model 11, subjected to all the ground motions.

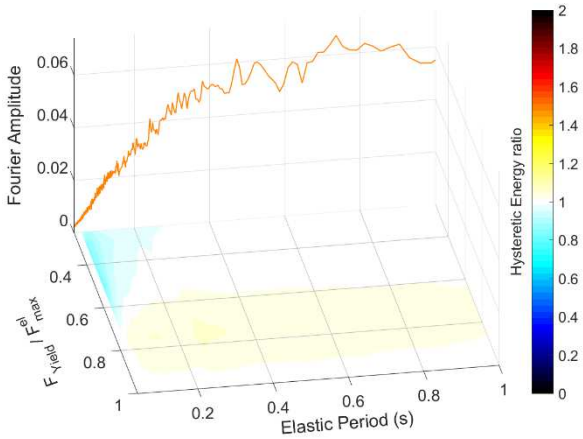

Figure 0.57. Mean total hysteretic energy ratios for the hysteretic model 11, subjected to all the ground motions.

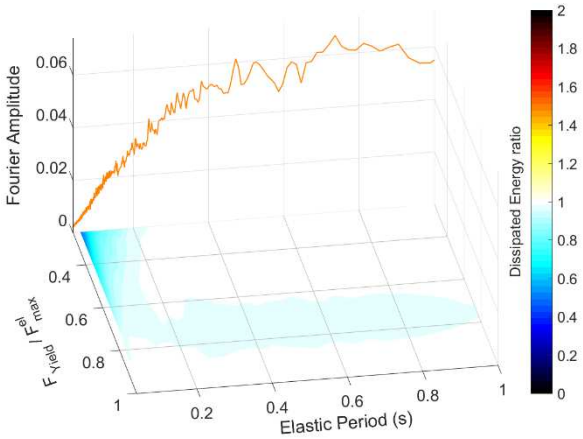

Figure 0.58. Mean total dissipated energy ratios for the hysteretic model 11, subjected to all the ground motions.

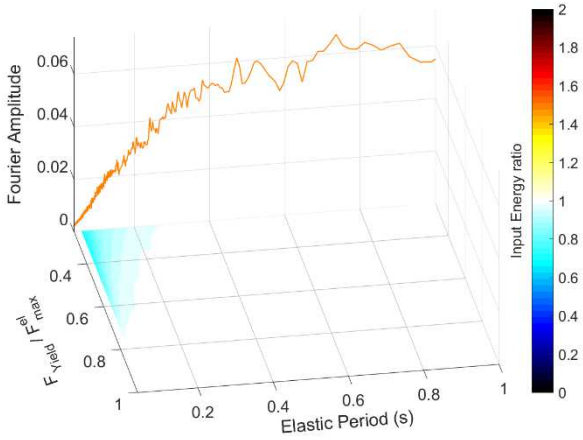

Figure 0.59. Mean total input energy ratios for the hysteretic model 11, subjected to all the ground motions.

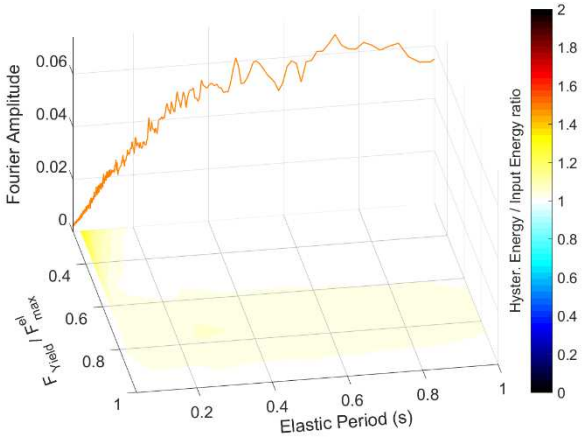

Figure 0.60. Mean ratios of the fractions of the hysteretic energy divided by the input energy for the hysteretic model 11, subjected to all the ground motions.

- *Model 12 (Elastoplastic with moderate strength deterioration)*

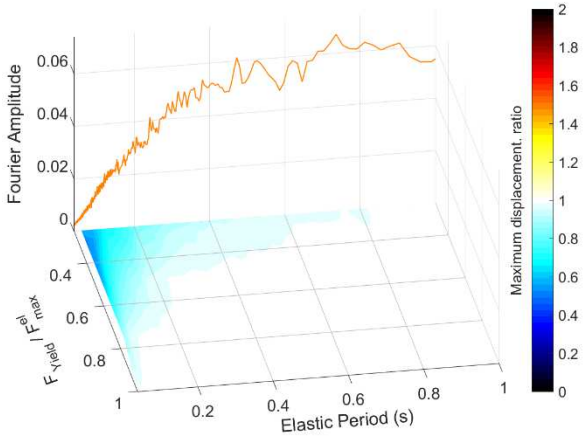

Figure 0.61. Mean maximum displacement ratios for the hysteretic model 12, subjected to all the ground motions.

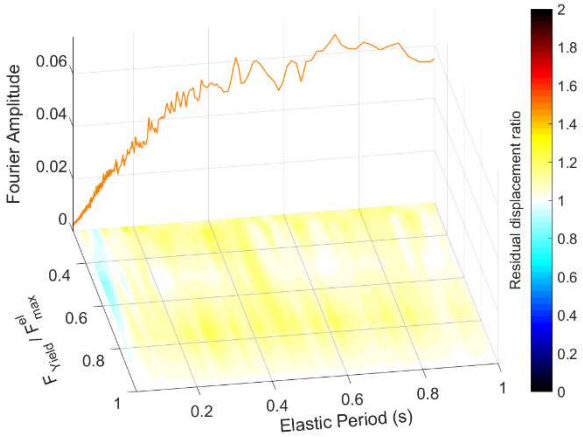

Figure 0.62. Mean residual displacement ratios for the hysteretic model 12, subjected to all the ground motions.

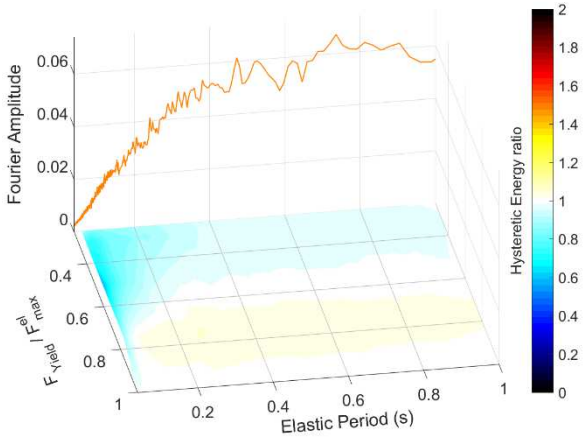

Figure 0.63. Mean total hysteretic energy ratios for the hysteretic model 12, subjected to all the ground motions.

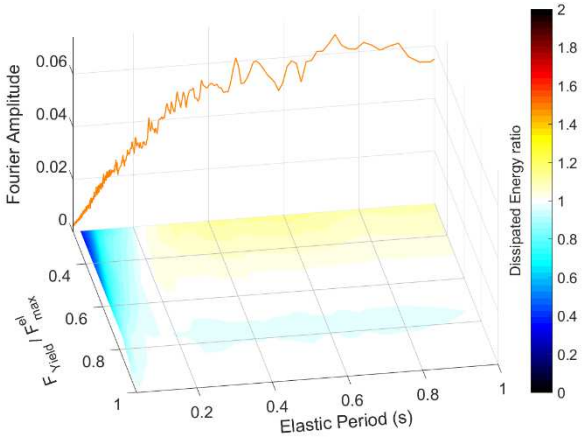

Figure 0.64. Mean total dissipated energy ratios for the hysteretic model 12, subjected to all the ground motions.

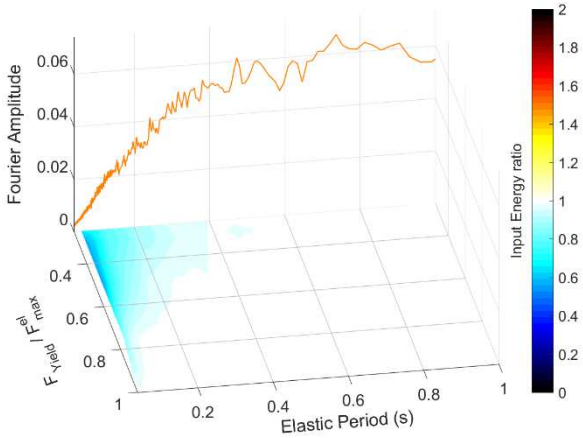

Figure 0.65. Mean total input energy ratios for the hysteretic model 12, subjected to all the ground motions.

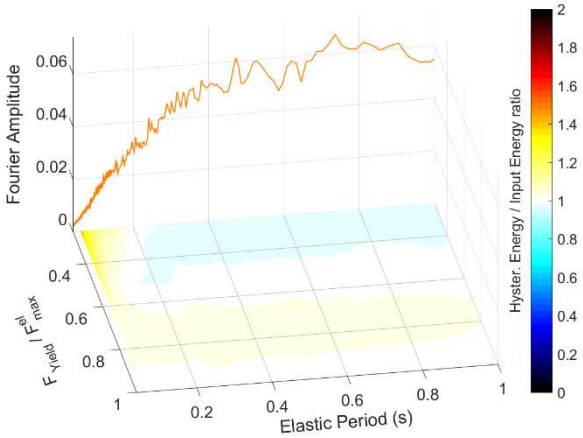

Figure 0.66. Mean ratios of the fractions of the hysteretic energy divided by the input energy for the hysteretic model 12, subjected to all the ground motions.

- *Model 13 (Elastoplastic with moderate strength deterioration)*

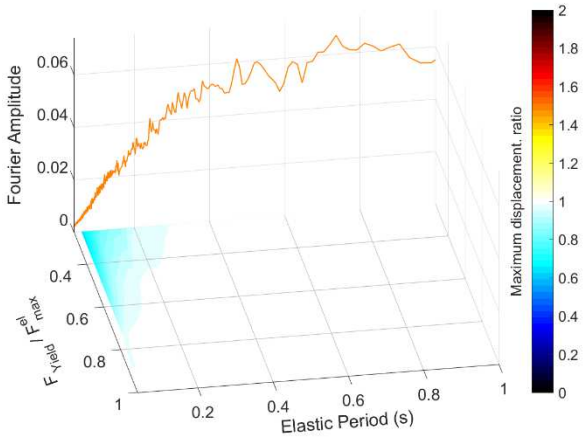

Figure 0.67. Mean maximum displacement ratios for the hysteretic model 13, subjected to all the ground motions.

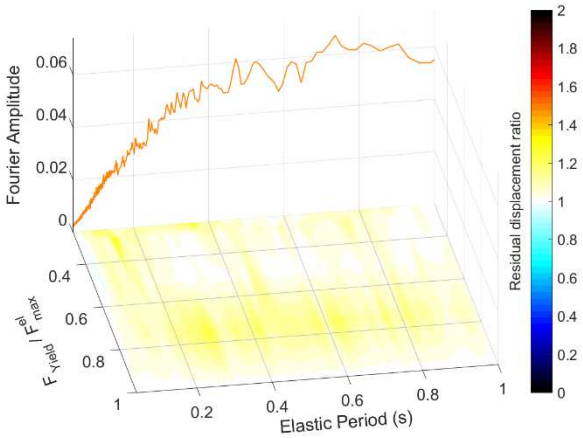

Figure 0.68. Mean residual displacement ratios for the hysteretic model 13, subjected to all the ground motions.

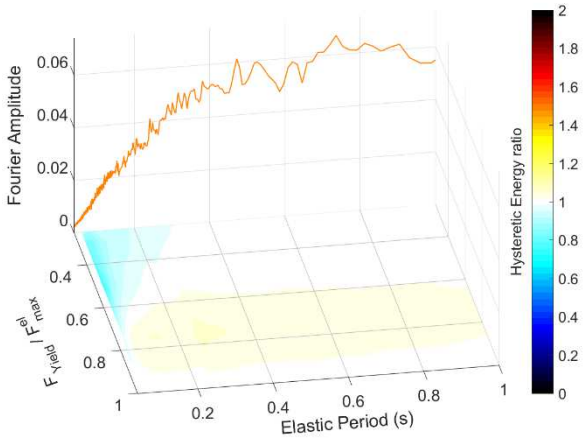

Figure 0.69. Mean total hysteretic energy ratios for the hysteretic model 13, subjected to all the ground motions.

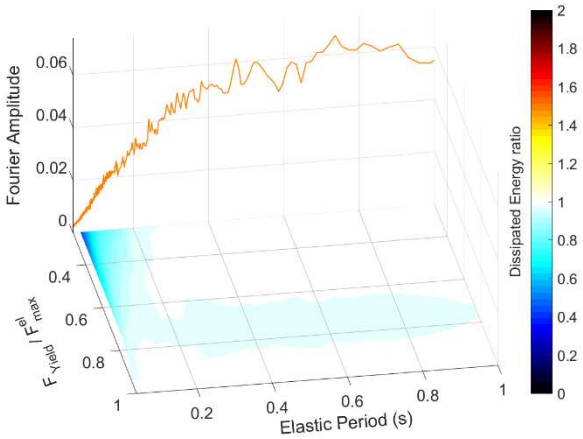

Figure 0.70. Mean total dissipated energy ratios for the hysteretic model 13, subjected to all the ground motions.

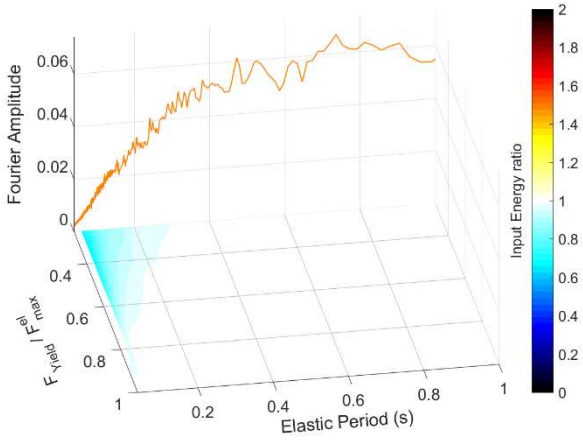

Figure 0.71. Mean total input energy ratios for the hysteretic model 13, subjected to all the ground motions.

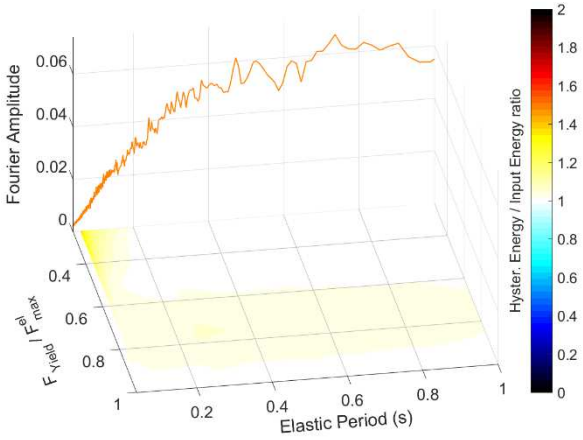

Figure 0.72. Mean ratios of the fractions of the hysteretic energy divided by the input energy for the hysteretic model 13, subjected to all the ground motions.

- *Model 14 (Elastoplastic with high strength deterioration)*

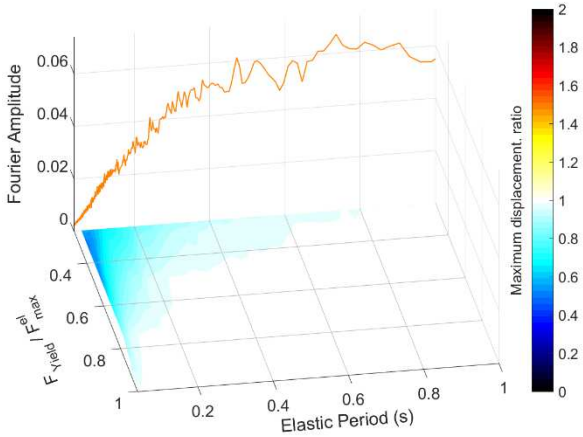

Figure 0.73. Mean maximum displacement ratios for the hysteretic model 14, subjected to all the ground motions.

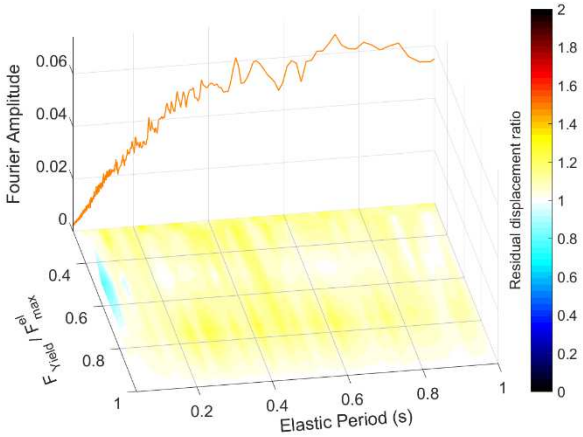

Figure 0.74. Mean residual displacement ratios for the hysteretic model 14, subjected to all the ground motions.

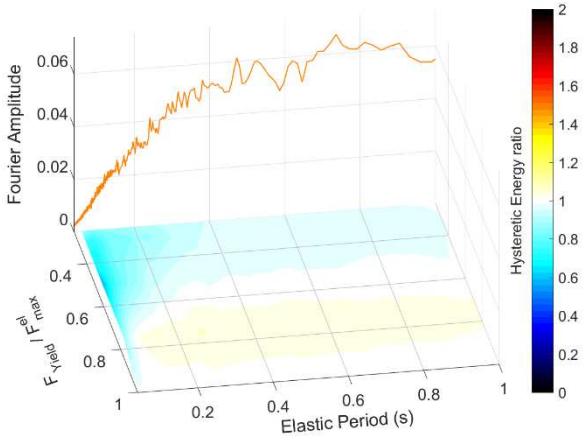

Figure 0.75. Mean total hysteretic energy ratios for the hysteretic model 14, subjected to all the ground motions.

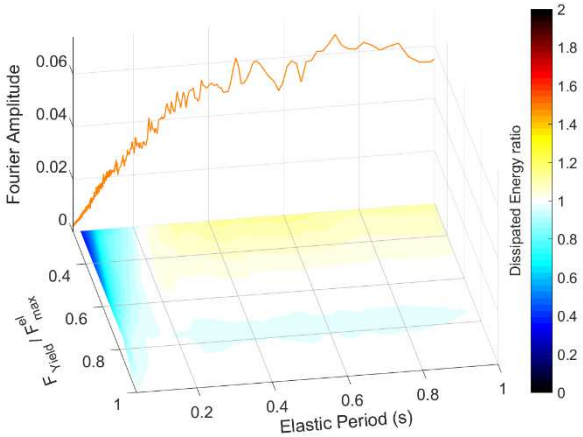

Figure 0.76. Mean total dissipated energy ratios for the hysteretic model 14, subjected to all the ground motions.

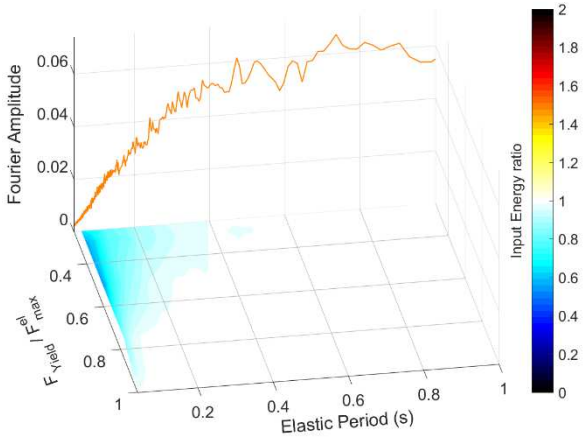

Figure 0.77. Mean total input energy ratios for the hysteretic model 14, subjected to all the ground motions.

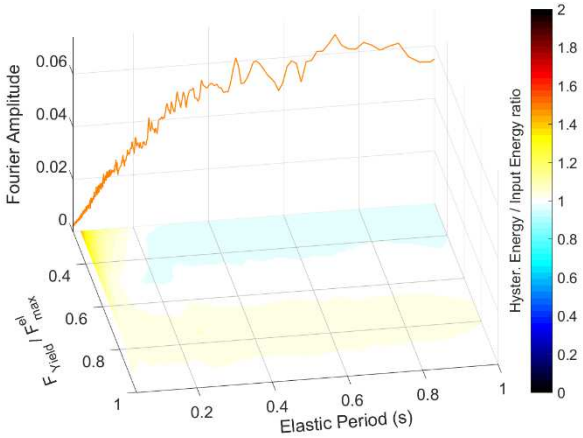

Figure 0.78. Mean ratios of the fractions of the hysteretic energy divided by the input energy for the hysteretic model 14, subjected to all the ground motions.

- *Model 15 (Strength hardening, with stiffness degradation and with low strength deterioration)*

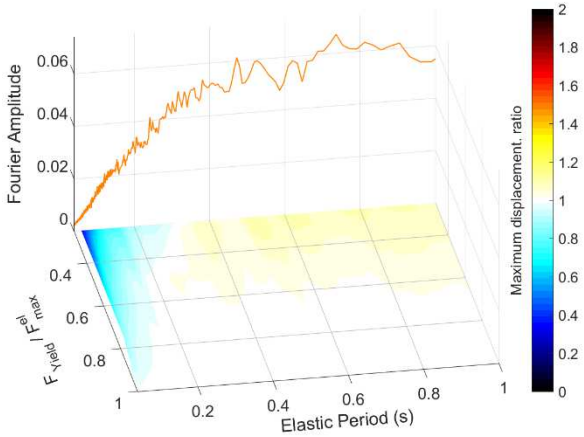

Figure 0.79. Mean maximum displacement ratios for the hysteretic model 15, subjected to all the ground motions.

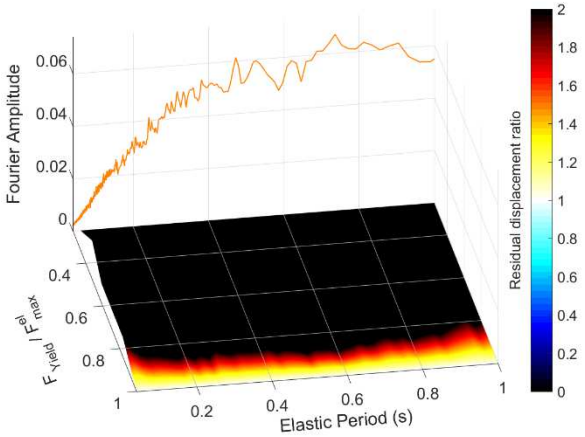

Figure 0.80. Mean residual displacement ratios for the hysteretic model 15, subjected to all the ground motions.

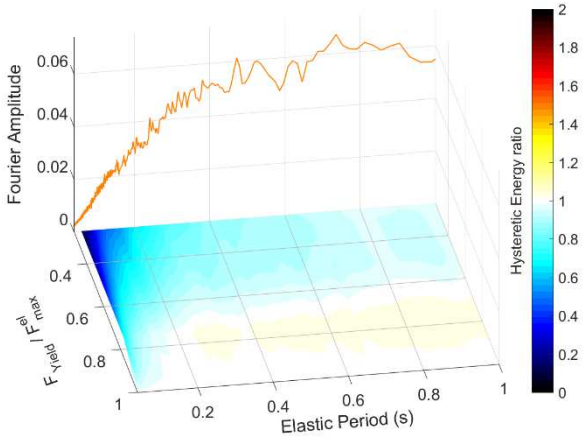

Figure 0.81. Mean total hysteretic energy ratios for the hysteretic model 15, subjected to all the ground motions.

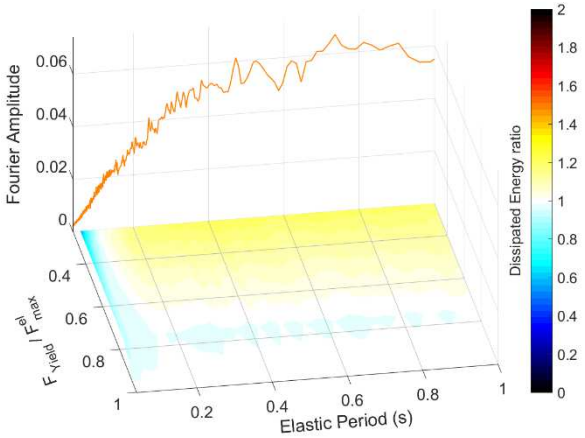

Figure 0.82. Mean total dissipated energy ratios for the hysteretic model 15, subjected to all the ground motions.

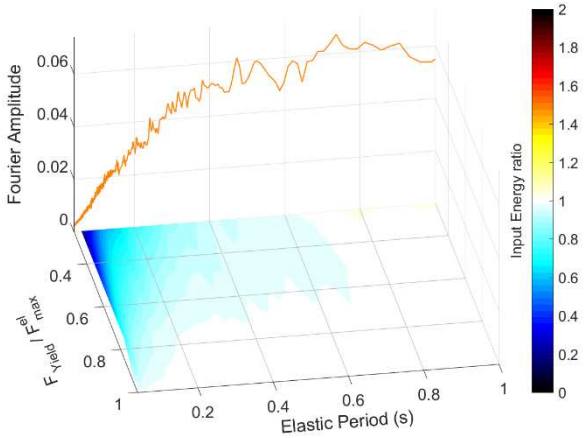

Figure 0.83. Mean total input energy ratios for the hysteretic model 15, subjected to all the ground motions.

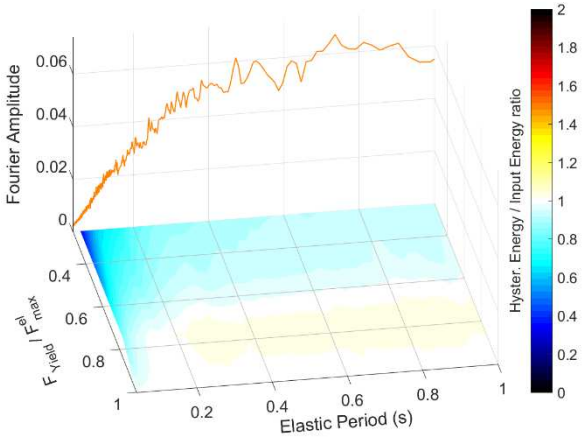

Figure 0.84. Mean ratios of the fractions of the hysteretic energy divided by the input energy for the hysteretic model 15, subjected to all the ground motions.

- *Model 16 (Strength hardening, with stiffness degradation and with moderate strength deterioration)*

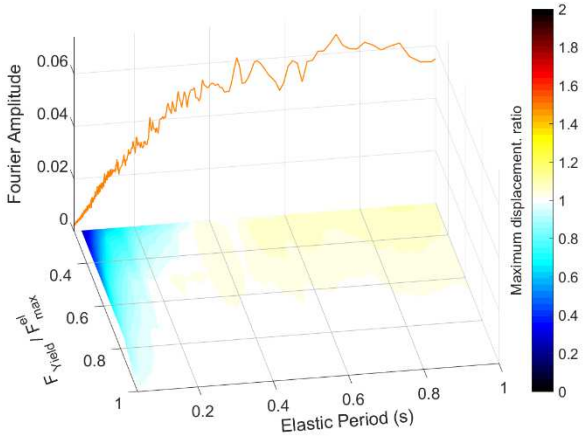

Figure 0.85. Mean maximum displacement ratios for the hysteretic model 16, subjected to all the ground motions.

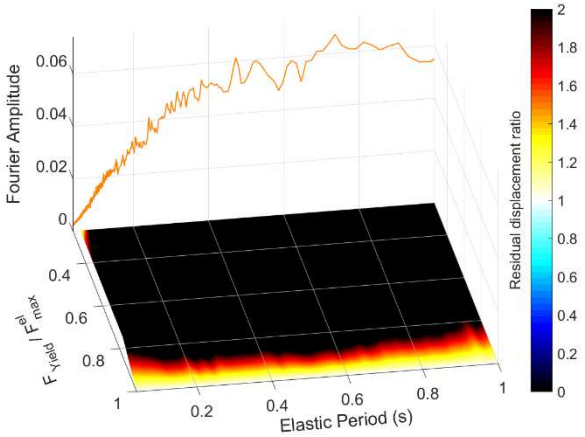

Figure 0.86. Mean residual displacement ratios for the hysteretic model 16, subjected to all the ground motions.

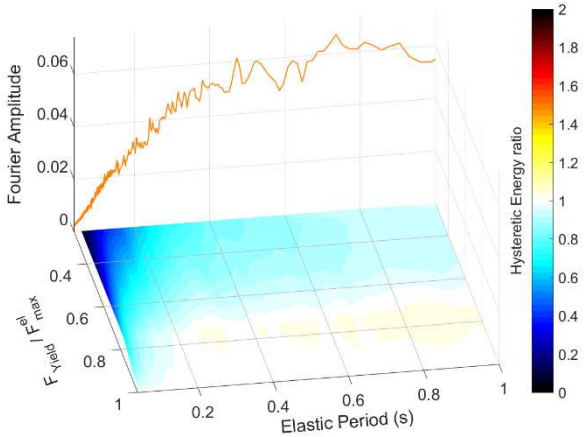

Figure 0.87. Mean total hysteretic energy ratios for the hysteretic model 16, subjected to all the ground motions.

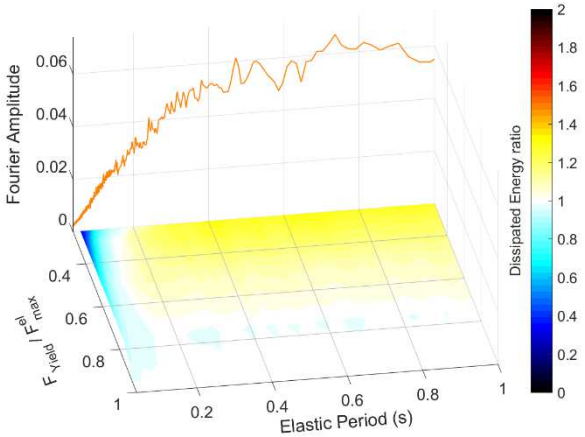

Figure 0.88. Mean total dissipated energy ratios for the hysteretic model 16, subjected to all the ground motions.

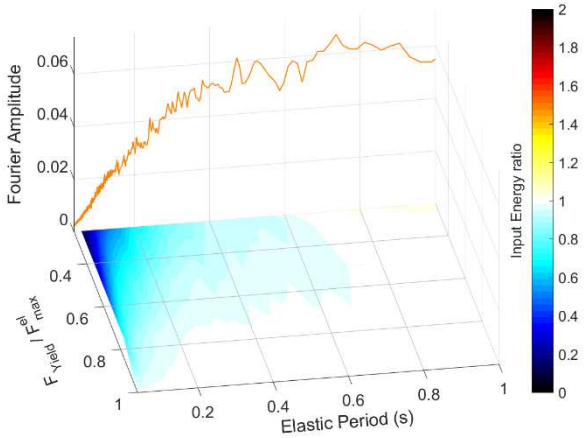

Figure 0.89. Mean total input energy ratios for the hysteretic model 16, subjected to all the ground motions.

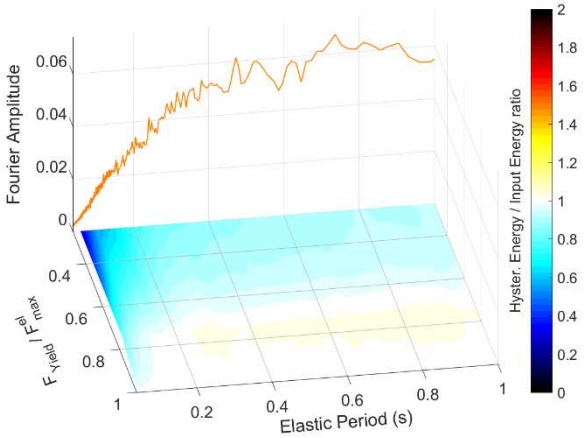

Figure 0.90. Mean ratios of the fractions of the hysteretic energy divided by the input energy for the hysteretic model 16, subjected to all the ground motions.

- *Model 17 (Strength hardening, with stiffness degradation and with moderate strength deterioration)*

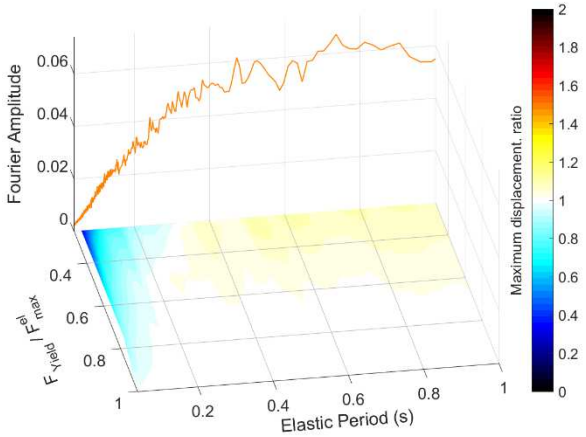

Figure 0.91. Mean maximum displacement ratios for the hysteretic model 17, subjected to all the ground motions.

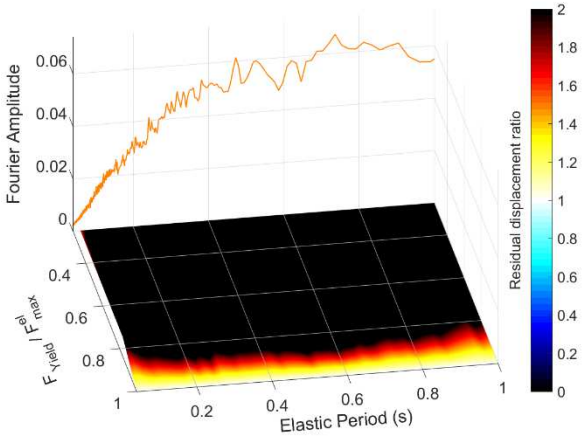

Figure 0.92. Mean residual displacement ratios for the hysteretic model 17, subjected to all the ground motions.

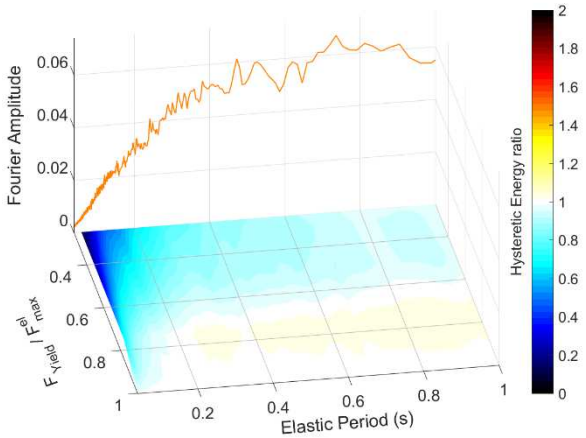

Figure 0.93. Mean total hysteretic energy ratios for the hysteretic model 17, subjected to all the ground motions.

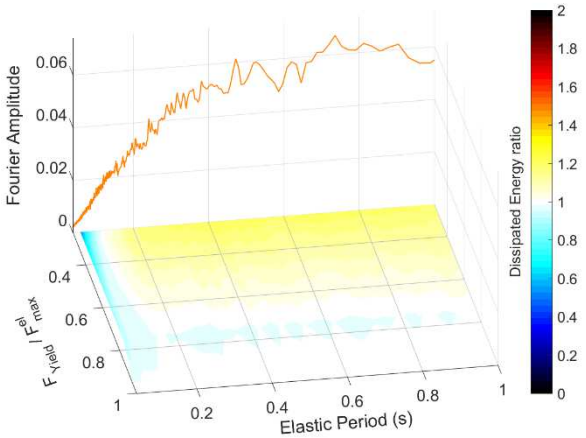

Figure 0.94. Mean total dissipated energy ratios for the hysteretic model 17, subjected to all the ground motions.

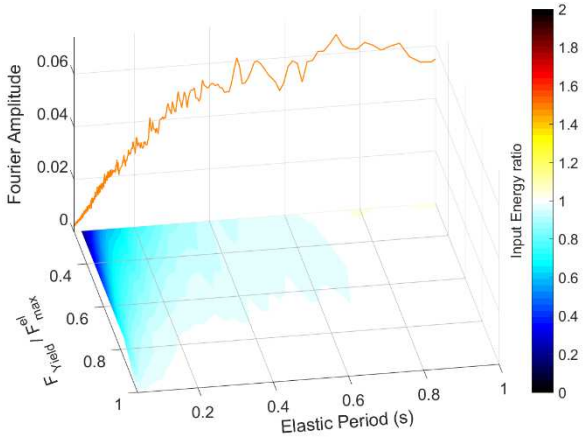

Figure 0.95. Mean total input energy ratios for the hysteretic model 17, subjected to all the ground motions.

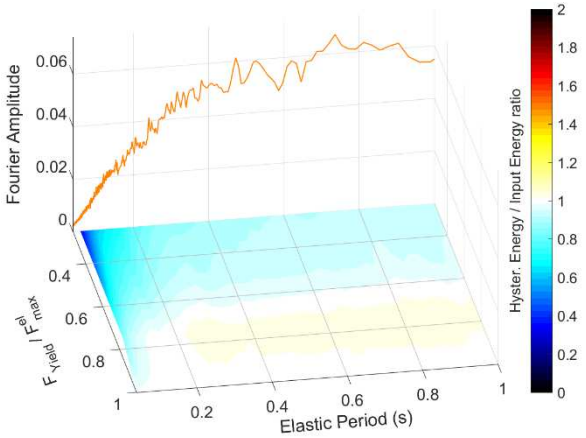

Figure 0.96. Mean ratios of the fractions of the hysteretic energy divided by the input energy for the hysteretic model 17, subjected to all the ground motions.

- *Model 18 (Strength hardening, with stiffness degradation and with high strength deterioration)*

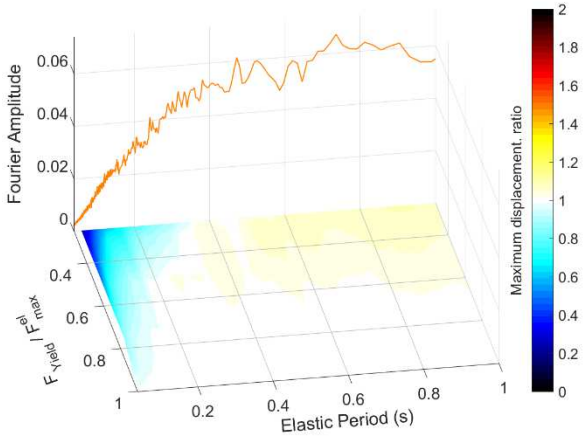

Figure 0.97. Mean maximum displacement ratios for the hysteretic model 18, subjected to all the ground motions.

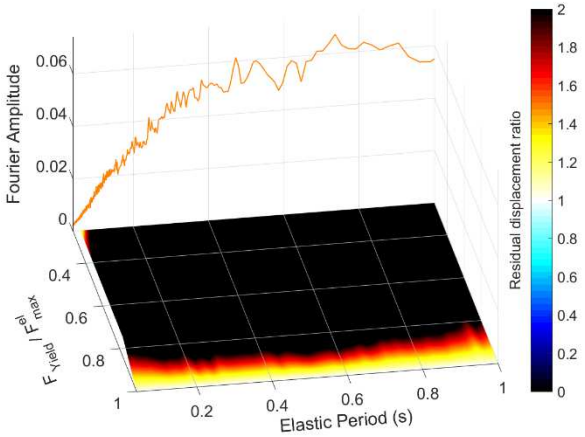

Figure 0.98. Mean residual displacement ratios for the hysteretic model 18, subjected to all the ground motions.

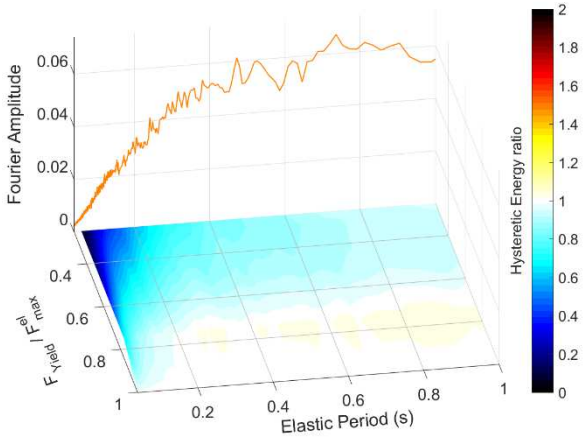

Figure 0.99. Mean total hysteretic energy ratios for the hysteretic model 18, subjected to all the ground motions.

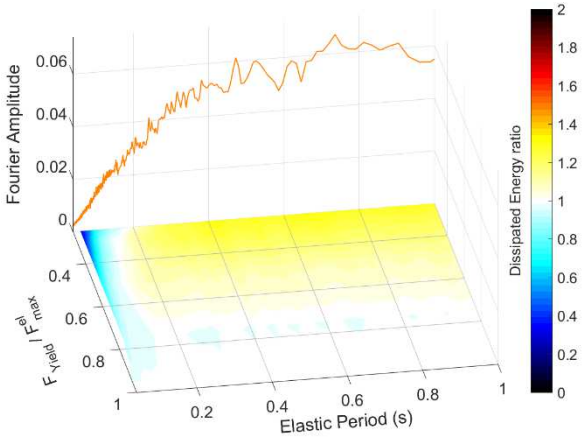

Figure 0.100. Mean total dissipated energy ratios for the hysteretic model 18, subjected to all the ground motions.

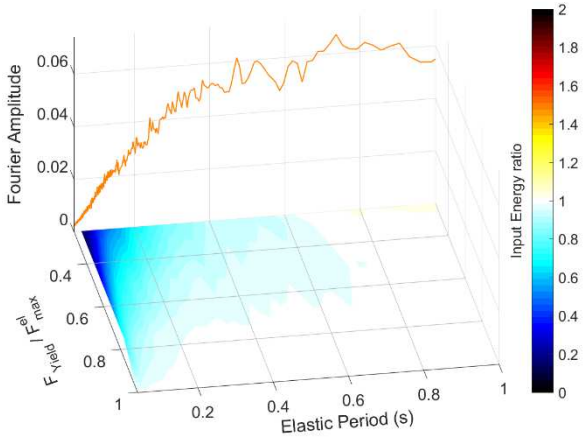

Figure 0.101. Mean total input energy ratios for the hysteretic model 18, subjected to all the ground motions.

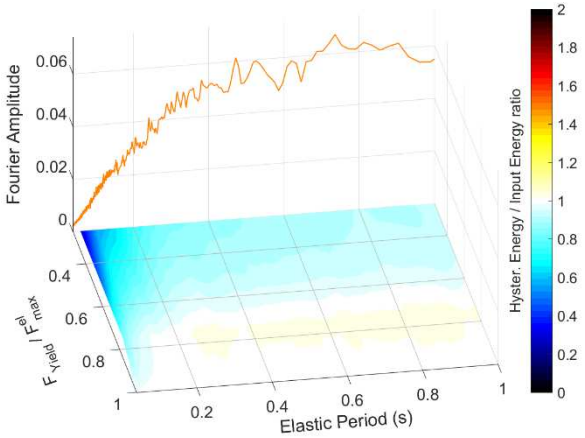

Figure 0.102. Mean ratios of the fractions of the hysteretic energy divided by the input energy for the hysteretic model 18, subjected to all the ground motions.

- *Model 19 (Elastoplastic with low pinching effect)*

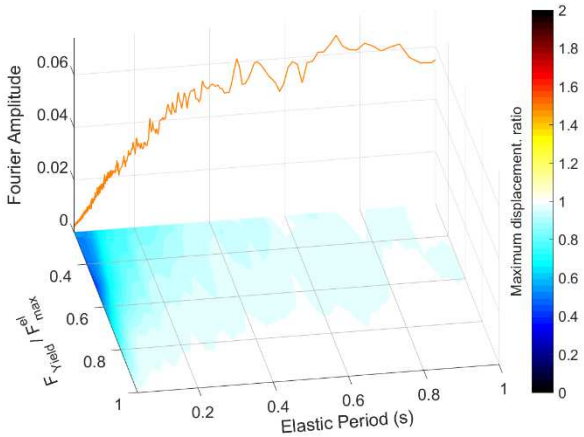

Figure 0.103. Mean maximum displacement ratios for the hysteretic model 19, subjected to all the ground motions.

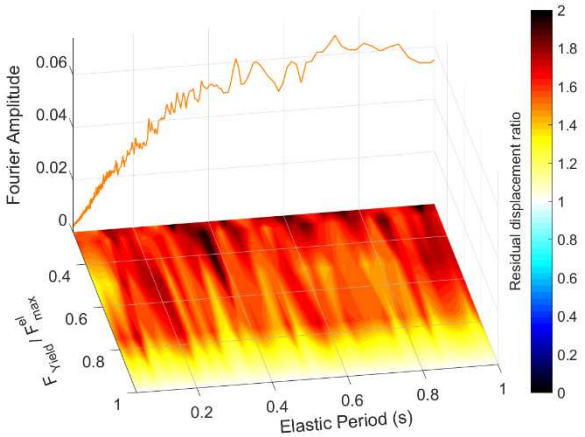

Figure 0.104. Mean residual displacement ratios for the hysteretic model 19, subjected to all the ground motions.

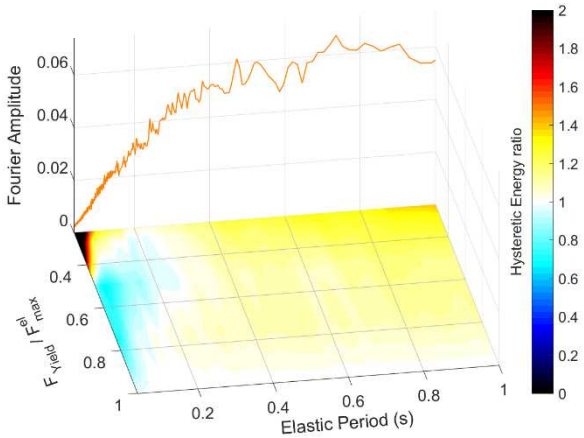

Figure 0.105. Mean total hysteretic energy ratios for the hysteretic model 19, subjected to all the ground motions.

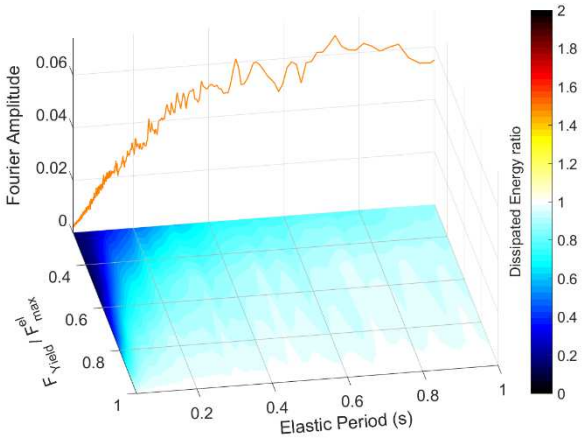

Figure 0.106. Mean total dissipated energy ratios for the hysteretic model 19, subjected to all the ground motions.

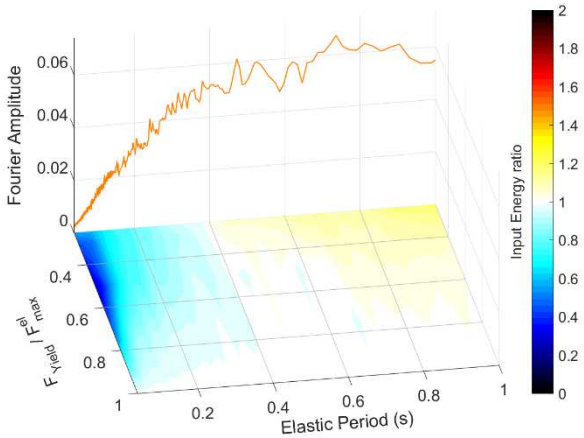

Figure 0.107. Mean total input energy ratios for the hysteretic model 19, subjected to all the ground motions.

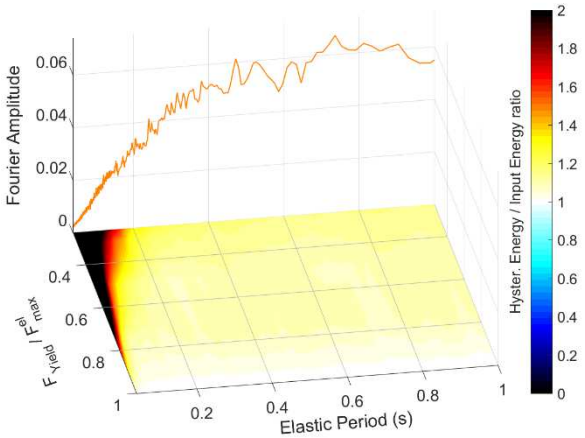

Figure 0.108. Mean ratios of the fractions of the hysteretic energy divided by the input energy for the hysteretic model 19, subjected to all the ground motions.

- *Model 20 (Elastoplastic with high pinching effect)*

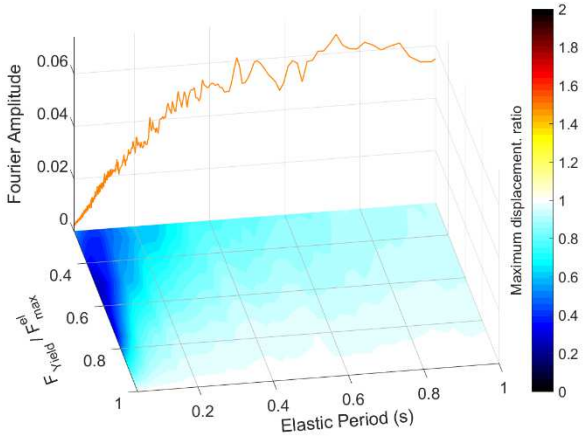

Figure 0.109. Mean maximum displacement ratios for the hysteretic model 20, subjected to all the ground motions.

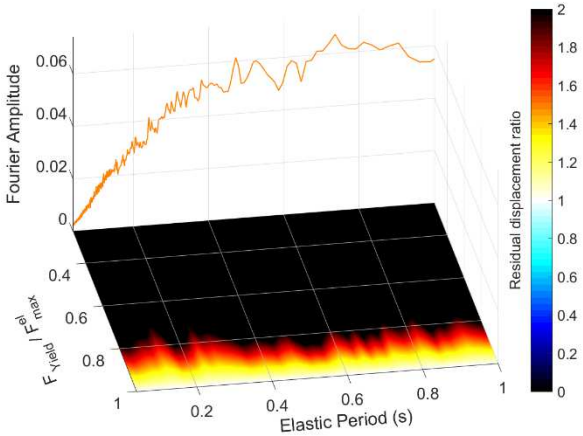

Figure 0.110. Mean residual displacement ratios for the hysteretic model 20, subjected to all the ground motions.

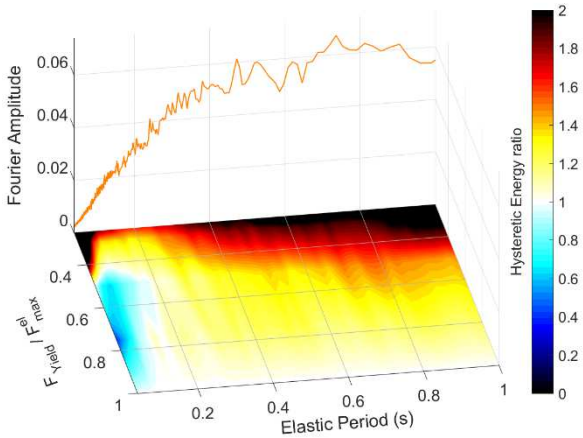

Figure 0.111. Mean total hysteretic energy ratios for the hysteretic model 20, subjected to all the ground motions.

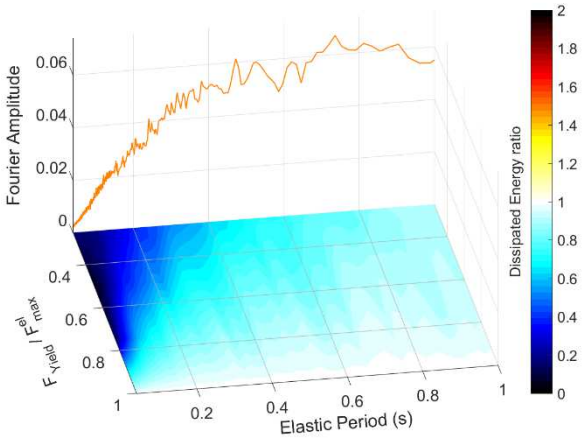

Figure 0.112. Mean total dissipated energy ratios for the hysteretic model 20, subjected to all the ground motions.

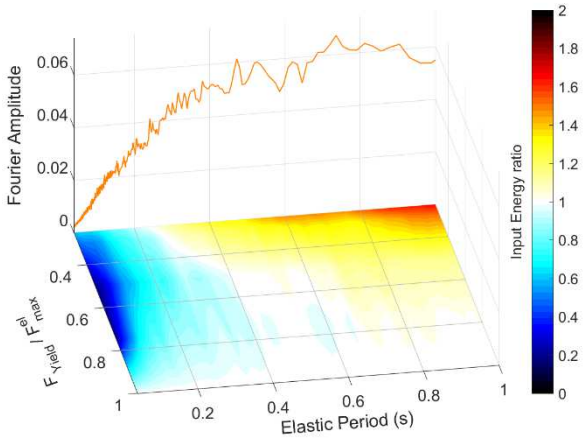

Figure 0.113. Mean total input energy ratios for the hysteretic model 20, subjected to all the ground motions.

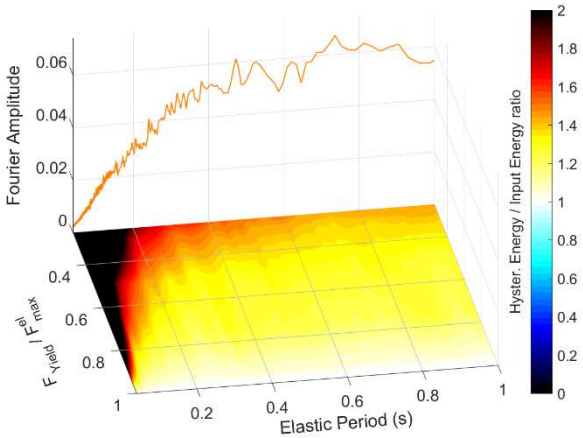

Figure 0.114. Mean ratios of the fractions of the hysteretic energy divided by the input energy for the hysteretic model 20, subjected to all the ground motions.

- *Model 21 (Strength hardening, with stiffness degradation, strength deterioration and low pinching)*

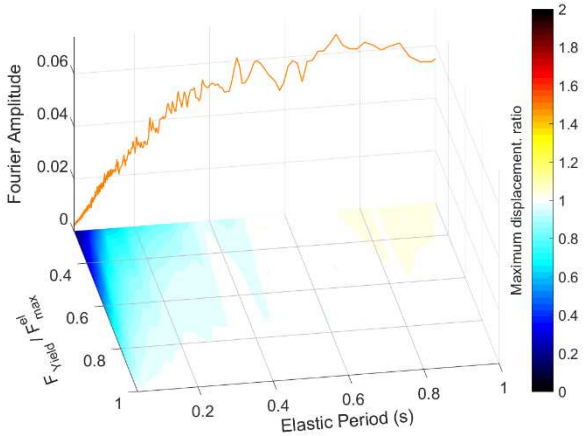

Figure 0.115. Mean maximum displacement ratios for the hysteretic model 21, subjected to all the ground motions.

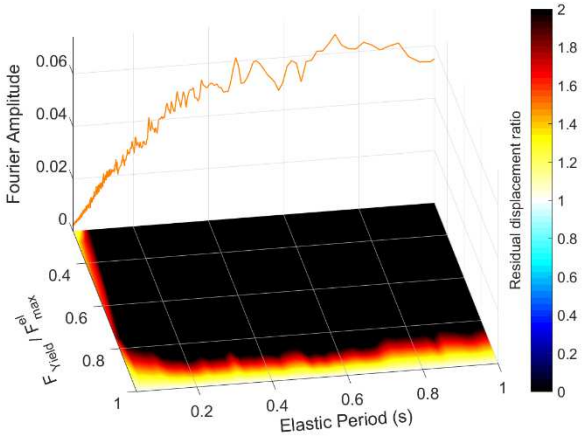

Figure 0.116. Mean residual displacement ratios for the hysteretic model 21, subjected to all the ground motions.

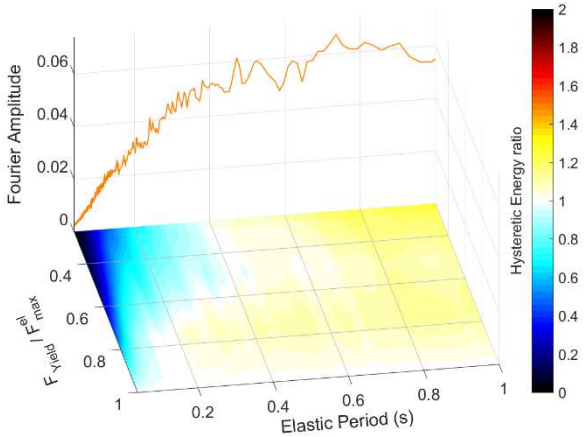

Figure 0.117. Mean total hysteretic energy ratios for the hysteretic model 21, subjected to all the ground motions.

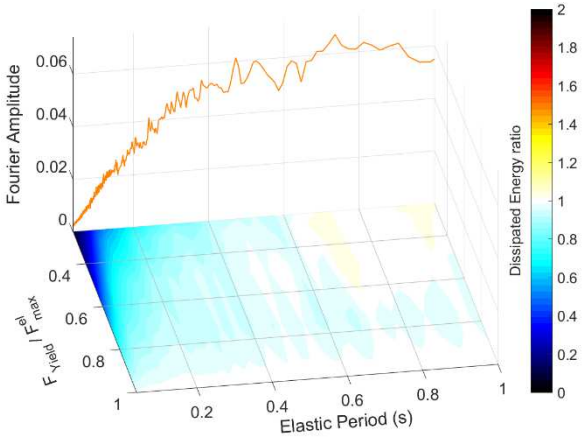

Figure 0.118. Mean total dissipated energy ratios for the hysteretic model 21, subjected to all the ground motions.

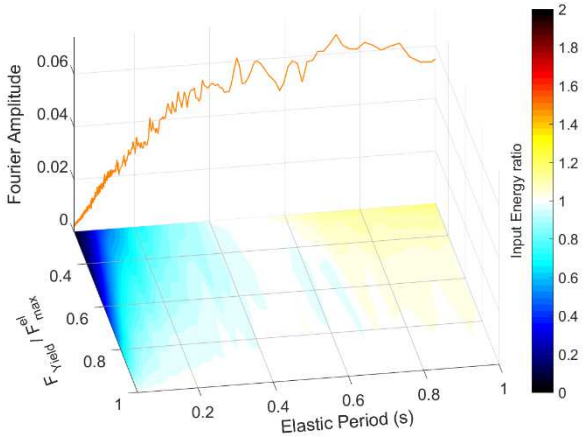

Figure 0.119. Mean total input energy ratios for the hysteretic model 21, subjected to all the ground motions.

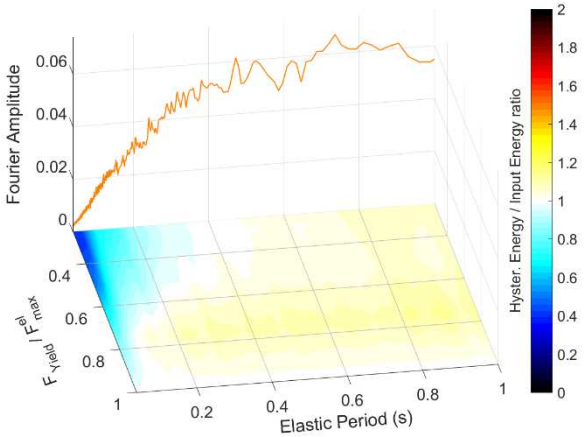

Figure 0.120. Mean ratios of the fractions of the hysteretic energy divided by the input energy for the hysteretic model 21, subjected to all the ground motions.

- *Model 22 (Strength hardening, with stiffness degradation, strength deterioration and high pinching)*

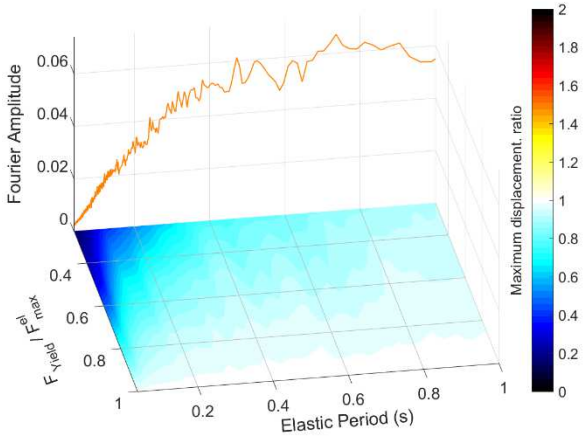

Figure 0.121. Mean maximum displacement ratios for the hysteretic model 22, subjected to all the ground motions.

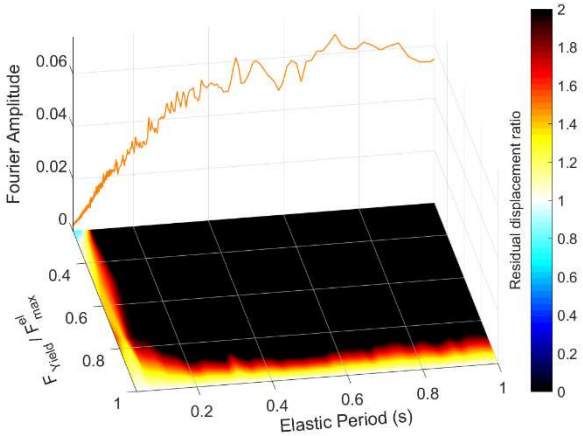

Figure 0.122. Mean residual displacement ratios for the hysteretic model 22, subjected to all the ground motions.

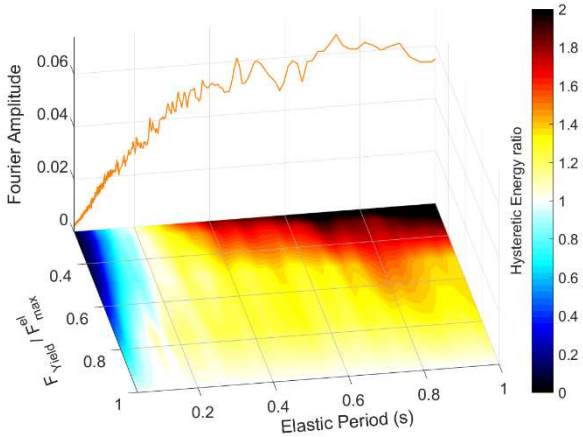

Figure 0.123. Mean total hysteretic energy ratios for the hysteretic model 22, subjected to all the ground motions.

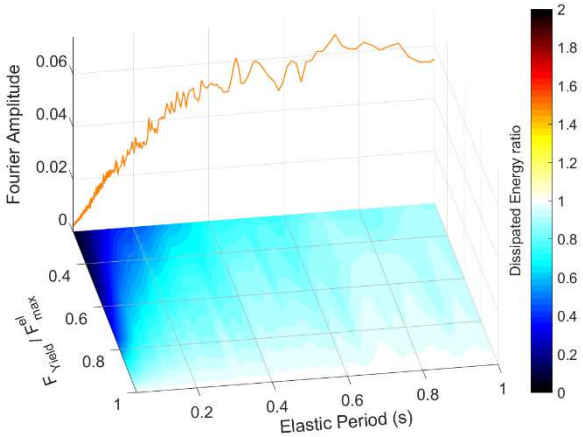

Figure 0.124. Mean total dissipated energy ratios for the hysteretic model 22, subjected to all the ground motions.

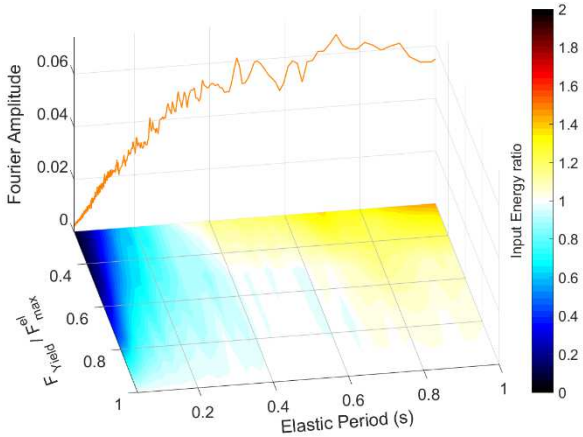

Figure 0.125. Mean total input energy ratios for the hysteretic model 22, subjected to all the ground motions.

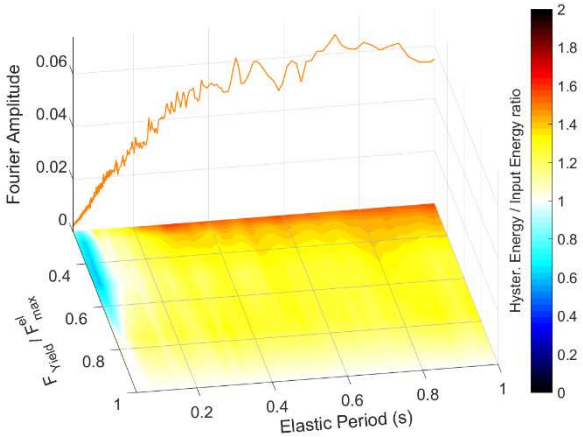

Figure 0.126. Mean ratios of the fractions of the hysteretic energy divided by the input energy for the hysteretic model 22, subjected to all the ground motions.

Record Sequence Number	Earthquake Name	Year	Station Name	Earthquake Magnitude	Pulse-like	Mechanism	5-95% Duration [s]	R_{rup} [km]	Vs_{30} [m/s]	Lowest Usable Freq [Hz]	PGA [g]	PGV [cm/s]	PGD [cm]
1	Helena, Montana-01	1935	Carroll College	6.00 (Mw)	No	strike slip	2.5	2.86	593	0.16	0.16	10.05	3.01
6	Imperial Valley-02	1940	El Centro Array #9	6.95 (Mw)	No	strike slip	24.2	6.09	213	0.25	0.23	31.30	18.45
96	Managua, Nicaragua-02	1972	Managua, ESSO	5.20 (Mw)	No	strike slip	8.1	4.98	289	0.13	0.23	22.00	7.70
126	Gazli, USSR	1976	Karakyr	6.80 (Mw)	No	Reverse	7.0	5.46	260	0.25	0.70	64.77	24.08
143	Tabas, Iran	1978	Tabas	7.35 (Mw)	Yes	Reverse	16.5	2.05	767	0.13	0.81	113.53	72.01
148	Coyote Lake	1979	Gilroy Array #3	5.74 (Mw)	Yes	strike slip	8.7	7.42	350	0.16	0.25	23.92	5.25
149	Coyote Lake	1979	Gilroy Array #4	5.74 (Mw)	Yes	strike slip	11.0	5.7	222	0.15	0.25	27.92	4.52
159	Imperial Valley-06	1979	Agrarias	6.53 (Mw)	Yes	strike slip	13.3	0.65	242	0.16	0.24	38.37	10.53
165	Imperial Valley-06	1979	Chihuahua	6.53 (Mw)	No	strike slip	24.0	7.29	242	0.23	0.27	28.71	7.78
170	Imperial Valley-06	1979	EC County Center FF	6.53 (Mw)	Yes	strike slip	13.2	7.31	192	0.08	0.22	52.42	37.43
171	Imperial Valley-06	1979	El Centro - Meloland Geot. Array	6.53 (Mw)	Yes	strike slip	8.2	0.07	265	0.10	0.31	83.52	34.71
173	Imperial Valley-06	1979	El Centro Array #10	6.53 (Mw)	Yes	strike slip	12.8	8.6	203	0.08	0.20	50.43	31.42
179	Imperial Valley-06	1979	El Centro Array #4	6.53 (Mw)	Yes	strike slip	10.3	7.05	209	0.06	0.38	79.11	55.11
180	Imperial Valley-06	1979	El Centro Array #5	6.53 (Mw)	Yes	strike slip	9.6	3.95	206	0.05	0.41	78.29	62.49
182	Imperial Valley-06	1979	El Centro Array #7	6.53 (Mw)	Yes	strike slip	6.8	0.56	211	0.08	0.44	82.68	46.01
183	Imperial Valley-06	1979	El Centro Array #8	6.53 (Mw)	No	strike slip	6.8	3.86	206	0.04	0.53	52.41	41.44
184	Imperial Valley-06	1979	El Centro Differential Array	6.53 (Mw)	Yes	strike slip	7.0	5.09	202	0.03	0.44	57.84	42.26
185	Imperial Valley-06	1979	Holtville Post Office	6.53 (Mw)	Yes	strike slip	12.8	7.5	203	0.08	0.24	52.29	37.92
235	Mammoth Lakes-02	1980	Mammoth Lakes H. S.	5.69 (Mw)	No	strike slip	3.9	9.12	347	0.16	0.42	24.10	3.65
252	Mammoth Lakes-07	1980	Green Church	4.73 (Mw)	No	strike slip	8.2	5.17	353	0.25	0.16	10.74	1.33
257	Mammoth Lakes-08	1980	Cashbaugh (CBR)	4.80 (Mw)	No	strike slip	10.9	9.64	338	0.19	0.12	4.98	0.38
261	Mammoth Lakes-08	1980	Long Valley Fire Sta	4.80 (Mw)	No	strike slip	9.9	5.95	377	0.25	0.02	1.55	0.29
285	Irpinia, Italy-01	1980	Bagnoli Irpinio	6.90 (Mw)	Yes	Normal	19.6	8.18	650	0.11	0.15	29.99	12.72
319	Westmorland	1981	Westmorland Fire Sta	5.90 (Mw)	No	strike slip	6.9	6.5	194	0.13	0.41	39.75	13.09
321	Mammoth Lakes-11	1983	Convict Creek	5.31 (Mw)	No	strike slip	10.1	7.7	382	0.25	0.12	9.16	1.82
368	Coalinga-01	1983	Pleasant Valley P.P. - yard	6.36 (Mw)	No	Reverse	9.1	8.41	257	0.18	0.52	46.58	15.77
445	New Zealand-01	1984	Turangi Telephone Exchange	5.50 (ML)	No	Normal	12.6	8.84	356	0.25	0.10	7.12	1.99
448	Morgan Hill	1984	Anderson Dam (Downstream)	6.19 (Mw)	No	strike slip	6.9	3.26	489	0.16	0.35	29.62	5.52
451	Morgan Hill	1984	Coyote Lake Dam - Southwest Abutment	6.19 (Mw)	Yes	strike slip	4.1	0.53	561	0.13	0.94	67.40	13.48
529	N. Palm Springs	1986	North Palm Springs	6.06 (Mw)	No	Reverse Oblique	5.2	4.04	345	0.25	0.68	50.67	11.87
547	Chalfant Valley-01	1986	Zack Brothers Ranch	5.77 (Mw)	No	strike slip	11.5	6.39	316	0.11	0.24	23.14	6.15
566	Kalamata, Greece-02	1986	Kalamata (bsmt) (2nd trigger)	5.40 (MS)	Yes	Normal	2.9	5.6	382	0.16	0.21	19.62	2.82
765	Loma Prieta	1989	Gilroy Array #1	6.93 (Mw)	No	Reverse Oblique	6.5	9.64	1428	0.08	0.43	32.70	13.13
779	Loma Prieta	1989	LGPC	6.93 (Mw)	No	Reverse Oblique	10.2	3.88	595	0.13	0.59	83.53	30.45
821	Erzican, Turkey	1992	Erzincan	6.69 (Mw)	No	strike slip	8.4	4.38	352	0.13	0.44	93.84	29.35
901	Big Bear-01	1992	Big Bear Lake - Civic Center	6.46 (Mw)	No	strike slip	10.4	8.3	430	0.12	0.52	28.40	4.28
982	Northridge-01	1994	Jensen Filter Plant Administrative Building	6.69 (Mw)	Yes	Reverse	12.5	5.43	373	0.20	0.52	97.62	33.83
1044	Northridge-01	1994	Newhall - Fire Sta	6.69 (Mw)	Yes	Reverse	5.9	5.92	269	0.12	0.65	86.67	25.79
1045	Northridge-01	1994	Newhall - W Pico Canyon Rd.	6.69 (Mw)	Yes	Reverse	8.8	5.48	286	0.13	0.36	99.73	33.82
1063	Northridge-01	1994	Rinaldi Receiving Sta	6.69 (Mw)	Yes	Reverse	9.1	6.5	282	0.10	0.71	114.40	30.74

Table 9. Earthquake ground motions used in this study.

Record Sequence Number	Earthquake Name	Year	Station Name	Earthquake Magnitude	Pulse-like	Mechanism	5-95% Duration [s]	R_{rup} [km]	Vs_{30} [m/s]	Lowest Usable Freq [Hz]	PGA [g]	PGV [cm/s]	PGD [cm]
1085	Northridge-01	1994	Sylmar - Converter Sta East	6.69 (Mw)	Yes	Reverse	7.4	5.19	371	0.23	0.69	89.00	25.22
1106	Kobe, Japan	1995	KJMA	6.90 (Mw)	Yes	strike slip	9.5	0.96	312	0.06	0.78	83.57	19.74
1111	Kobe, Japan	1995	Nishi-Akashi	6.90 (Mw)	No	strike slip	11.2	7.08	609	0.13	0.47	39.49	11.85
1114	Kobe, Japan	1995	Port Island (0 m)	6.90 (Mw)	Yes	strike slip	11.5	3.31	198	0.13	0.32	73.09	35.27
1120	Kobe, Japan	1995	Takatori	6.90 (Mw)	Yes	strike slip	11.3	1.47	256	0.13	0.67	121.69	34.25
1244	Chi-Chi, Taiwan	1999	CHY101	7.62 (Mw)	Yes	Reverse Oblique	30.4	9.94	259	0.05	0.38	91.28	60.73
1501	Chi-Chi, Taiwan	1999	TCU063	7.62 (Mw)	Yes	Reverse Oblique	33.1	9.78	476	0.04	0.16	63.52	46.96
1545	Chi-Chi, Taiwan	1999	TCU120	7.62 (Mw)	No	Reverse Oblique	32.4	7.4	459	0.04	0.23	42.95	48.56
1551	Chi-Chi, Taiwan	1999	TCU138	7.62 (Mw)	No	Reverse Oblique	34.0	9.78	653	0.04	0.21	38.77	31.18
1605	Duzce, Turkey	1999	Duzce	7.14 (Mw)	No	strike slip	11.1	6.58	282	0.10	0.43	78.70	48.74
1611	Duzce, Turkey	1999	Lamont 1058	7.14 (Mw)	No	strike slip	13.4	0.21	529	0.08	0.10	14.64	12.03
1615	Duzce, Turkey	1999	Lamont 1062	7.14 (Mw)	No	strike slip	16.1	9.14	338	0.06	0.21	14.63	8.97
1617	Duzce, Turkey	1999	Lamont 375	7.14 (Mw)	No	strike slip	13.1	3.93	454	0.19	0.68	27.89	6.12
2628	Chi-Chi, Taiwan-03	1999	TCU078	6.20 (Mw)	No	Reverse	5.4	7.62	443	0.05	0.43	40.76	13.17
2632	Chi-Chi, Taiwan-03	1999	TCU084	6.20 (Mw)	No	Reverse	15.6	9.32	665	0.06	0.12	16.95	7.17
2734	Chi-Chi, Taiwan-04	1999	CHY074	6.20 (Mw)	Yes	strike slip	7.4	6.2	553	0.08	0.32	38.94	13.57
3965	Tottori, Japan	2000	TTR008	6.61 (Mw)	Yes	strike slip	18.5	6.88	139	0.02	0.39	44.73	25.50
3966	Tottori, Japan	2000	TTR009	6.61 (Mw)	No	strike slip	11.1	8.83	420	0.13	0.62	33.10	14.56
4031	San Simeon, CA	2003	Templeton - 1-story Hospital	6.5 (Mw)	No	Reverse	10.3	6.22	411	0.09	0.43	30.73	12.71
4064	Parkfield-02, CA	2004	PARKFIELD - DONNA LEE	6.00 (Mw)	No	strike slip	6.3	4.93	657	0.13	0.34	14.95	2.57
4066	Parkfield-02, CA	2004	PARKFIELD - FROELICH	6.00 (Mw)	No	strike slip	5.4	3.19	227	0.13	0.41	13.55	3.01
4069	Parkfield-02, CA	2004	PARKFIELD - JACK CANYON	6.00 (Mw)	No	strike slip	11.1	9.46	576	0.13	0.16	9.14	1.33
4074	Parkfield-02, CA	2004	PARKFIELD - VINEYARD CANYON	6.00 (Mw)	No	strike slip	12.4	5.15	340	0.13	0.24	17.56	3.53
4081	Parkfield-02, CA	2004	Parkfield - Cholame 5W	6.00 (Mw)	No	strike slip	12.6	6.87	237	0.08	0.23	14.97	2.27
4083	Parkfield-02, CA	2004	PARKFIELD - TURKEY FLAT #1 (0M)	6.00 (Mw)	No	strike slip	8.8	5.29	907	0.19	0.20	13.11	1.76
4102	Parkfield-02, CA	2004	Parkfield - Cholame 3W	6.00 (Mw)	Yes	strike slip	6.5	3.63	231	0.25	0.41	34.26	6.16
4104	Parkfield-02, CA	2004	Parkfield - Cholame 4AW	6.00 (Mw)	No	strike slip	7.6	5.53	283	0.25	0.28	21.39	3.88
4107	Parkfield-02, CA	2004	Parkfield - Fault Zone 1	6.00 (Mw)	Yes	strike slip	9.4	2.51	178	0.19	0.64	67.33	10.83
4108	Parkfield-02, CA	2004	Parkfield - Fault Zone 3	6.00 (Mw)	No	strike slip	9.9	2.73	212	0.13	0.37	22.41	3.14
4109	Parkfield-02, CA	2004	Parkfield - Fault Zone 4	6.00 (Mw)	No	strike slip	14.1	2.65	221	0.25	0.12	14.52	2.31
4112	Parkfield-02, CA	2004	Parkfield - Fault Zone 8	6.00 (Mw)	No	strike slip	8.5	3.95	309	0.25	0.48	20.46	2.25
4113	Parkfield-02, CA	2004	Parkfield - Fault Zone 9	6.00 (Mw)	Yes	strike slip	10.4	2.85	372	0.13	0.13	19.53	4.50
4117	Parkfield-02, CA	2004	Parkfield - Fault Zone 15	6.00 (Mw)	No	strike slip	11.7	2.67	308	0.13	0.21	23.57	5.84
4118	Parkfield-02, CA	2004	Parkfield - Gold Hill 1W	6.00 (Mw)	No	strike slip	15.4	2.67	214	0.16	0.14	7.70	2.34
4134	Parkfield-02, CA	2004	Parkfield - Vineyard Cany 3W	6.00 (Mw)	No	strike slip	6.9	5.21	309	0.13	0.31	22.00	5.54
4140	Parkfield-02, CA	2004	PARKFIELD - UPSAR 03	6.00 (Mw)	No	strike slip	16.2	9.95	441	0.09	0.21	13.60	2.88
4142	Parkfield-02, CA	2004	PARKFIELD - UPSAR 06	6.00 (Mw)	No	strike slip	15.9	9.61	441	0.06	0.23	15.41	3.15
4143	Parkfield-02, CA	2004	PARKFIELD - UPSAR 07	6.00 (Mw)	No	strike slip	14.8	9.61	441	0.13	0.38	18.20	3.06
4145	Parkfield-02, CA	2004	PARKFIELD - UPSAR 09	6.00 (Mw)	No	strike slip	15.9	9.34	466	0.13	0.23	18.87	3.60
4146	Parkfield-02, CA	2004	PARKFIELD - UPSAR 10	6.00 (Mw)	No	strike slip	16.6	9.14	342	0.13	0.29	22.15	3.40

Table 10. Earthquake ground motions used in this study.

Record Sequence Number	Earthquake Name	Year	Station Name	Earthquake Magnitude	Pulse-like	Mechanism	5-95% Duration [s]	R_{rup} [km]	Vs_{30} [m/s]	Lowest Usable Freq [Hz]	PGA [g]	PGV [cm/s]	PGD [cm]
4148	Parkfield-02, CA	2004	PARKFIELD - UPSAR 12	6.00 (Mw)	No	strike slip	18.5	9.47	466	0.10	0.25	19.06	3.14
4210	Niigata, Japan	2004	NIG020	6.63 (Mw)	No	Reverse	95.9	8.47	332	0.09	0.47	28.05	10.69
4218	Niigata, Japan	2004	NIG028	6.63 (Mw)	No	Reverse	5.6	9.79	431	0.08	0.65	35.75	6.04
4289	Umbria-02, Italy	1979	Norcia	3.7 (Mw)	No	Normal	4.4	6.25	678	0.25	0.02	0.78	0.14
4337	Umbria Marche (foreshock)	1997	Colfiorito	5.7 (Mw)	No	Normal	4.8	4.02	317	0.25	0.30	21.83	4.01
4349	Umbria Marche, Italy	1997	Colfiorito	6 (Mw)	No	Normal	11.4	6.92	317	0.16	0.20	16.53	3.33
4365	Umbria Marche (aftershock 1)	1997	Colfiorito-Casermette	5.5 (Mw)	No	Normal	5.3	6.3	405	0.13	0.19	8.58	1.18
4373	Umbria Marche (aftershock 6)	1997	Colfiorito-Casermette	4.5 (Mw)	No	strike slip	2.8	2.55	405	0.25	0.10	2.17	0.18
4374	Umbria Marche (aftershock 6)	1997	Nocera Umbra-Biscontini	4.5 (Mw)	No	strike slip	6.4	9.76	442	0.13	0.07	1.78	0.09
4396	Umbria Marche (aftershock 11)	1997	Nocera Umbra-Biscontini	4.3 (Mw)	No	strike slip	5.4	9.97	442	0.18	0.03	0.72	0.09
4399	Umbria Marche (aftershock 12)	1997	Sellano Ovest	4.6 (Mw)	No	Normal	2.5	8.65	509	0.13	0.04	1.93	0.13
4403	Umbria Marche (aftershock 13)	1997	Sellano Ovest	4.9 (Mw)	No	Normal	3.8	5.82	509	0.23	0.05	2.18	0.23
4451	Montenegro, Yugo.	1979	Bar-Skupstina Opstine	7.10 (Mw)	Yes	Reverse	21.3	6.98	462	0.25	0.37	49.59	14.14
4458	Montenegro, Yugo.	1979	Ulcinj - Hotel Olimpic	7.10 (Mw)	Yes	Reverse	26.0	5.76	319	0.16	0.25	47.93	17.40
4480	L'Aquila, Italy	2009	L'Aquila - V. Aterno - Centro Valle	6.30 (Mw)	Yes	Normal	7.7	6.27	475	0.13	0.56	40.87	5.48
5619	Iwate	2008	IWT011	6.90 (Mw)	No	Reverse	39.7	8.44	279	0.04	0.19	17.92	10.31
5657	Iwate	2008	IWTH25	6.90 (Mw)	No	Reverse	13.7	4.8	506	0.08	1.35	64.88	29.18
6897	Darfield, New Zealand	2010	DSLC	7.00 (Mw)	Yes	strike slip	19.6	8.46	296	0.08	0.25	54.81	61.33
6906	Darfield, New Zealand	2010	GDLC	7.00 (Mw)	Yes	strike slip	16.0	1.22	344	0.06	0.73	117.10	77.59
6911	Darfield, New Zealand	2010	HORC	7.00 (Mw)	Yes	strike slip	9.5	7.29	326	0.13	0.47	77.77	48.27
6975	Darfield, New Zealand	2010	TPLC	7.00 (Mw)	Yes	strike slip	24.5	6.11	249	0.06	0.24	64.40	64.05
8066	Christchurch, New Zealand	2011	Christchurch Hospital	6.2 (Mw)	No	Reverse Oblique	10.6	4.85	194	0.06	0.38	59.37	22.03
8118	Christchurch, New Zealand	2011	Papanui High School	6.2 (Mw)	No	Reverse Oblique	13.9	9.06	263	0.05	0.21	40.87	20.86
8119	Christchurch, New Zealand	2011	Pages Road Pumping Station	6.2 (Mw)	Yes	Reverse Oblique	4.3	1.98	206	0.10	0.65	89.15	39.45
8123	Christchurch, New Zealand	2011	Christchurch Resthaven	6.2 (Mw)	Yes	Reverse Oblique	11.2	5.13	141	0.10	0.52	69.49	27.05
8124	Christchurch, New Zealand	2011	Riccarton High School	6.2 (Mw)	No	Reverse Oblique	9.5	9.44	293	0.08	0.28	27.11	12.81
8369	Yorba Linda	2002	Yorba Linda; Diemer Filtration Plant	4.27 (Mw)	No	strike slip	12.3	7.06	374	0.21	0.03	1.35	0.17
8630	40204628	2007	Mt. Pleasant High School	5.45 (Mw)	No	strike slip	12.6	9.36	377	0.19	0.09	6.48	1.21
8648	40204628	2007	San Jose; Laneview School Warmwood Ln.	5.45 (Mw)	No	strike slip	17.6	8.83	363	0.15	0.09	5.62	1.11
8671	40204628	2007	Calaveras Reservoir #2	5.45 (Mw)	No	strike slip	4.2	4.29	519	0.18	0.09	3.03	0.47
9444	21465580	2005	Martis Creek Dam (Dwn Stream)	4.77 (Mw)	No	strike slip	4.5	8.65	422	0.21	0.11	2.78	0.34
10876	14312160	2007	Simi Valley - Katherine Rd & Sylvan	4.66 (Mw)	No	Reverse	3.8	9.5	351	0.19	0.15	3.61	0.27
10896	14312160	2007	Granada Hills - Porter Ranch Fire Station 8	4.66 (Mw)	No	Reverse	2.4	8.79	450	0.10	0.14	4.49	0.31
10898	14312160	2007	Chatsworth; Fire Station 96 Marilla St.	4.66 (Mw)	No	Reverse	6.5	9.42	283	0.21	0.05	2.92	0.28
11064	21522424	2006	Gilroy - Hwy 101 & Cohansey	4.30 (Mw)	No	strike slip	17.0	9.75	324	0.19	0.01	1.05	0.21
11065	21522424	2006	Coyote Lake Dam - Southwest Abutment	4.30 (Mw)	No	strike slip	6.5	5.88	561	0.15	0.03	1.25	0.14
11066	21522424	2006	Gilroy Array #6	4.30 (Mw)	No	strike slip	2.7	7.88	663	0.18	0.11	3.79	0.24
11608	21262721	2003	Hollister - City Hall Annex	4.30 (Mw)	No	strike slip	9.1	7.7	273	0.16	0.11	6.31	0.70
11648	51183708	2007	San Juan Bautista, 24 Polk St	4.20 (Mw)	No	strike slip	8.2	9.42	336	0.16	0.05	1.44	0.15
11651	51183708	2007	SJB Overpass, Bent 3 g.l.	4.20 (Mw)	No	strike slip	6.4	7.42	367	0.19	0.07	2.86	0.16

Table 11. Earthquake ground motions used in this study.

Record Sequence Number	Earthquake Name	Year	Station Name	Earthquake Magnitude	Pulse-like	Mechanism	5-95% Duration [s]	R_{rup} [km]	Vs_{30} [m/s]	Lowest Usable Freq [Hz]	PGA [g]	PGV [cm/s]	PGD [cm]
11663	40234037	2009	Coe Ranch	4.30 (Mw)	No	strike slip	5.2	5.71	400	0.23	0.03	1.81	0.18
11686	40234037	2009	Lick Observatory, Mt. Hamiliton	4.30 (Mw)	No	strike slip	1.4	6.85	710	0.10	0.06	4.16	0.40
11772	9173365	2001	Sylmar - County Hospital Grounds	4.26 (Mw)	No	Reverse	6.5	8.68	421	0.11	0.04	1.40	0.15
11872	9703873	2001	Beverly Hills Pac Bell Bsmt	4.24 (Mw)	No	strike slip	4.2	6.48	460	0.15	0.08	3.47	0.53
12045	14116972	2005	San Bernardino - Sycamore FS	4.42 (Mw)	No	strike slip	2.5	8.27	631	0.24	0.03	0.85	0.05
12055	14116972	2005	San Bernardino - Fire Sta. #9	4.42 (Mw)	No	strike slip	6.1	9.34	326	0.25	0.04	1.93	0.15
12112	30225889	2003	Santa Rosa Fire Station #1	4.12 (Mw)	No	strike slip	4.4	2.8	389	0.13	0.13	9.24	1.11
12157	30225889	2003	Taylor Mountain	4.12 (Mw)	No	strike slip	7.9	8.28	760	0.16	0.02	0.90	0.11
12200	40199209	2007	Oakland; Fire Station 03 14th St.	4.20 (Mw)	No	strike slip	15.4	9.66	258	0.19	0.02	0.89	0.10
12204	40199209	2007	Berkeley; Fire Station 03 Russell Str.	4.20 (Mw)	No	strike slip	1.5	8.3	415	0.18	0.18	6.03	0.33
12245	40199209	2007	Oakland; Fire Station 29 66th St.	4.20 (Mw)	No	strike slip	9.0	5.87	285	0.14	0.03	0.90	0.13
12246	40199209	2007	Oakland; Fire Station 16 13th St.	4.20 (Mw)	No	strike slip	6.3	4.96	377	0.11	0.04	2.55	0.30
12257	40199209	2007	Oakland; Fire Station 12 Alice St.	4.20 (Mw)	No	strike slip	7.7	7.83	286	0.15	0.04	1.65	0.18
12258	40199209	2007	Alameda - Posey & Webster Geotech Array	4.20 (Mw)	No	strike slip	7.4	8.73	208	0.10	0.05	3.30	0.26
12259	40199209	2007	Orinda - BART Station Grounds	4.20 (Mw)	No	strike slip	4.8	8.19	469	0.15	0.06	1.99	0.12
12260	40199209	2007	Orinda - Valley View & Moraga	4.20 (Mw)	No	strike slip	2.7	5.77	515	0.14	0.14	3.63	0.22
12261	40199209	2007	Oakland - Hwys 13 & 24	4.20 (Mw)	No	strike slip	1.3	6.22	511	0.19	0.31	11.40	0.87
12267	40199209	2007	Piedmont Jr. High School Grounds	4.20 (Mw)	No	strike slip	1.8	5.22	597	0.15	0.12	4.28	0.36
12270	40199209	2007	Byerly Seismographic Vault, Berkeley	4.20 (Mw)	No	strike slip	3.1	8.89	522	0.10	0.04	2.23	0.26
12890	14282008	2007	Joshua Ridge: China Lake	4.11 (Mw)	No	Normal	4.4	6.72	623	0.15	0.03	0.69	0.06
12974	30226086	2003	Healdsburg; Fire Station	4.00 (Mw)	No	strike slip	5.4	7.65	378	0.24	0.02	0.73	0.05
13044	21305648	2003	Byerly Seismographic Vault, Berkeley	4.00 (Mw)	No	strike slip	3.8	9.77	522	0.23	0.01	0.24	0.02
13348	10285533	2007	Table Mountain 2	4.20 (Mw)	No	Reverse Oblique	4.7	8.34	586	0.11	0.02	0.69	0.05
14923	21549979	2006	Hollister - City Hall Annex	3.70 (Mw)	No	strike slip	12.8	4.92	273	0.14	0.04	1.80	0.21
14924	21549979	2006	Hollister - Airport Bldg #3	3.70 (Mw)	No	strike slip	9.4	6.93	289	0.18	0.02	2.59	0.29
14925	21549979	2006	San Juan Bautista, 24 Polk St	3.70 (Mw)	No	strike slip	7.4	7.01	336	0.19	0.02	1.88	0.23
14926	21549979	2006	Hollister - South & Pine	3.70 (Mw)	No	strike slip	9.7	5.32	282	0.18	0.06	1.94	0.17
15992	9644101	2001	Serrano	3.64 (Mw)	No	strike slip	8.0	8.48	441	0.15	0.01	0.23	0.03
16403	30226452	2003	Byerly Seismographic Vault, Berkeley	3.50 (Mw)	No	strike slip	5.5	9.26	522	0.11	0.00	0.16	0.01
16461	51203888	2008	Round Hill	3.50 (Mw)	No	strike slip	3.6	8.95	481	0.19	0.02	0.77	0.06
16982	14360416	2008	China Lake	3.59 (Mw)	No	strike slip	4.1	9.4	1464	0.19	0.01	0.10	0.00
17945	10477949	2009	Owens Lake	4.04 (Mw)	No	strike slip	7.3	8.7	323	0.19	0.02	0.36	0.02
17993	10488901	2009	Owens Lake	3.67 (Mw)	No	strike slip	3.6	6.9	323	0.21	0.01	0.35	0.03
18415	21401170	2004	Bear Valley Ranch, Parkfield	4.88 (Mw)	No	strike slip	10.0	9.54	528	0.16	0.04	1.43	0.21
18473	21456837	2005	Parkfield - Vineyard Cany 2E	4.48 (Mw)	No	strike slip	5.4	9.46	468	0.14	0.09	4.37	0.32
18500	51182151	2007	Parkfield - Fault Zone 4	4.01 (Mw)	No	strike slip	13.7	8.72	221	0.20	0.01	0.64	0.09
18569	51182114	2007	Mt. Pleasant High School	3.50 (Mw)	No	strike slip	9.9	9.27	377	0.23	0.00	0.09	0.01
18919	71337451	2010	Calaveras Reservoir #2	3.73 (Mw)	No	Reverse Oblique	2.7	9.69	519	0.20	0.03	0.82	0.04
19059	51213534	2008	Mount Johnson	4.00 (Mw)	No	strike slip	9.8	8.57	486	0.16	0.03	0.48	0.02
19167	51215567	2009	Mount Johnson	3.80 (Mw)	No	strike slip	6.4	9.66	486	0.21	0.01	0.21	0.01

Table 12. Earthquake ground motions used in this study.

- Signals similar to Groningen ground motions

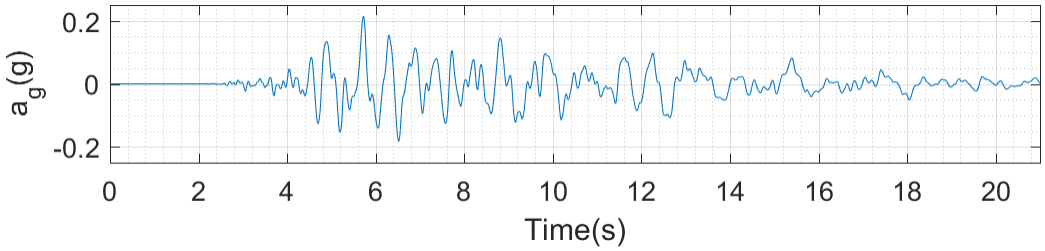

FigureD.1. Signal 1: Signal spectrally matched to the ground motions recorded in Groningen.

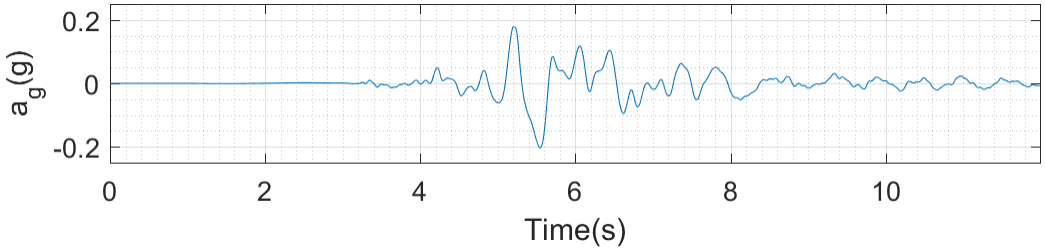

FigureD.2. Signal 2: Signal spectrally matched to the ground motions recorded in Groningen.

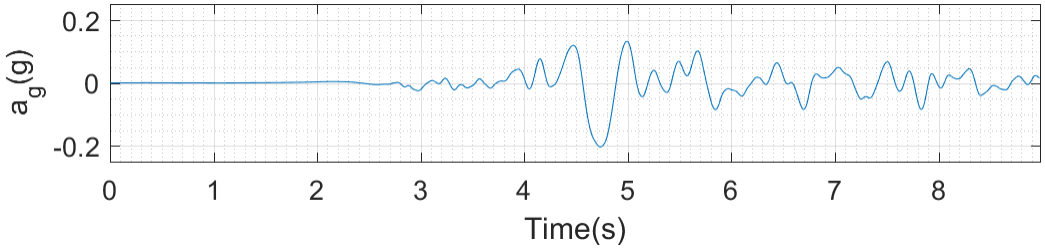

FigureD.3. Signal 3: Signal spectrally matched to the ground motions recorded in Groningen.

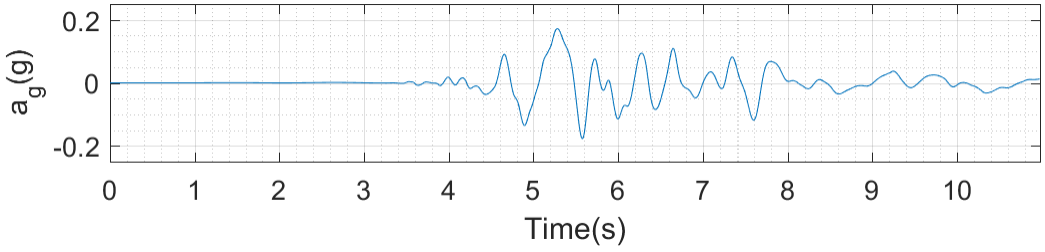

FigureD.4. Signal 4: Signal spectrally matched to the ground motions recorded in Groningen.

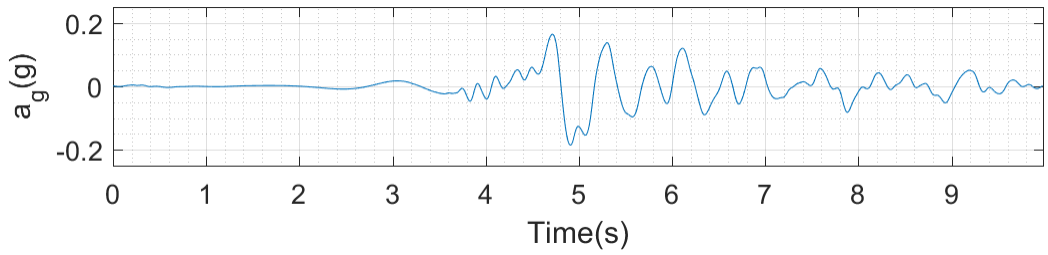

FigureD.5. Signal 5: Signal spectrally matched to the ground motions recorded in Groningen.

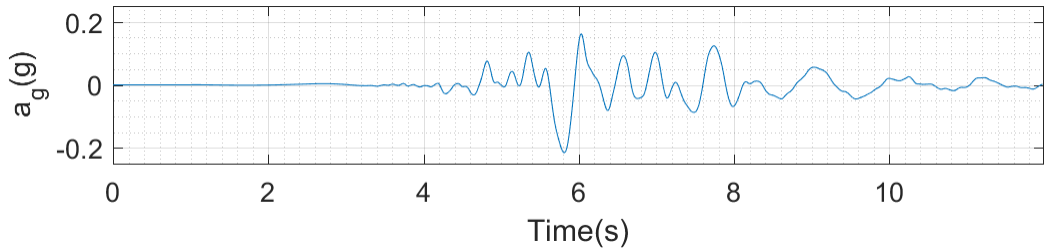

FigureD.6. Signal 6: Signal spectrally matched to the ground motions recorded in Groningen.

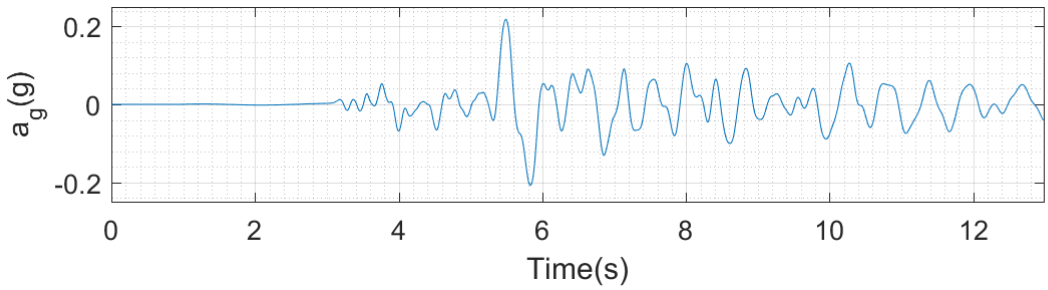

FigureD.7. Signal 7: Signal spectrally matched to the ground motions recorded in Groningen.

References

Akkar, S., 2014. *Basic Earthquake Engineering, from seismology to analysis and design*, Switzerland: Springer International Publishing.

Baber, T.T. & Noori, M.N., 1985. Random vibration of degrading, pinching systems. *Journal of Engineering Mechanics*, 111(8), pp.1010–1026.

Banon, H., Irvine, H.M. & Biggs, J.M., 1981. Seismic damage in reinforced concrete frames. *Journal of the Structural Division*, 107(9), pp.1713–1729.

Banon, H. & Veneziano, D., 1982. Seismic safety of reinforced concrete members and structures. *Earthquake Engineering and Structural Dynamics*, 10, pp.179–193.

Bayat, M. et al., 2010. The approximate analysis of non-linear behavior of structure under harmonic loading. *International Journal of the Physical Sciences*, 5(July), pp.1074–1080.

Bayat, M., Bayat, M. & Bayat, M., 2011. An analytical approach on a mass grounded by linear and non-linear springs in series. *International Journal of the Physical Sciences*, 6(2), pp.229–236.

Bayat, M. & Pakar, I., 2013. On the approximate analytical solution to non-linear oscillation systems. *Shock and Vibration*, 20, pp.43–52.

Bojorquez, E. et al., 2010. Energy-based damage index for steel structures. *Steel and Composite Structures*, 10(4), pp.331–348.

Bojórquez, E. & Ruiz-García, J., 2011. Evaluation of Residual Drift Demands in Steel Frames Subjected to Narrow-Band Earthquake Ground Motions. *15th World Conference on Earthquake Engineering (15WCEE)*.

Bojórquez, E. & Ruiz, S.E., 2004. Strength reduction factors for the valley of Mexico, considering low-cycle fatigue effectss. In *13th World Conference on Earthquake Engineering*.

Bommer, J. & Martinez-Pereira, A., 1999. The effective duration of earthquake strong motion. *Journal of Earthquake Engineering*, 3(2), pp.127–172. Available at: http://www.tandfonline.com/doi/full/10.1080/13632469909350343.

Bouc, R., 1967. Forced vibration of mechanical system with hysteresis. *Forth Confenrence on Non-linear Oscillations*.

Bozorgnia, Y. & Bertero, V. V., 2002. Improved damage parameters for post-earthquake applications. In *SMIP02*. pp. 61–82.

Bozorgnia, Y. & Campbell, K.W., 2004. Earthquake engineering: from engineering seismology to performance-based engineering. *CRC Press LLC*.

Bracci, J.M. et al., 1989. Deterministic Model for Seismic Damage Evaluation of Reinforced Concrete Structures. Technical Report. *Technical Report NCEER-89-0033, National Center for Earthquake Engineering Reasearch, State University of New York at Buffalo*.

Caughey, T.K., 1960. Sinusoidal Excitation of a System With Bilinear Hysteresis. *Journal of Applied Mechanics*, December, pp.640–643.

Chai, Y.H., Romstad, K.M. & Bird, S.M., 1995. Energy-based linear damage model for high- intensity seismic loading. *Journal of Structural Engineering*, 121(5), pp.857–864.

Charalampakis, A.E., 2009. Ανελαστική δυναμικη αναλυση φορέων με προσομοίωση κατα Bouc-Wen (Inelastic Dynamic analysis of structures using Bouc-Wen hysteretic models). *PhD Thesis*.

Chopra, A.K., 2012. *Dynamics of structures, theory and applications to earthquake engineering* Fourth Edi. W. J. Hall, ed., NJ 07458: Prentice Hall.

Chung, Y.S., Meyer, C. & Shinozuka, M., 1987. Seismic damage assessment of reinforced concrete members. *Technical Report NCEER-87-0022, National Center for Earthquake Engineering Reasearch, State University of New York at Buffalo*.

Clough, R.W. & Johnston, S.B., 1966. Effects of stiffness degradation on earthquake ductility requirements. *Second Japan Earthquake Engineering Symposium*, pp.227–232.

Colombo, A. & Negro, P., 2005. A damage index of generalised applicability. *Engineering Structures*, 27(8), pp.1164–1174.

Comité Européen de Normalisation, 2004. Eurocode 8: Design of structures for earthquake resistance. , pp.1–229.

Cosenza, E. & Manfredi, G., 2000. Damage indices and damage measures. *Progress in Structural Engineering and Materials*, 2(1), pp.50–59.

Darwin, D. & Nmai, C.K., 1986. Energy dissipation in RC beams under cyclic load. *ASCE Journal of Structural Engineering*, 112(8), pp.1829–1846. Available at: http://ascelibrary.org/doi/abs/10.1061/(ASCE)0733-9445(1986)112:8(1829).

Degarmo, E.P., J T. Black & Kohser, R. a, 2003. *Materials and Process in Manufactoring* Ninth., John Wiley & Sons, Inc.

Elwood, K.J. & Moehle, J.P., 2003. Shake table tests and analytical studies on the gravity load collapse of reinforced concrete frames. *PEER Report 2003/01, Pacific Earthquake Engineering Research Center, University of California, Berkeley, California*.

Fajfar, P., 1992. Equivalent ductility factors, taking into account low-cycle fatigue. *Earthquake Engineering & Structural Dynamics*, 21(10), pp.837–848.

Fajfar, P. & Krawinkler, H., 1997. *Seismic design methodologies for the next generation of codes*, A.A. Balkema.

FEMA P440A, 2009. Effects of Strength and Stiffness Degradation on Seismic Response. *Federal Emergency Management Agency, National Earthquake Hazards Reduction Program ()*, (June), p.312.

Ghobarah, A., 2001. Performance-based design in earthquake engineering : state of development. , 23, pp.878–884.

Ghobarah, A., Abou-Elafth, H. & Ashraf, B., 1999. Response-based damage assessment of structures. *Earthquake Engineering and Structural Dynamics*, 168(April 1998), pp.27–34.

Goel, S.C. & El-tayem, A.A., 1987. Cyclic load behaviour of angle X-Bracing. *Journal of Structural Engineering*, 112(11), pp.2528–2539.

Gosain, N.K., Jirsa, J.O. & Brown, R.H., 1977. Shear requirements for load reversals on R/C members. *Journal of the Structural Division*, 103(7), pp.1461–1476.

Hadzima-Nyarko, M., Morić, D. & Španić, M., 2014. Spectral functions of RC frames using a new formula for damage index. *Tehnički vjesnik*, 21(1), pp.163–171.

Hancock, J. & Bommer, J., 2006. A state-of-knowledge review of the influence of strong-motion duration on structural damage. *Earthquake Spectra*, 22(3), pp.827–845.

He, Y.-B. et al., 2014. The modification on the discreteness of Park-Ang damage index based on Bayesian methodology. *Journal of Harbin Institute of Technology*, 21(1), pp.102–108.

Ibarra, L.F., Medina, R.A. & Krawinkler, H., 2005. Hysteretic models that incorporate strength and stiffness deterioration. *Earthquake Engineering and Structural Dynamics*, 34(12), pp.1489–1511.

Jeong, G.D. & Iwan, W.D., 1988. The effect of earthquake duration on the damage of structures. *Earthquake Engineering and Structural Dynamics*, 16(April), pp.1201–1211.

Kalmár-Nagy, T. & Shekhawat, A., 2009. Non-linear dynamics of oscillators with bilinear hysteresis and sinusoidal excitation. *Physica D: Non-linear Phenomena*, 238(17), pp.1768–1786. Available at: http://dx.doi.org/10.1016/j.physd.2009.06.016.

Kappos, A.J., 1998. Evaluation of behaviour factors on the basis of ductility and overstrength studies. *Journal of Engineering Structures*, (21), pp.823–835.

Kappos, A.J., 1997. Seismic damage indices for RC buildings: evaluation of concepts and procedures. *Progress in Structural Engineering and Materials*, (I), pp.78–87.

Kottari, A.K., Charalampakis, A.E. & Koumousis, V.K., 2014. A consistent degrading Bouc – Wen model. *Engineering Structures*, 60(2), pp.235–240.

Kramer, S.L. & Stewart, J.P., 2004. *Geotechnical Aspects of Seismic Hazards*,

Kratzig, W.B., Meyer, I.F. & Meskouris, K., 1989. Damage evolution in reinforced concrete members under cyclic loading. In *Int. Conf. on Struct. Safety and Reliability*. pp. 795–802.

Kunnath, S.K. et al., 1997. Cumulative seismic damage of reinforced concrete bridge piers. *Technical Report NCEER-97-0006, National Institute of Standards and Technology*.

Kunnath, S.K., Mander, J.B. & Fang, L., 1997. Parameter identification for degrading and pinched hysteretic structural concrete systems. *Journal of Engineering Structures*, 19(3), pp.224–232.

Kunnath, S.K., Reinhorn, A.M. & Park, Y.J., 1990. Analytical modeling of inelastic seismic response of R/C structures. *Journal of Structural Engineering*, 116(4), pp.996–1017.

L.Kramer, S., 1997. Geotechnica Earthquake Engineering. , p.168.

Liu, C.-S. & Huang, Z.-M., 2004. The steady state responses of s.d.o.f. viscous elasto-plastic oscillator under sinusoidal loadings. *Journal of Sound and Vibration*, 273(1–2), pp.149–173. Available at: http://linkinghub.elsevier.com/retrieve/pii/S0022460X03004231.

Liu, C.S., 2000. The steady loops of sdof perfectly elastoplastic structures under sinusoidal loadings. *Journal of Marine Science and Technology*, 8(1), pp.50–60.

Liu, J. & Astaneh-asl, A., 2004. Moment – rotation parameters for composite shear tab connections. *Journal of Structural Engineering*, 130(9), pp.1371–1380.

Lybas, J.M. & Sozen, M.A., 1977. *Effect of beam strength and stiffness on dynamic behavior of reinforced concrete coupled walls*,

Macrae, G. a & Kawashima, K., 1997. Post-earthquake residual displacements of bilinear oscillators. *Earthquake Engineering and Structural Dynamics*, 26, pp.701–716. Available at: http://dx.doi.org/10.1002/(SICI)1096-9845(199707)26:7%3C701::AID-EQE671%3E3.0.CO;2-I.

Medina, R.A. & Krawinkler, H., 2004. Influence of Hysteretic Behavior on the Non-linear Response of Frame Structures. *13 th World Conference on Earthquake Engineering*, (239).

Mehanny, S.S.F. & Deierlein, G.G., 2001. Seismic damage and collapse assessment of composite moment frames. *Journal of Structural Engineering*, 127(9), pp.1045–1053.

Van Melick, H.G.H., Govaert, L.E. & Meijer, H.E.H., 2003. On the origin of strain hardening in glassy polymers. *Polymer*, 44(8), pp.2493–2502.

Mihaiță, M., 2013. A theoretical review of the damage indices used to model the dynamic non-linear behavior of reinforced concrete structures. *Buletinul Institutului Politehnic din Iași*, LIX (LXIII(2), pp.109–119.

Miller, B.G.R. & Butler, M.E., 1988. Periodic response of elastic-perfectly plastic SDOF oscilator. , 114(3), pp.536–550.

Miranda, E., 1993. Evaluation of site-dependent Inelastic seismic design spectra. , 119(5), pp.1319–1338.

Mirzaaghabeik, H. & Vosoughifar, H.R., 2015. Comparison between quality and quantity seismic damage index for LSF systems. *Engineering Science and Technology, an International Journal*, 19(1), pp.497–510. Available at: http://www.sciencedirect.com/science/article/pii/S2215098615001470.

Naeim, F., Skliros, K. & Reinhorn, A.M., 2000. Influence of Hysteretic Deteriorations on Seismic Response of Multistory Steel Frame Buildings. In *12th World Conference on Earthquake Engineering*. pp. 1–8. Available at: http://ascelibrary.org/doi/abs/10.1061/40492(2000)107.

NEHRP, 2009. Recommended Seismic Provisions for New Buildings and Other Structures. *Fema P-750 (National Earthquake Hazards Reduction Program)*, I. Available at: http://www.fema.gov/media-library-data/20130726-1730-25045-1580/femap_750.pdf.

Newmark, N.M. & Emilio, R., 1971. *Fundamentals of earthquake engineering*,

Nishigaki, K. & Mizuhata, K., 1983. Experimental study on low-cycle fatigue on reinforced concrete columns. *Transaction of the Architectural Institute of Japan*.

Niu, D. & Ren, L., 1996. A modified seismic damage model with double variables for reinforced concrete structures. *Journal of Earthquake Engineering and Engineering Vibration*, 16, pp.44–55.

Oh, Y., Han, S.W. & Lee, L., 2000. Effect of hysteretic models on the inelastic design spectra. In *12th World*

Conference on Earthquake Engineering. pp. 1–8.

Park, R., 1988. State-of-the-art report: Ductility evaluation from laboratory analytical testing. In *Ninth world conference on earthquake engineering*. pp. 605–616.

Park, Y. & Ang, A.H.S., 1985. Mechanistic seismic damage model for reinforced concrete. , 111(4), pp.722–739.

Park, Y.J., Reinhorn, A.M. & Kunnath, S.K., 1987. IDARC: Inelastic damage analysis of reinforced concrete frame - shear-wall structures. *Technical Report NCEER-87-0008, National Center for Earthquake Engineering Reasearch, State University of New York at Buffalo*.

Park, Y.J., Reinhorn, A.M. & Kunnath, S.K., 1988. Seismic damage analysis of reinforced concrete buildings. In *Proceedings of the 9th World Conference of Earthquake Engineering*. pp. 211–216.

Di Pasquale, E. & Camak, A.S., 1987. Detection and assessment of seismic structural damage. *Technical Report NCEER-87-0015, National Center for Earthquake Engineering Reasearch, State University of New York at Buffalo*. Available at: http://www.ncbi.nlm.nih.gov/pubmed/1790541.

Di Pasquale, E. & Camak, A.S., 1989. On the relation between local and global damage indices. *Technical Report NCEER-89-0034, National Center for Earthquake Engineering Reasearch, State University of New York at Buffalo*.

Powell, G. h. & Allahabad, R., 1988. Seismic damage prediction by deterministic methods : concepts and procedures. *Earthquake engineering and structural dynamics*, 16(October 1987), pp.719–734.

Pratap, R. & Mukherjee, S., 1994. Dynamic behavior of a bilinear hysteretic elasto-plastic oscillator, Part1 free oscillations. *Journal of Sound and Vibration*, 172(3), pp.321–337.

Pratap, R., Mukherjee, S. & Moon, F.C., 1994. Dynamic behavior of a bilinear hysteretic elasto-plastic oscillator, Part II: oscillations under periodic impulse forcing. *Journal of Sound and Vibration*, 172(3), pp.339–358. Available at: http://www.sciencedirect.com/science/article/pii/S0022460X84711795.

Rahnama, M. & Krawinkler, H., 1993. *Effects of soft soil and hysteresis model on seismic demands, Report No. 108*,

Ravenshorst, G. et al., 2016. *Structural behaviour of a calcium cilicate brick masonry assemblage: quasi-static cyclic pushover and dynamic identification test*,

Ray, T. & Reinhorn, A., 2014. Enhanced smooth hysteretic model with degrading properties. *Journal of Structural Engineering*, 140(1), pp.4013028–1, 4013028–10. Available at: http://0-ascelibrary.org.wam.city.ac.uk/doi/abs/10.1061/(ASCE)ST.1943-541X.0000798.

Reinhorn, A.M. et al., 2009. IDARC2D Version 7.0: A program for the inelastic damage analysis of structures. *Technical Report MCEER-09-0006, University at Buffalo, State University of New York*.

Reinhorn, A.M., Kunnath, S.K. & Panahshahi, N., 1988. Modelling of RC building strucutres with flexible floor diaphragms (IDARC2).

Rodgers, Janise E.; Mahin, S.A., 2004. Effects of Hysteretic Deterioration on Seismic Response of Steel Moment Frames. *13th World Conference on Earthquake Engineering*, (1581).

Rodriguez, M.E. & Aristizabal, J.C., 1999. Evaluation of a seismic damage parameter. *Earthquake Engng. Struct. Dyn*, 477, pp.463–477.

Rodriguez, M.E. & Padilla, D., 2009. A Damage Index for the Seismic Analysis of Reinforced Concrete Members. *Journal of Earthquake Engineering*, 13(3), pp.364–383.

Rodriguez Gomez, S. & S., C.A., 1990. Evaluation of Seismic Damage Indices for Reinforced Concrete Structures.pdf.

Roufaiel, M.S.L. & Meyer, C., 1982. Analysis of damaged concrete frames for cyclic loads. *EARTHQUAKE ENGINEERING AND STRUCTURAL DYNAMICS*, 11, pp.208–228.

Roufaiel, M.S.L. & Meyer, C., 1987a. Analytical modeling of hysteretic be- havior of R/C frames. *Journal of Structural Engineering*, 113(3), pp.429–444.

Roufaiel, M.S.L. & Meyer, C., 1987b. Analytical modeling of hysteretic behavior or R/C frames. *Journal of Structural Engineering*, 113(3), pp.429–444.

Roufaiel, M.S.L. & Meyer, C., 1987. Reliability of concrete frames damaged by earthquakes. *Journal of Structural Engineering*, 113(3), pp.445–457.

Ruiz-García, J. & Miranda, E., 2003. Inelastic displacement ratios for evaluation of existing structures. *Earthquake Engineering and Structural Dynamics*, 32(8), pp.1237–1258.

Ruiz-García, J. & Miranda, E., 2006. Inelastic displacement ratios for evaluation of structures built on soft soil sites. *Earthq. Eng. Struct. Dynam*, 35, pp.679–694.

Ruiz-García, J. & Miranda, E., 2006. Residual displacement ratios for assessment of existing structures. *Earthquake Engineering and Structural Dynamics*, 35(3), pp.315–336.

Seidel, M.J., Reinhorn, A.M. & Park, Y.J., 1989. Seismic damageability assessment of R/C buildings in Eastern U.S. *Journal of Structural Engineering*, 115(9), pp.2184–2203.

Sinha, R. & Shiradhonkar, S.R., 2012. Seismic Damage Index for Classification of Structural Damage – Closing the Loop. *Proc: 15th World Conference on Earthquake Engineering*, 98.

Sivaselvan, M. & Reinhorn, A.M., 2000. Hysteretic models for deteriorating inelastic structures. *Journal of Engineering Mechanics*, 126(6), pp.633–640.

Sivaselvan, M. V., 2013. Hysteretic models with stiffness and strength degradation in a mathematical programming format. *International Journal of Non-Linear Mechanics*, 51, pp.10–27.

Sivaselvan, M. V. & Reinhorn, A.M., 1999. Hysteretic Models for Cyclic Behavior of Deteriorating Inelastic Structures. *Technical Report NCEER-99-0018, National Center for Earthquake Engineering Reasearch, State University of New York at Buffalo*.

Sozen, M., 1981. Review of earthquake response of reinforced concrete buildings with a view to drift control. *State-of-the-Art in Earthquake Engineering, Turkish National Committee on Earthquake Engineering*, pp.383–418.

Spetzler, J. & Dost, B., 2016. Probabilistic Seismic Hazard Analysis for Induced Earthquakes in Groningen. *KNMI report*, June(June), pp.1–14.

Sreekala, R. et al., 2011. Development of a simplified damage model for beams aiding performance based design. *Advances in Structural Engineering*, 14(2), pp.307–317.

Stephens, J.E. & Yao, J.T.P., 1987. Damage assessment using response measurements. *Journal of Structural Engineering*, 113(4), pp.787–801.

Takeda, Sozen & Nielsen, 1970. Reinforced Concrete Response to Simulated Earthquakes. *Journal of the Structural Division*, 96(12), pp.2557–2573. Available at: http://cedb.asce.org/cgi/WWWdisplay.cgi?17038.

Teran-gilmore, A., Jirsa, J.O. & Eeri, M., 2005. A damage model for practical seismic design that accounts for low. *Earthq. Eng. Struct. Dynam*, 36(3), pp.383–404.

Thyagarajan, R.S., 1989. Modeling and analysis of hysteretic structural behaviour. *Report No. EERL 89-03, California Institute of Technology, Pasadena, California*.

Toussi, S. & Yao, J.T.P., 1983. Hysteresis identification of existing structures. *Journal of Engineering Mechani*, 109(5), pp.1189–1202.

Trifunac, M.D.. & Brady, A.G., 1975. A study on the duration of strong earthquake ground motion. *Bull. Seis. Soc. Am.*, 65, pp.581–626.

Uriz, P. & Mahin, S.A., 2004. Seismic performance assessment of concentrially braced steel frames. *13 th World Conference on Earthquake Engineering*.

Velde, J., 2010. *3D Nonlocal damage modeling for steel structures under earthquake loading*,

Venti, M. & Engelhardt, M.D., 1999. Brief report of steel moment connection test specimen DBBW (Dog Bone - Bolted Web). *SAC Joint Venture - Steel Project, Internal SAC Phase 2 Background Report*, 2.

Visintin, A., 1994. *Deifferential models of hysteresis*, Berlin Heidelberg: Springer-Verlag.

Wang, M.-L. & Shah, S.P., 1987. Reinforced concrete hysteresis model based on the damage concept. *Earthquake Engineering and Structural Dynamics*, 15(8), pp.993–1003.

Wang, Y., 1996. an Analytical Solution for Periodic Response of Elastic-Friction Damped Systems. *Journal of*

Sound and Vibration, 189(3), pp.299–313. Available at: http://www.sciencedirect.com/science/article/pii/S0022460X96900218.

Wen, Y.K., 1976. Method of random vibration of hysteretic systems. *Journal of the Engineering Mechanics Division*, 102(2), pp.249–263.

Whitworth, H.A., 1998. A stiffness degradation model for composite laminates under fatigue loading. *Composite structures*, 40(2), pp.95–101.

Yao, J.T.P. & Munse, W.H., 1962. Low-cycle fatigue behavior of axially loaded specimens of mild steel. *American society for testing and materials*, pp.5–24.

Yazgan, U., 2010. The Use of Post-Earthquake Residual Displacements. *PhD Thesis*, (Institute of Structural Engineering Swiss Federal Institute of Technology).